TECHNISCHE UNIVERSITÄT MÜNCHEN
Wissenschaftszentrum Weihenstephan für Ernährung, Landnutzung und Umwelt
Lehrstuhl für Aquatische Systembiologie

Extraction of parameters for aquatic reed status determination by exploring UAV-RGB and airborne Green-LiDAR data

Nicolás Corti Meneses

Vollständiger Abdruck der von der Fakultät Wissenschaftszentrum Weihenstephan für Ernährung, Landnutzung und Umwelt der Technischen Universität München zur Erlangung des akademischen Grades eines

Doktors der Naturwissenschaften

genehmigten Dissertation.

Vorsitzender: Prof. Dr. Thomas Knoke

Prüfer der Dissertation:

1. Prof. Dr. Jürgen Geist
2. Prof. Dr. Matthias Braun
3. Prof. Dr. Johannes Kollmann

Die Dissertation wurde am 27.05.2019 bei der Technischen Universität München eingereicht und durch die Fakultät Wissenschaftszentrum Weihenstephan für Ernährung, Landnutzung und Umwelt am 15.10.2019 angenommen.

Preface

This dissertation aims to contribute to the development of efficient and effective monitoring of reed beds by analysing remote sensing (RS) data. Considering the problem of declining aquatic reed consisting of *Phragmites australis,* data collected with Unmanned Aerial Vehicles (UAV) and airborne Green-LiDAR (Light Detection and Ranging) was analysed in order to extract biometric parameters. Quantitative variables are essential to evaluate a reed bed stock, to assess the vegetation status, and to develop conservation or restoration measures. The present dissertation starts with a description of aquatic reed beds and their importance for the lake ecosystem, as well as documented factors causing their decline. The introduction also illustrates the already used monitoring methods and the new opportunities offered by UAV and LiDAR technologies for describing this type of vegetation. Following the introduction, three detailed thematic studies dealing with the extraction, and measuring of biometric reed parameters in RS data are presented. Each specific topic has been published (Chapter 2, 3, and 4) as autonomous research papers in a slightly modified form (according to the specific journal requirements). The dissertation provides a general discussion on the suitability of UAV and Green-LiDAR in delivering relevant information for characterizing aquatic reed beds and the advantages, and potential constraints, when implementing this system in reed bed monitoring projects. The feature extraction, classification and mapping as well as the conclusions drawn from the results suggest that the proposed approach may be useful for other application areas such as agriculture or forestry.

Abstract

Aquatic reed beds are of essential importance for freshwater lake ecosystems. They protect the shores from erosion, constitute a habitat for several species, and provide an important structural element in the lake landscape. Their population decline has been observed in long-term monitoring projects. Discussed causes triggering aquatic reed decrease are of mechanical, hydrological, climatic, anthropogenic and biological origin. For instance, high frequency of extreme droughts, floods, strong winds and thunderstorms in addition to the more frequent boat traffic and recreational activities at Bavarian lakes increase the pressure on aquatic reed populations. Monitoring the status of the aquatic reed bed at intervals shorter than the three years, recommended by the authorities, appears to be necessary. Terrestrial mapping and visual interpretation of aerial images followed by manual delineation has been commonly used to assess and quantify the development aquatic reed beds. The difficulties in the implementation and execution make these methods ineffective. Modern remote sensing technologies, in support of terrestrial inventories, are expected to reduce monitoring time and costs, and allow a higher update frequency with increased accuracy.

This dissertation deals with the task of extracting quantitative and essential biometric information of aquatic reed beds health and distribution. For this purpose, based on data gathered by Unmanned Aerial Vehicles (UAVs) and airborne Green Light Detection and Ranging (Green-LiDAR), two new classification strategies are developed based on data points defined by a given coordinate system (point clouds). These classification strategies were derived based on mapping structural parameters and vegetation status for aquatic reed beds consisting of *Phragmites australis*.

The investigations presented in this dissertation were published as three detailed thematic studies. The first study presents an efficient and empirical approach for determining the required parameters for image alignment and feature extraction for point cloud calculation of sparse aquatic reed beds, with the lowest Root Mean Square (RMS) reprojection error. Aimed at finding differences in biometric features extracted on data collected by Rotary- (RW) and Fixed-Wing (FW) UAVs, images were recorded with the same sensor system mounted on both aerial vehicles. Image processing and feature extraction were executed in a Structure from Motion (SfM) environment and based on bundle adjustment.

The determined point clouds from the first study were used in the second study, which presents the classification method developed for determining frontline, extent, density and status of aquatic reed beds. The extent was validated by comparing it against cross sections measured in the field. Density and vegetation status was assessed against independent aerial imagery in addition to field data. The Root Mean Square Error and an Error Matrix were applied for this task.

The third study presents the combination and adaption of UAV developed classification rules to Green-LIDAR data for extracting the same fundamental parameters (height, density, and extent) of aquatic reeds. A rule-based algorithm was developed for the automatic classification of Green-LiDAR point clouds. Green-LiDAR data allowed for the delimitation of the aquatic reed frontline and shoreline therefore providing an accurate quantification of extents. Digital Surface Models (DSM), calculated from point clouds, similarly showed a high level of agreement in the derived heights of flat surfaces and in the complex surface of aquatic reed heights.

The results of the studies proved the suitability of UAVs and Green-LiDAR on mapping diagnostic structural parameters of aquatic reed beds by examining point clouds. Independently of the type of system used the height of aquatic red beds were extracted. This was achieved through Green-LiDAR point cloud analysis or photogrammetry, which are procedures with high potential for automatic

feature extraction. The results showed that height and density (sparse and dense) could be evaluated by analysing height variations. Lakeward expansion front (frontline) of aquatic reed beds was allocated using UAV and LiDAR data. Green-LiDAR data also demonstrated its suitability in identifying the shoreline. Spectral information in UAV point clouds contributed to the status assessment of aquatic reed. The three spectral bands (red, green, blue) of each point offered opportunities for calculation of vegetation indexes (e.g. NDVI). Secondary biometric parameters such as the amount of leaves or flowers could potentially be assessed using the laser beam amplitude (intensity) in combination with point geometry, however this is still to be determined. Vegetation mapping with both remote sensing systems appeared to be more practicable than onsite measurements and delivered, in some cases, more accurate quantitative information (height, density, extent) with no disturbance of the habitat. The research shows that complex transitional zones (water-vegetation-land) can be assessed using these remote sensing technologies. Analysing remotely collected monitoring data with the presented classification procedure improved the efficiency, reproducibility, and accuracy of the quantification of aquatic reed beds status. Based on the objectivity, comparability and repeatability, it is clearly recommended that UAV or LiDAR based data collection methods are used for monitoring aquatic reed beds.

To my father and mother:
Long is the way through teaching, short and effective through the example.

Contents

List of Figures

List of Tables

1. Introduction

1.1. Reed beds as a study object and their importance for lake ecosystems

Common reed is a grass type plant with a special adaptability. It occurs in shallow shores of standing or slowly flowing waters, and swamps (Dittrich 2014). The high genetic variability allows the growing not only in nutrient-poor lake shores, but also in brackish water locations (Grosser et al. 1997). Although reproduction happens occasionally with seeds, reed proliferates almost exclusively through rhizome sprouts. Shoots can grow up to 4.5 cm/day and stems can reach heights of 4 meters (Dittrich 2014; Ostendorp 1993b). The high productivity allows the reed to reach its maximum height within 4-5 months (Ostendorp 1991; Grosser et al. 1997). However, the growth rate varies according to the different ecological zones. Along a horizontal gradient, from lakeside towards the bank, reed stocks are classified into three different ecological zones, which occur either in land, transitional, and aquatic zones (Figure 1.1). Land reed beds are located in areas above water level, comprise an onshore/shoreward stock of not only reeds but multiple plant species, and usually grow in meadows. Transitional reed stands are not permanently flooded, correspond to the landside, are pure stands of *Phragmites australis*, and characterized for its increment in stem density, length, and fertility. Aquatic reed beds grow in locations flooded throughout the year. They are also pure stands of *Phragmites australis*, which correspond to lakeside stocks that grow directly in sediment and are characterized for their low culm density and longer sparse fertility (Grosser et al. 1997). The aquatic reed at the expansion front of a stand is considered the most sensitive zone. In spring, aquatic reeds have a faster development since it needs to emerge from water for breathing and perform photosynthesis. At the middle of summer, aquatic reeds reach 85% of its maximal length, whilst the uniform development of transitional and land reed grow only 80% by the time (Grosser et al. 1997). Between the middle of summer to mid-autumn the flowering phase takes place, and aquatic reed stocks often carry no panicles (Grosser et al. 1997).

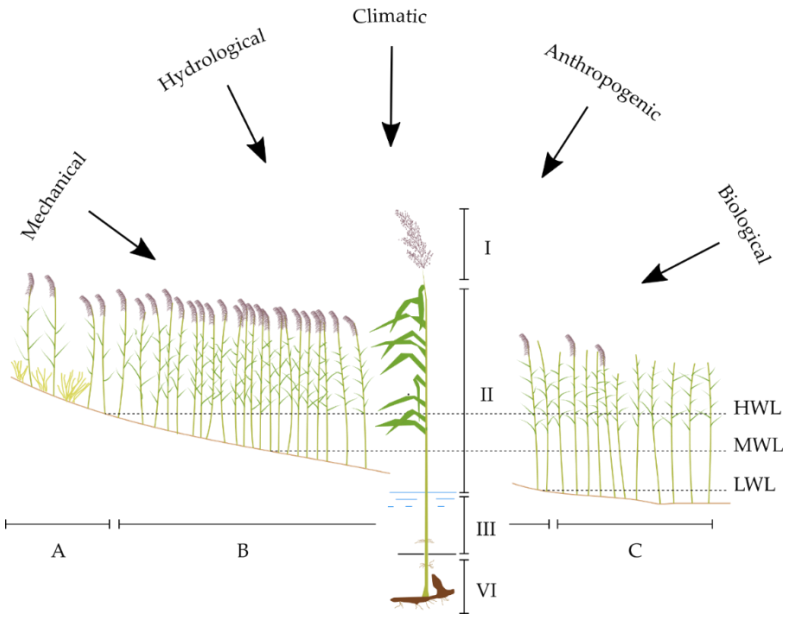

Figure 1.1 Vertical and horizontal classification of reed beds depending on water level, and reasons for decline. I) Stem tips and panicles area, II) emerged stem and leaves, III) submerged stem, IV) sediment and rhizome zone. A) Land reed: the water level is lower than the ground surface, B) Transitional reed: not constantly flooded, C) Aquatic Reed: flooded throughout the year. HWL) High water level, MWL) middle water level, LWL) low water level. Adapted from (Ostendorp 1993b)

Many investigations have shown the ecological impact of reeds in lakeshore ecosystems. On a landscape level reed beds contribute to the species conservation, shore protection, and pollution control (Ostendorp 1993a). "*They are ecotones between land and water, which attract many kinds of wildlife, economic, cultural and recreational uses and human settlement*" (Schmieder 2004). For specialized fauna, reed stands constitute a structural element and food source. Reed beds establish the habitat for fish, birds, and mammals, and its high productivity is the food basis for many primary consumers, parasites and secondary decomposers (Ostendorp 1989). The oxygen entry in combination with the length of the root system make the ideal habitat for different species of fungus and bacteria. Reed beds are also natural structures that protect against sediment movement and bank erosion. The allocation of reed stems reduces the wind and wave energy, therefore stabilizing the shorelines of lakes, rivers, reservoirs, and channels (Grosser et al. 1997). The nutrient retention capacity contributes to the self-purification potential of contaminated lakes or rivers. Reed beds contribute to the cleaning of runoff from agricultural fields or tributaries (Grosser et al. 1997). The ability of reeds to release oxygen in water and soil promotes the microbial decomposition of organic matter by oxygen-specialized bacteria, which settles in large quantities of capillaries on the reed roots (Dittrich 2014). The significance of reeds varies according to the ecological zones. Land and transitional reeds are stabile zones and their stem density and height allow ideal habitat for birds and small mammals. The growing organisms in aquatic reed beds offer instead adequate ecological conditions for molluscs and diatoms. Fish, reptiles, and amphibians avoid transitional zones and remain in undisturbed areas for spawning (Grosser et al. 1997). In addition, reed beds have also an aesthetic significance. Reed beds are a dominating element of the landscape at most of the European lakes. Located at the shore of lakes, they are associated with near-natural landscape images, which is considered as an important aspect for recreation (Holsten et al. 2013). The mentioned ecosystem services and functions give the reed belts on lakeshores also a fundamental economic significance. For instance, conservation of fish species contributes to the livelihoods of local anglers on which they partially depend on. Environmental protection measurements for enhancing water quality and erosion control are reduced, since respectively the nutrient load of surface runoff from used agricultural areas as well as the wave and wind energy are diminished. The biodiversity in reed belts are the perfect wildlife reserves that attract tourists (Ostendorp 1989).

1.2. Factors causing reed decline

Reed beds have experienced a recession during the past decades (Ostendorp 1989; van der Putten 1997; Brix 1999; Fogli et al. 2002; Vermaat et al. 2016). Diminishing of reed beds had already been documented in some Swiss lakes since the middle of the past century, in which almost only aquatic reeds were affected (Grosser et al. 1997). The identified stressing factors can be grouped as mechanical, hydrological, climatic, anthropogenic, and biological causes. Mechanical damage of reed culms is produced by wind, frequent strong waves produced by sailing or boot traffic, and transported materials by water currents. Recreational activities such as bathing, surfing or paddling have also been documented of causing mechanical damage to the reeds through cutting or stepping. In the same way, similar disturbances have been recognized but provoked by browsing animals (e.g. Goose, muskrat) below the water line (Dittrich 2014; Grosser et al. 1997; Sukopp and Markstein 1989; Stark and Dienst 1989). Flooding is the main factor documented as a hydrological cause. Flooding of reed stems produces early yellowing and hinders the accumulation of nutrients for the next vegetation period. In addition, the inundation of broken reed culms hinders the provision of oxygen to the rhizome through the aerenchym (Grosser et

al. 1997; Stark and Dienst 1989; Ostendorp 1991; Rea 1996; Rücker et al. 1999). Water level fluctuations lead to the freezing or washing out of rhizomes (Dittrich 2014). Long-term climate changes have also a modifying effect on reed development. The exposure time to sunlight and temperature variability shorten the growing season affecting the growth and spread of reeds (Rücker et al. 1999). As anthropogenic causes have been identified based on the changes in land use. For instance, land reclamation, wetland draining, the construction of houses, beaches, and landing sites for boats, are some anthropogenic changes that have a negative impact to the reed stocks (Ostendorp 1989; Sukopp and Markstein 1989). Shades caused by constructions or tree plantations is a side effect which influences the normal development of reeds (Dittrich 2014). High nutrient content (eutrophication) facilitates the generation of algal mats, which are driven by wind or waves to reed belts causing culm breaking, and poisoning the rhizome through the decomposition products (Dittrich 2014; Stark and Dienst 1989). Eutrophication also causes the accumulation of detritus in littoral zones and the high generation of H_2S damages the rhizome and is considered as a cause of reed die-back (Grosser et al. 1997). Although a stimulus for growth may possibly be the increment of nutrients, the excessive intensification of nutrients in highly eutrophic waters may cause physiological stress (Den Hartog et al. 1989). Genetic variations in reeds have been recognized as biological cause. Specific genotypes die through changes in environmental conditions, but are replaced with new adapted forms. However, on a long term this process causes a genetic loss since the reproduction is mainly vegetative (Grosser et al. 1997). Consequently, loss of genetic diversity within a reed population may lead to a lack of adaptability of the reed to environmental changes (Dittrich 2014).

1.3. Remote sensing methods used in the monitoring of aquatic reed beds

Global, regional or local, remote sensing technologies provide data for different degrees of detail. Available information from satellite constellations with multispectral and hyperspectral sensors have been applied in the global research of reed beds. *Phragmites australis* has been ecologically assessed using multi-season SPOT-5 scenes (Poulin et al. 2010; Davranche et al. 2010), as well as the conservation status with data from Geoeye and Worldview 2 (Villa et al. 2013). Large-scale management of common reed for paper production has been also supported Landsat ETM, TM and ASTER imagery (Brix et al. 2014). The effectiveness in large-scale mapping of lakeshore habitat has also been assessed with the new European satellite Sentinel 2 (Stratoulias et al. 2015a). Interpretation of aerial photographs has normally been focused more on regional and local scale analysis of reed development, extent, structure, or health. It has been used to map reed decline in large lakes (Krumscheid et al. 1989), to define possible decline causes through analysis of historical imagery (Rücker et al. 1999), to investigate the development of reed and consequently to create conservation plans (Melzer et al. 2001), or to outline the effects of extreme floods on spatial dynamics and stand structure of reed belts (Schmieder et al. 2002). Implementation of aerial imagery with an additional band in the infrared wavelength of the electromagnetic spectrum contributed not only in mapping vitality of reed beds. The spectral differences measureable in the infrared wavelength have been used to delimitate proportions of stands with dead stems and thus the degree of damage of a reed cut can be estimated (Schmieder et al. 2002; Ostendorp et al. 2003; Schmieder et al. 2004; Dienst et al. 2004).

These remote sensing data have contributed in the analysis of large-scale reed beds. Interpretation of aerial and satellite imagery with spatial resolutions from approximately 1 to 30 m has achieved good results in mapping healthy and large reed stands. Healthy land reed beds are characterized for the slow replacement of sedge or woodland communities or by unfertilized grasslands. On the other hand,

healthy aquatic reed beds are homogeneous, dense and with a regular lake frontline without lanes or gaps, shaping a uniform fringe, decreasing gradually in stems length, but all stalks of one stand of similar height (Ostendorp 1989; Hoffmann and Zimmermann 2000). Die-back or unhealthy aquatic reed beds are characterized instead by:

- sparse and parallel stripes along the reed bed edge (due to either floods, wind storms, or driftwood accumulation),
- a lane/aisle perpendicular to the shore (for docks, boot traffic, bathing, fish traps),
- the disintegration of reed beds though decreasing stem density, frayed, ripped, not zoned reed edge and in single clumps (through erosion or flood), and seaward stubble fields of past reed beds (Hoffmann and Zimmermann 2000).

In order to detect stress in aquatic reed beds, these characteristics are fundamental for image interpretation and it is here where the limitations of aerial and satellite imagery are noticeable. Spatial resolution and mixed spectral signature in each pixel (e.g. water and vegetation) hinders the accurate allocation of lakeside frontline, and even in aerial imagery, this cannot be distinguished (Hoffmann and Zimmermann 2000). It is crucial to detect degradation of aquatic reed beds during succession in land-water ecotones by monitoring for the following typical indicators: deep water retreat, gradual thinning, clumped growth patterns, die-back in brackish water, and the natural degeneration of reed (van der Putten 1997). State-of-the-art remote sensing methods (UAV and Green-LiDAR) may contribute in the assessment of structure (height, density, extent) and vitality by combining three dimensional (3D) information and spectral signature or light intensity.

1.4. Unmanned Aerial Vehicles (UAV) and airborne Green Light Detection and Ranging (Green-LiDAR)

The advances in remote sensing technologies may offer new opportunities in the monitoring of sparse aquatic reed beds. Height information of reed beds would potentially solve the problems faced with the detection and quantification of sparse reed beds. Considering the height differences of water surface and reed stems, lakeside frontline could be accurately defined and consequently the total vegetal coverage calculated. Collection of points defined by a given coordinate system (point clouds) that represent a 3D (three-dimensional) shape or feature can be obtained from Light Detection and Ranging (LiDAR) sensors or through photogrammetric measurements applied in optical imagery recorded for instance by imaging sensors mounted on Unmanned Aerial Vehicles (UAV). Airborne LiDAR generate positions (coordinates) for points on the Earth's surface out of three sources: laser sensor, Inertial Measurement Unit (IMU) of the aircraft, and Global Positioning System (GPS) (Large and Heritage 2009). These three instruments are necessary for corrections and accurate measurement of coordinate points (Figure 1.2) which, as a whole, are called point clouds. LiDAR systems measures the time-of-flight (TOF) of green or infrared light from emission to reception. Green light, in contrast to infrared, penetrates in water by reflecting off the bottom surface, or in medium content materials (Mandlburger et al. 2013). In addition, green light not only propagates in water but can also reflect off land surfaces. These characteristics make the Green-LiDAR scanner suitable in mapping bathymetry (Costa et al. 2009), bottom structures (Wedding et al. 2008; Tulldahl and Wikström 2012), or even for topo-bathymetric applications (Mandlburger et al. 2015; Yamamoto et al. 2012). Extents are important in the monitoring of aquatic reed beds where the mapping of the shoreline and the frontline are crucial. The technological benefits of a Green-LiDAR scanner could contribute to the accurate mapping of reed bed boundaries. The frontline is scanned from reed stems and leaves above the water surface, thanks to light propagation.

Since Green-LiDAR propagates in water, additional elements such as lake bottom, water surface, and shoreline can also be obtained.

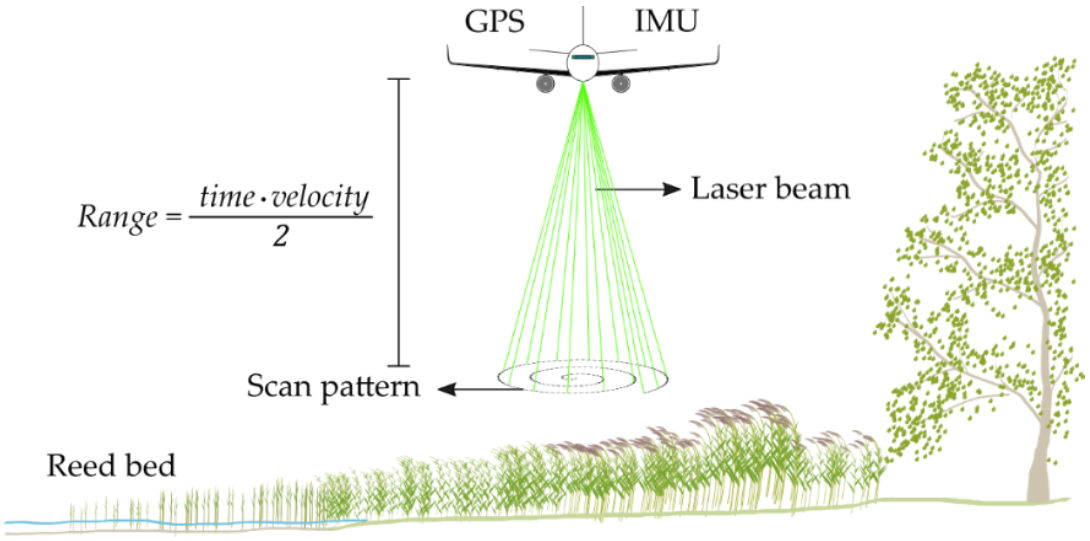

Figure 1.2 Brief explanation of LiDAR functionality. Coordinate of objects on the earth surface are determined using the measured laser beam range and coordinates of the point of origin (aeroplane), which are obtained through GPS and IMU systems

Regarding UAV data, point clouds are generated after photogrammetrically processing optical data (Figure 1.3). Photogrammetric measurements have been applied to imagery obtained from platforms deployed in outer space, air, land and even in aquatic environments (Stratoulias et al. 2015b; Fernandes et al. 2013; Villa et al. 2015; Davranche et al. 2010; Dienst et al. 2004). Recent developments of low flying aerial systems provide a comparatively convenient alternative to using close-range aerial imagery. Bundle triangulation represents "*the most powerful and accurate method of image orientation and point determination in photogrammetry*" (Luhmann et al. 2014). In order to reconstruct an object in 3D, this method merges single images into an overall model by using tie points. With a series of overlapping images, objects can be matched and the geometric accuracy is improved while the probability of occlusions (shadowed or invisible areas in an image) is reduced. Therefore, the generating of image-based point clouds requires images with a high-spatial resolution and a multi-image overlap (White et al. 2013). Since close-range aerial imagery has a very high spatial resolution and spectral information in three bands (red, green and blue), generated clouds have a high point density and every point has a spectral information stored. The fusion of 3D and spectral information is declared as "state of the art" for characterizing ecosystem vegetation and improves the understanding of vegetation status compared to the application of only the structure or the spectral reflectance (Dandois et al. 2017). The implementation of spectral and geometrical information could also contribute in the characterization of reed beds structure, as well as vitality.

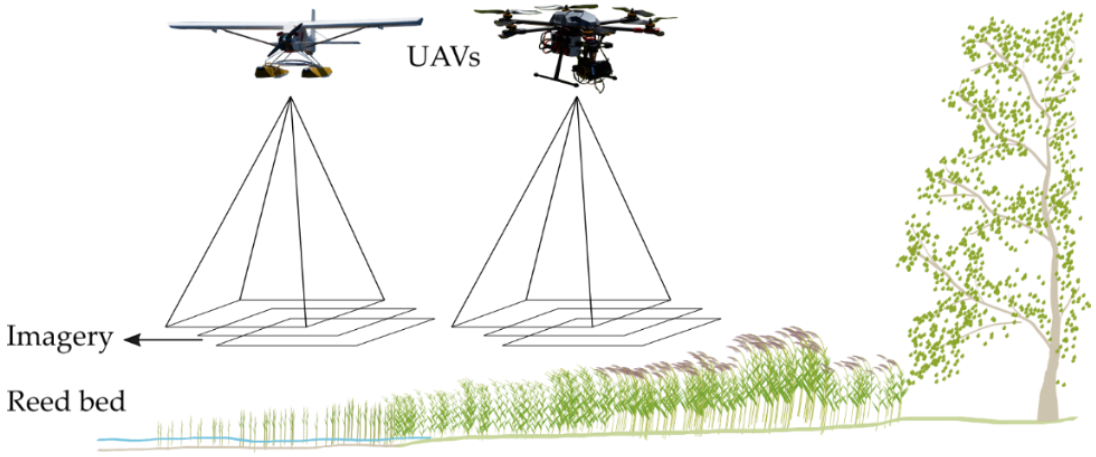

Figure 1.3 Gathering of imagery for photogrammetric processing using Unmanned Aerial Vehicles from Fixed and Rotary-Wings platforms

1.5. Objectives

Previous research identified the continuous decrease of aquatic reed beds and in order to successfully conserve the remaining stands, the implementation of appropriate and accurate monitoring methods is crucial. Aquatic reed beds consisting of *Phragmites australis* are of particular interest because it is a well-known ecotone that attracts many kinds of wildlife, contribute to water purification, provide habitat for many species, and protect against sediment movement and bank erosion. Traditionally, research focused in the assessment of aquatic reed stands was performed by means of field work and complemented with interpretation of optical imagery. However, the success of these processes diminished when implemented separately and as stand-alone monitoring strategies. To increase the knowledge about methods for aquatic reed bed monitoring which are accurate, operational, easy to implement, and without habitat disturbance, the overall objective of this work concentrates on extracting quantitative and essential biometric information of aquatic reed beds in point clouds derived from Unmanned Aerial Vehicles (UAVs) and airborne Green Light Detection and Ranging (Green-LiDAR) data.

The primary objectives of this thesis were:

i. Extract heights of aquatic reed beds using photogrammetry in close-range aerial imagery.

   With a focus on extent quantification and characterization of aquatic reed beds, the first objective focuses firstly on the question of whether close-range aerial photogrammetry is capable of extracting heights of sparse aquatic reed beds. The parameters for image alignment set in a Structure from Motion (SfM) environment were determined by measuring the lowest Root Mean Square (RMS) reprojection error. Aiming at differencing extracted biometric features in data collected by Rotary- (RW) and Fixed-Wing (FW) UAVs, imagery was recorded with the same sensor system mounted on both aerial vehicles.

ii. Mapping vegetation coverage, height, density and derive its status by analysing UAV point clouds.

In terms of mapping products, the second objective faced the challenge of developing an approach, which is consistent with the official monitoring method. This study assessed the classification of aquatic reed beds using high-resolution imagery and point clouds extracted from close-range aerial imagery. Geometry and spectral information in UAV point clouds were assessed for mapping extent, density and vegetation status.

iii. Evaluating of Green-LiDAR for mapping extent, density, and height of aquatic reed beds

The third objective was to evaluate the applicability of Green-LiDAR technology in aquatic reed monitoring. A rule-based algorithm was developed for the automatic classification of Green-LiDAR point clouds. The same fundamental parameters (height, density, and extent) of aquatic reeds were also considered for this goal.

2. Extracting Heights of Sparse Aquatic Reed (*Phragmites Australis*) Using Structure from Motion Point Clouds derived from Rotary- and Fixed-Wing Unmanned Aerial Vehicle (UAV) Data

A similar version of this chapter was published: Meneses, Nicolás Corti; Baier, Simon; Reidelstürz, Patrick; Geist, Juergen; Schneider, Thomas (2018): Modelling heights of sparse aquatic reed (Phragmites australis) using Structure from Motion point clouds derived from Rotary- and Fixed-Wing Unmanned Aerial Vehicle (UAV) data. In *Limnologica* 72, pp. 10–21. DOI: 10.1016/j.limno.2018.07.001.

2.1. Abstract

Aquatic reed beds consisting of *Phragmites australis* play an important role in lake ecosystems. Digital Elevation Models (DEM) provide essential information in identifying and quantifying these stocks. This study modelled sparse aquatic reed beds with aerial images collected from Rotary- (RW) and Fixed-Wing (FW) Unmanned Aerial Vehicles (UAV) by the same imaging system. Image processing was executed in a Structure from Motion (SfM) environment and based on bundle adjustment. The DEMs were referenced with Ground Control Points (GCPs) and validated with independent Reference Points (RPs) of heights from reed and flat surfaces. Root Mean Squared (RMS) reprojection error showed that imagery taken with FW could be better aligned than the RW dataset. Quality assessment proved that RW gathers sharper data and lowers image blur resulting in slightly more accurate DEM, while FW showed better area coverage. The results from both configurations proved the efficiency of the methodology in deriving diagnostic relevant features for monitoring sparse aquatic reed beds.

2.2. Introduction

Aquatic reed beds consisting of *Phragmites australis* play an important role in lake ecosystems. They contribute to water purification, provide habitat for many species and protect against sediment movement and bank erosion (Ostendorp 1993a, 1993b, 1989). However, aquatic reed beds are threatened and their decline has already been documented (Hotes et al. 2005; Rücker et al. 1999; Grosser et al. 1997; van der Putten 1997; Krumscheid et al. 1989; Ostendorp 1989). Changes in water level, temperature alterations, overpopulation of water birds, leisure and tourism pressures, shore erosion, lake and river driftwood or solid waste, are some examples of stressors which are suspected of causing reed decline (Grosser et al. 1997). Standard procedures for monitoring the status of aquatic reed beds typically rely on physical field mapping, supported by visual interpretation of either orthophoto or stereo pairs of aerial photographs (Dienst et al. 2004; Schmieder et al. 2004; Ostendorp et al. 2003; Schmieder et al. 2002; Krumscheid et al. 1989). Based on these methodologies, dense reed beds can be routinely identified and quantified, but sparse aquatic reed stocks represent a challenge for these methodologies. A study at Lake Chiemsee in Germany revealed that spatial resolution of aerial imagery (spatial resolution lower than 20 cm) constrained the accurate identification and quantification of sparse aquatic reed stocks (Hoffmann and Zimmermann 2000). This study was based on official aerial photographs provided by the Bavarian State Survey (Landesamt für Digitalisierung, Breitband und Vermessung – LDBV). Survey objectives and logistic constraints do not allow data to be gathered all at once and within short timeframes. Therefore, any kind of vegetation is recorded in different phenological stages. Likewise, illumination conditions cause spectral differences of the same object to be recorded in different images. The extent of quantification and status assessment of aquatic reeds becomes inaccurate when using these official data sources and therefore this mapping methodology was supported with field work.

However, onsite inspection and manual imagery interpretation involve high personnel, time and financial efforts (Schmieder and Woithon 2004b) and depend on the experience of the interpreter. In this way, the frequency and quality of environmental monitoring is reduced by the accuracy of the results, and economic and time constraints.

The advances in Remote Sensing technologies may offer new opportunities in the monitoring of sparse aquatic reed beds. Photogrammetric measurements are applied to imagery obtained from platforms deployed in outer space, air, land and even in aquatic environments (Stratoulias et al. 2015b; Fernandes et al. 2013; Villa et al. 2015; Davranche et al. 2010; Dienst et al. 2004). Recent developments of low flying aerial systems provide a comparatively convenient alternative using close-range aerial imagery. Software performance, availability, and computing capacity of electronic devices has led to an incremental progress in remote sensing applications with Unmanned Aerial Vehicles (UAV) (Colomina and Molina 2014). Fixed Wing (FW) and Rotary Wing (RW) platforms are nowadays mostly deployed in close-range aerial photogrammetry (Colomina and Molina 2014).

Weaknesses and strengths of UAVs configured as FW and RW are commonly analysed in close-range aerial photogrammetry. Although both platforms can perform the same tasks, when executing missions the differences between them are remarkable. Fixed Wings are not as manoeuvrable as RW, but are more efficient since they only need energy to move forward and not to hold themselves up in the air. This results in longer flight times, and consequently in larger areal coverage (Long et al. 2016; Chen et al. 2015; Zarco-Tejada et al. 2014). Flight time endurance of RW is still a drawback and for bigger areas (>150 hectares) several flight missions have to be deployed (Tonkin et al. 2014; Neugirg et al. 2016). However, RW is more suitable when flying at lower altitudes, and it can better stabilize imaging systems and during the same flight can take photographs at different angles such as NADIR, high oblique, and/or low oblique (Clapuyt et al. 2016; Jaud et al. 2016).

One important factor in digital surface modelling is to have imagery of the same object taken at different angles. This contributes to more accurate feature extraction in a Structure from Motion (SfM) environment (Jensen and Mathews 2016). Stabilizing systems (gimbal) in RW allow camera angles to be readjusted when flying. Regarding FW, which are commonly built without gimbals, several missions in autopilot mode, but with different camera angles may have to be deployed. In close-range aerial photogrammetry missions, UAVs are deployed in autopilot mode. It requires less expertise and flight experience than manually controlling (Chen et al. 2015; Wiseman and Van Sluijs 2015; Harvey et al. 2016; Kršák et al. 2016), therefore is a common applied strategy for amateur operators. However, in monitoring aquatic reed beds the laborious and time-consuming tasks of landing, changing the camera angle, and launching the FW again poses a serious limitation to the operability. In order to make the recording of data more efficient and operable, UAVs deployed in manual mode could be an effective solution in aquatic reed feature extraction. Manual control of UAVs records imagery by default from different points of view and within the same flight, and good overlap is achieved by making several passes over the same area. However, this faces the question whether the quality of imagery collected by flying in manual mode is good enough for extracting heights of sparse aquatic reed beds.

The type of imaging sensor or camera system is essential in close-range UAVs missions. The quantity of picture elements (pixels), number of bits per pixel (colour depth), photon recording technology, and resolving power are some elements to be considered in the planning phase. Sharpness is also discussed

in the branch of close-range aerial photogrammetry. Sharpness not only depends on the number of effective pixels available, but also on the stabilizing technology, sensor resolving power and filtering, as well as demosaicing processes in camera sensors. For instance, sensors with a high quantity of small pixels deliver data at a higher resolution, but this compromises the colour depth. Sensors with very high resolutions are normally used in bigger cameras (e.g., Canon EOS 5DS, Nikon D810, Sony SLT Alpha 99 II). On the other hand, compact cameras (weight lower than 200 grams) are easier for use in FW (Jensen and Mathews 2016; Puliti et al. 2015; Cunliffe et al. 2016; Chen et al. 2015). Resolutions between 12 and 18 Megapixels (MP) are most commonly applied in close-range aerial photogrammetry. The recent development of mirrorless or system cameras with sensor such as APS-C, Four Thirds, Foveon X3 have been seen as the best trade-off between quality and weight (Zarco-Tejada et al. 2014; Uysal et al. 2015; Pérez-Ortiz et al. 2016).

Regarding the processing of recorded imagery, several methods have been applied for image alignment and their photogrammetric reconstruction. Bundle triangulation represents *'the most powerful and accurate method of image orientation and point determination in photogrammetry'* (Luhmann et al. 2014). In order to reconstruct an object in three dimensions, this method merges single images into an overall model by using tie points. The alignment process is executed by matching algorithms available in commercial and open source software. Agisoft Photoscan is one of the most applied computer programs for feature extraction by using SfM algorithms. Agisoft Photoscan is preferred mainly due to its ability to automatically generate data points in a specific coordinate system to represent the external surface of an object (point clouds) with a high degree of accuracy (Santoso et al. 2016), to calculate DEM and orthophoto in a specific coordinate system (Uysal et al. 2015), to better allocate resources (i.e., higher computational efficiency) (Cunliffe et al. 2016), its greater suitability to UAV image processing (Long et al. 2016), and for being user-friendly (Reshetyuk and Mårtensson 2016). The software offers several parameters for controlling image alignment. However, the information about suitable settings for alignment is limited and is normally derived by either trial and error approaches (Puliti et al. 2015), leaving the default values, or applying Agisoft Photoscan tutorials recommendations (Jaud et al. 2016). Finally, assessing the quality of the features extracted in form of a DEM process is of major importance within the photogrammetric modelling chain. There are several statistical approaches to assess the quality of derived models. In this context, standard deviation, linear regression, or root mean square error (RMSE) of residuals are examples of the most widely applied statistical tests or indicators. The RMSE is the square root of the arithmetic mean of the squares of a set of differences between the measured and expected observations (Luhmann et al. 2014). Comparisons of either DGPS/total station point surveying and generated DEM (Uysal et al. 2015; Cunliffe et al. 2016; Zarco-Tejada et al. 2014; Chen et al. 2015), LIDAR data and DEM (Tonkin et al. 2016; Clapuyt et al. 2016), total station, Point cloud and DEM (Wiseman and Van Sluijs 2015), or Terrestrial Laser Scanning (TLS) and DEM (Reshetyuk and Mårtensson 2016), are some examples how accuracies have been evaluated.

2.2.1. Objectives

Digital Elevation Models (DEM) derived from UAV imagery have been applied in different fields like geothermal monitoring (Harvey et al. 2016), erosion quantification (Neugirg et al. 2016), weed mapping for precision agriculture (Pérez-Ortiz et al. 2016), glaciers degradation (Tonkin et al. 2016), or open-pit mining features characterization (Chen et al. 2015). In the same way, UAVs have already been deployed for monitoring phenology changes based on spectral response and vegetation indexes (Venturi et al.

2016). Nevertheless, the implementation of UAVs for height extraction of sparse aquatic reed and its potential for extent quantification is still unknown.

In the monitoring aquatic reed beds, the quantification of extent is the most important variable to be considered. Its area of surface is obtained by calculating the vegetation coverage from shoreline to the expansion front seawards. The official shoreline determines the aquatic reed boundaries on the land side. Frontline is however harder to delimitate when analysing long-range optical imagery (Satellite or Aeroplane). Considering the change in elevation that occur in the frontline, heights obtained from DEMs may contribute to the delimitation of the break line between water surfaces and emerged vegetation (aquatic reed).

For a future extent quantification and characterization of sparse aquatic reed beds, the presented study focuses firstly on the question of whether close-range photogrammetry (imaging distance less than 300 m (Luhmann et al. 2014)) is capable of extraction height of sparse aquatic reed beds. The geometry of objects plays an important role in photogrammetry. For instance, a house with flat surfaces (roof and walls) would be easier to model in comparison to a bush (uneven structures). In addition, the geometry also changes if the object moves while is imaged. In this sense, the extraction of sparse aquatic reed beds faces the following challenges. First, *Phragmites australis* has an uneven geometry and is not a static object. Second, the problematic of reconstructing a RGB (Red, Green, Blue) image by imaging sensors when recording data from aquatic surfaces (e.g. sunglint). Third, the need of recording imagery rapidly and at different view angles. Fourth, there is little knowledge about the adequate parameters used for an accurate image alignment. Considering this, the core research questions addressed in this study are:

- Which parameters for image alignment allow point cloud calculation of sparse aquatic reed beds with the lowest Root Mean Square (RMS) reprojection error?
- How accurate is the estimated height in DEM of sparse aquatic reed beds, interpolated from point clouds photogrammetrically, and modelled with imagery collected with Fixed Wing (FW) and Rotary Wing (RW) UAVs?

2.3. *Material and Methods*

2.3.1. Study Area

Lake Chiemsee is located approximately 80 km southeast of Munich at an altitude of 518 meters above sea level (masl). Compared to much greater declines in other Bavarian lakes, reed beds at Lake Chiemsee have declined by approximately 50% within half a century (Grosser et al. 1997), which allows for the comparison of a wide range of stock densities with different spatial extent. Aquatic reed beds were defined as vegetation growing in permanently flooded areas (Ostendorp 1993b). First, reed stocks were identified in the field based on their extent and spatial distribution. According to the last reed inventory from 2000, the most representative stocks of aquatic reed beds can be found on the north-west side of Lake Chiemsee and at Herreninsel (Hoffmann and Zimmermann 2000). Second, field observations were further needed for selecting potential Areas of Interest (AOI). The description of sparse aquatic reeds defined in the last survey (Hoffmann and Zimmermann 2000) was the main criterion used for the random selection of AOIs. Sparse aquatic reed beds are characterized by sparse and parallel stripes along the reed bed edge (due to either floods, wind storms, or driftwood accumulation), a lane/aisle perpendicular to the shore (for docks, boot traffic, bathing, fish traps), the dissolution of reed beds

though decreasing stem density, frayed, ripped, not zoned reed edge and in single clumps (through erosion or flood), and seaward stubble fields of past reed beds (Hoffmann and Zimmermann 2000). Using the same methodology for photogrammetric reconstruction, imagery collected with the same imaging system mounted in two different close-range aircraft and deployed in manual flight mode contributed in reaching the goals of this study.

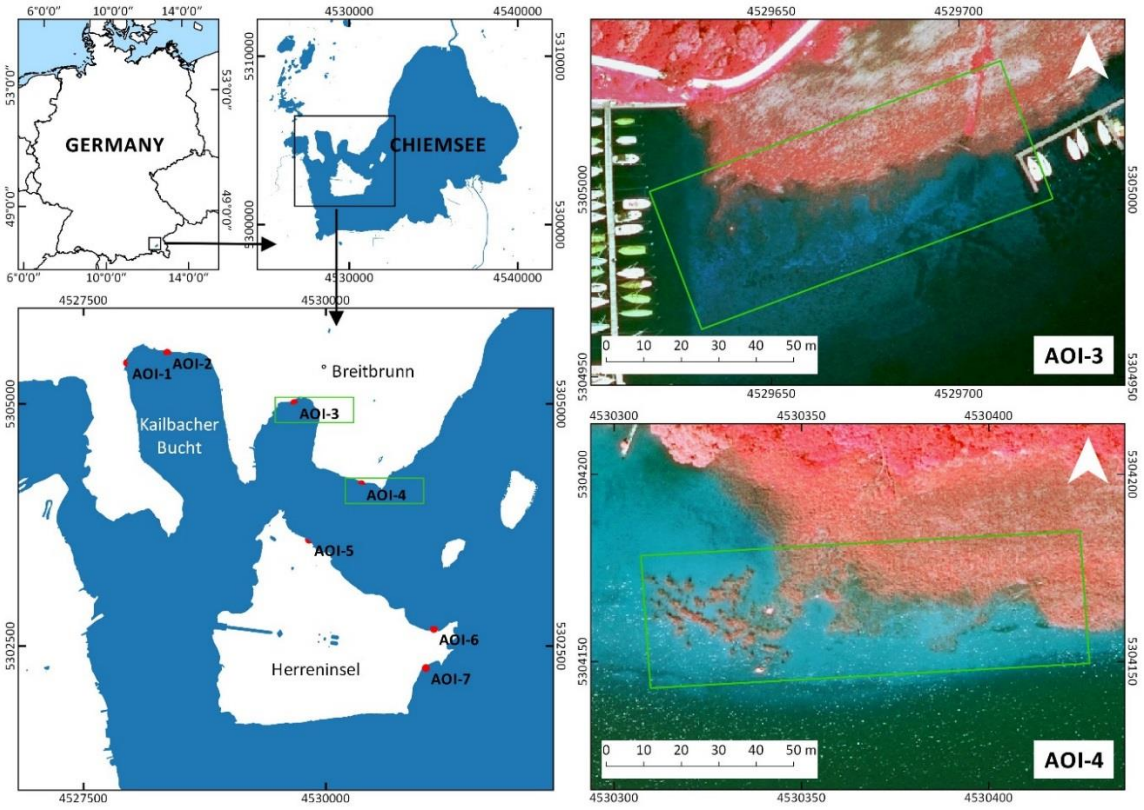

Figure 2.1 Location of study area in Germany and distribution of AOIs at Lake Chiemsee. AOI-3 and AOI-4 represent aquatic sparse reed beds. Background is an orthorectified aerial photograph in false colour (4,2,1) of the LDBV, 2015. Coordinate System is DHDN Gauss Krüger Zone 4 (EPSG 31468)

Seven AOI with a mean surface of 3000 m² (100 m long and 10-40 m width) each solely comprising *Phragmites australis* were selected. AOI-1 and -2 are located at Kailbacher Bucht, AOI-3 and -4 on the shores of town Breitbrunn, and AOI-5, -6, -7 at Herreninsel. Three of the AOIs were flown over with RW (AOI-2, -3, -7) and four with FW (AOI-1, -4, -5, -6) while testing different imaging strategies. In the following sections, the accuracies resulting from photogrammetric analysis of the two UAV systems are compared on behalf of AOI-3 (RW) and AOI-4 (FW) (Figure 2.1) in this study. Imagery from this two AOIs were registered with a short time difference under the same flight strategy and mostly similar illumination conditions.

2.3.2. UAVs configuration and data acquisition

For RW a hexacopter Tarot FY680 was used (Figure 2.2a). The power unit consisted of 6 brushless motors configured with 6 serial Lithium-Polymer (6S-LiPo) batteries (22.2 V, 10000 – 15000 mAh, 25C) enabled a flight time of up to 30 min, a maximum speed over 65 km/h, a climbing altitude over 400 m height and a payload up to 6.6 kg, while the 'Jeti Duplex' wireless allowed range of up to 1.5 km. With the integrated 'DJI Naza' flight controller, functions such as Altitude-Hold, Position-Hold, and Return-

to-Launch (RTL) were implemented. As a failsafe, the RTL and Landing were integrated in case of signal loss. Foldable landing skids were optimized for camera circumspection.

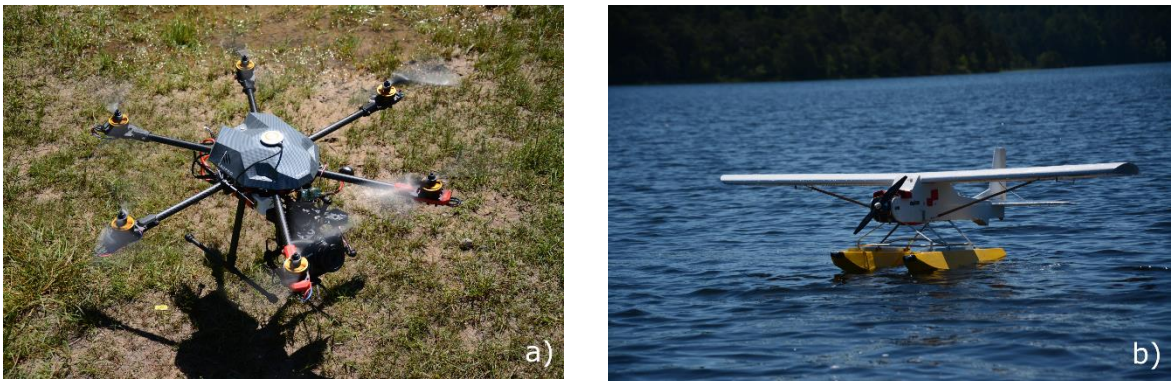

Figure 2.2 UAVs configuration deployed for the measurements campaigns. Tarot FY680 hexacopter (a) and a strongly modified Hype Trainer 70 (b)

The second platform was a strongly modified 'Hype Trainer 70' configured as FW (Figure 2.2b). Originally it was a classical wood constructed RC-Trainer with a wingspan of 1.9 m designated for a 70 cubic-inch methanol engine with take-off weight about 3.4 kg. It was modified to increase the payload up to 1.5 kg as well as to be able to fly in rough and wet conditions. The fuselage under the wings was heightened to allow integration of larger sensors (e.g., multispectral camera Mini MCA 6). Flaps were also integrated to ensure increased lift for short starts and landings with steep approaches as well as slow flight capabilities. A brushless outrunner engine in slow speed configuration (420 rpv) in combination with a high-end electric speed control was installed and the parameters RPM, voltage, amps, and temperature were retrieved in real time through telemetry. The drive was configured with LiPo batteries with a 6S configuration and 8000 mAh capacity, allowing for a flight time of over 40 minutes with an integrated payload of up to 1 kg. Additionally, two air scoops were installed to cool down the ESC without compromising its waterproof capability. The FW was manually controlled through a Jeti Duplex radio control system with a programmed fail-safe function in case of signal loss. Air control regulations in Upper Bavaria (Germany) in 2015 limited the weight of UAVs to five kilograms. Under this ordinance, the company Geodatenflug GmbH set up the UAVs and obtained the required flying permits.

A digital single lens Mirrorles (DSLM) camera was chosen for this study. The system camera CANON EOS-M is equipped with a Canon APS-C Sensor (18 MP – 4.3 µ pixel size – colour depth 22.1 bits). A small and lightweight 'Pancake' 22 mm (f1/2.0) lens was used (Canon EF-M Bayonet lock). With the given adapter, any Canon lens with EF/EF-S bayonet catch can be mounted (e.g., Canon 50 mm – f 1/1.8). However, all test flights confirmed that the 22mm 'Pancake' lens had the perfect angle of view for the given flight configurations and flight strategy, especially considering that it is equivalent to former analogue image format of the given APS-C Sensor with a 1:1.6 crop factor.

For the RW configuration, the DSLM camera was mounted on a two axis (pitch and roll) brushless gimbal to reduce image blur. This could not be implemented for the FW, due to the aircraft's closeness to the water surface. Integrating the camera into the fuselage and designing a flap which was able to open and close resolved this problem. Exposure time was chosen to 1/2000 and flight height (102 m) was calculated for a minimum mapping unit of 2 cm/pixel. All flights were manually controlled and directly piloted from the boat. The mean flying altitude was 48 and 146 meters for RW and FW UAVs

respectively. The flight strategy was chosen by considering the physical characteristics of sparse aquatic reed beds, the surrounding vegetation, and weather conditions. It was executed based on the view angle, and the resulting image blur by given airspeed, considering flight height, focal length, shutter speed, aperture and ISO parameters. In order to ensure strong overlap (greater than 80%), the AOIs were flown over several times (3 to 6 flights) and therefore multiple images were taken. The photographic camera was triggered by a PWM-IR (Pulse Width Modulation – InfraRed) adapter. Platforms were deployed under windless conditions and clear sky for avoiding exaggerated moving of reeds and adequate illumination during recording.

2.3.3. Verification Data Collection

The reference data was collected along cross sections and within square sample plots. First, a one-hundred meter line parallel to the shore was established. Every ten meters along this line, a measuring tape was placed perpendicular to it (cross sections). Measurements were recorded from water to shore line (i.e. where water and land have the same height). At every meter along the measuring tape, water depth and reed-stem height were measured to the nearest centimetre and decimetre, respectively (Figure 2.3). Since extraction of heights is based on images which have recorded stems in natural status (curved), the stem heights were measured with a 2 m long meter stick from lake bottom to highest point (e.g. curved stem or florescence). The obtained value was the average of stems within a square meter. Additionally, one square meter sample plots in dense and sparse reed beds were placed. The parameters measured were density (stems/m²), stem diameter, number of stems with and without shoots, as well as the number of green and dried (brown) stems.

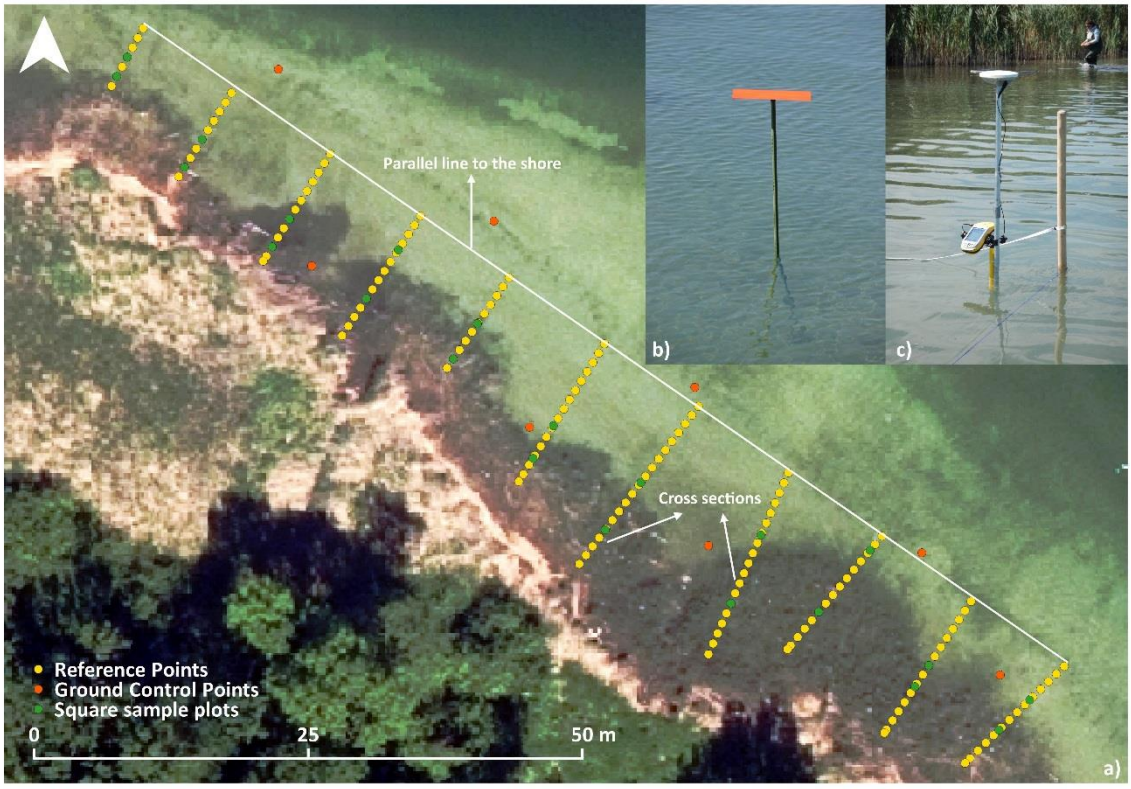

Figure 2.3 Reference Points (RP) and Ground Control Points (GCP) in AOI-5 a). Targets are coloured in fluorescent orange for georeferencing b). Measurement of cross-transects with a DGPS Trimble GTX

and an antenna Hurricane L1 c). Background is an orthorectified aerial photograph in true colour of the LDBV, 2015. Coordinate System is DHDN Gauss Krüger Zone 4 (EPSG 31468)

2.3.4. Photogrammetric Processing Chain

The photogrammetric process was performed with Agisoft Photoscan Professional - Version 1.2.6 (Agisoft LLC 2017). The 110 and 83 images of RW and FW respectively were loaded into Agisoft, and with the available tools, image quality was assessed and camera parameters were defined. In this study, settings parameters for image alignment were not chosen according to default values or trial and error procedures. Contrarily, the most suitable settings were obtained through several alignment tests based on a quality assessment according to the number of images aligned and RMS reprojection error. The maximum number of points Photoscan will extract from each photo (Key Point Limit – KPL) and the limit at which tie-points with the lower number of projections will be removed (Tie Point Limit – TPL) were then determined. The defined values for KPL and TPL, which led to a low RMS reprojection error and a higher number of aligned images, were then used for the final feature detection and image matching (i.e. build sparse point cloud). Outliers were removed based on the parameters offered in Photoscan; reprojection error (RE), reconstruction uncertainty (RU), and projection accuracy (PA). Consequently, the resulting sparse point cloud was georeferenced and finally the dense point cloud was reconstructed. After removing the outliers by manual editing, a dense point cloud was exported and the DEM and orthomosaics were generated (Figure 2.4).

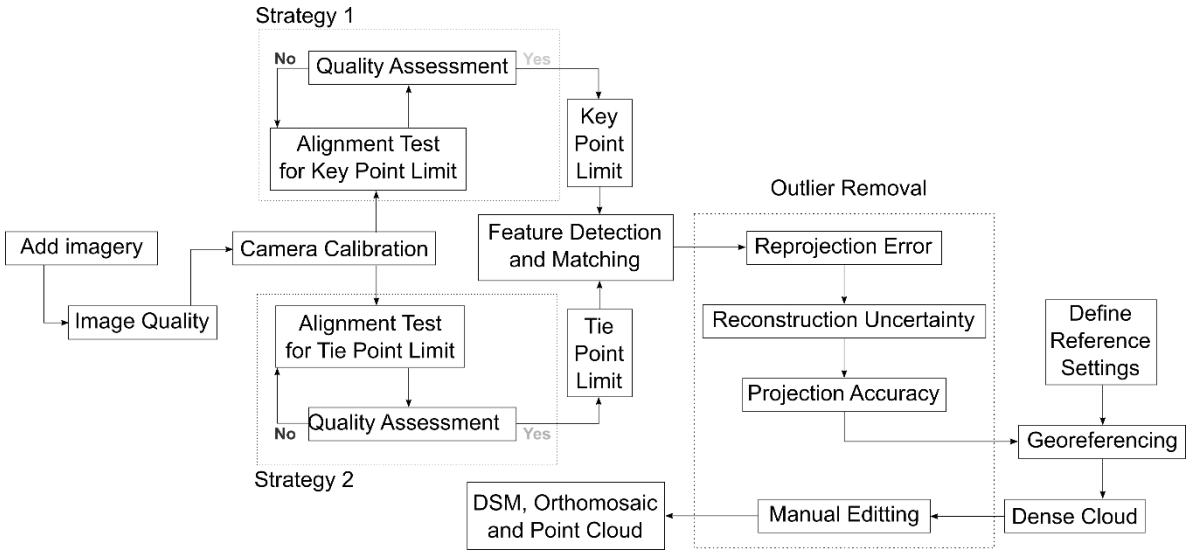

Figure 2.4 Photogrammetric processing chain applied for extracting of aquatic reed beds. Strategy 1 and 2 were applied to define Key and Tie Point Limits for image alignment with the lowest RMS reprojection error

Due to the requirements of 3D photogrammetric reconstruction, high quality images were selected. Photoscan supports a tool (Estimate Image Quality) to assess image quality. The closer to 1 the calculated coefficient value is, the sharper the image. Camera calibration parameters were extracted from EXIF (Exchangeable Image File) data (camera type, pixel size and focal length). Auto calibration was selected and fix calibration and GPS/INS Offset were disabled, since missions were executed in manual mode. The camera interior parameters were then estimated based on the focal length and pixel

size information. Camera positions were derived after first image alignment and according to the projections of every tie point.

To optimize reconstruction, general (accuracy and pair selection) and advanced (KPL, TPL, and adaptive camera model fitting) matching parameters were set. Highest accuracy was selected and pair selection was set to *'Generic'* because flight was executed in manual mode. The exact settings were chosen for RW and FW imagery. Activation of *'Adaptive Camera Model Fitting'* allowed the automatic calculation of interior parameters. This enables the automatic selection of camera parameters to be included in adjustments based on their reliability estimates.

The definition of values for KPL and TPL was accomplished by applying two strategies to FW and RW datasets. In Strategy-1 (S1), several alignments were executed, while always maintaining a TPL of 0 and progressively incrementing the value for KPL. In Strategy-2 (S2), the alignments were executed with a different TPL and a fixed KPL of 0. The first alignment executed in every dataset was always performed with a value of 0 for KPL and TPL. Consequently, at every alignment either the KPL (S1) or TPL (S2) were progressively incremented by a defined value. The changes in the values obtained for RMS reprojection error and the number of aligned images were used to define the threshold value that KPL or TPL should be incremented to before an alignment. When the RMS reprojection error did not change after several alignments, the tests were terminated. This point was inferred as the lowest RMS reprojection which can be obtained for a specific dataset. The set with the most number of images aligned and with the lowest RMS reprojection error were used to define the most appropriate KPL and TPL.

The next step in the photogrammetric processing chain was the removal of outliers in the sparse point cloud. Three criteria available in Agisoft were implemented to automatically select and remove outliers. First, Reprojection Error (RE) was selected and the threshold value was defined according to the obtained RMS reprojection error of the sparse point cloud for a FW or RW dataset. Second, Reconstruction Uncertainty (RU) was implemented to detect points reconstructed from nearby photos with a small baseline (high RU values). Third, projection accuracy (PA) was used to find the error of projection of a key point, which is directly proportional to the key point size. Points with RU and PA values greater than the 75% limit were removed. Detailed information about these criteria can be found in Photoscan's user manual (Agisoft LLC 2017).

GCPs collected before UAVs deployment were used for georeferencing point clouds. Physical characteristics (water and reeds) of AOIs hindered the placement of scale bars. Since the mean vertical accuracy of GCP in centimeters is 48.3 for AOI-3 and 36.4 for AOI-4, a value of 40 and 30 centimeters was set in the marker accuracy of the reference settings in Photoscan. As with the RP and GCP, the coordinate system used was DHDN Gauss Krüger Zone 4 (EPSG 31468). A dense point cloud was then computed using the highest quality available, '*Ultra High'*, and with a depth filtering of '*Mild'* (Agisoft LLC 2017). More features of aquatic reed beds can be modelled when selecting the highest quality. Depth filtering contributed to obtaining points where reed stems are sparse, without removing either important points or generating a large number of outliers. Evident points outside the reconstructed aquatic reed beds (outliers higher than 4 meters and lower than -0.5 meters) were then manually removed (manual editing option offered by Agisoft). Finally, a DEM and orthophotos were generated.

2.3.5. Assessment of vertical accuracy

Vertical accuracy assessment of the resulting DEM was undertaken based on two analyses. First, the onsite measured height values from a flat surface (dock) were compared to the modelled ones. Second, the height values corresponding to reed stems were compared with those of the RP collected at each AOI (Section 2.3.3). These two analysis were implemented to define any displacement in the Z axis (height). If residuals were normally distributed and most of the outliers were removed, three separate quantitative analyses were implemented (Table 2.1). Through these statistics, the closeness agreement between the independently observed and expected measurements from the extracted point cloud and DEM were evaluated. In order to know if the residuals were normally distributed, sample skewness and its significance was calculated.

Table 2.1 Accuracy measures for DEMs presenting normal distribution of errors

Mean Error	$\mu = \frac{1}{n}\sum_{i=1}^{n} \Delta h_i$	(Höhle and Höhle 2009)
Standard Deviation	$\sigma = \sqrt{\frac{1}{(n-1)}\sum_{i=1}^{n} (\Delta h_i - \mu)^2}$	(Höhle and Höhle 2009)
Root Mean Square Error	$\mathrm{RMSE} = \sqrt{\frac{1}{n}\sum_{i=1}^{n} \Delta h_i^2}$	(Höhle and Höhle 2009; Luhmann et al. 2014)

n is the number of tested points in the sample (sample size) and Δh_i represents the difference between RP and DEM for a point i.

The relative stem height (RSH) of the reed was used to assess vertical accuracy. The absolute height of aquatic reed beds was defined as the measured length from top (reed flower) to bottom (ground). RSH was calculated by subtracting stem height (absolute height) minus water depth at every RP measured. The absolute altitude of the water surface on the day of measurement was obtained from the water level gauge Stock-Prien in the Chiemsee. The absolute height of the water surface during imaging was 517.19 meters above sea level. This value was used to obtain the RSH from the calculated DEM.

2.4. Results

2.4.1. Alignments of RW and FW imagery

Alignments were executed for imagery with coefficient values greater than 0.82 (RW) and 0.7 (FW) resulting in 110 (AOI-3) and 83 (AOI-4) images, respectively. After analysing processing times and reprojection errors in units of tie point scale for this selection of imagery, the most suitable value determined for alignment test was 10000 for KPL in S1 and 2000 for TPL in S2. Using these settings, a total of 54 alignments for RW and 99 for FW were conducted until the lowest reprojection error was obtained. It was identified that even in extreme cases where only reed beds were recorded by the imaging system, the implemented matching algorithm in Agisoft was able to define tie points. With respect to the amount of images aligned, the KPL allowed a greater image match. For RW imagery, a

KPL higher than 100000 aligned all the possible iamges (105) as well as a KPL higher than 510000 for FW imagery (78 images aligned) (Figure 2.5).

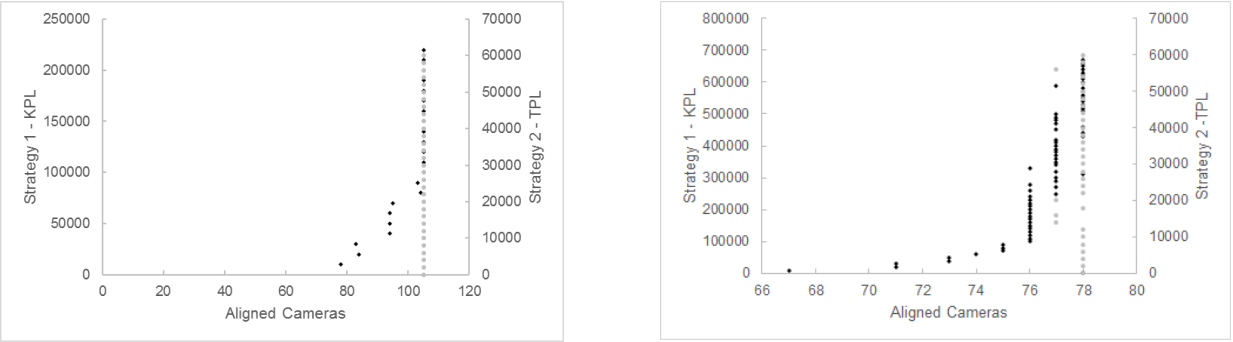

Figure 2.5 Aligned cameras (images) results from the alignment tests of imagery obtained with RW (left) and FW (right) UAV. Black points represent to S1-KPL and grey points to S2-TPL

The RMS reprojection errors in the sparse point cloud from RW and FW decreased similarly when incrementing the KPL and TPL. Regarding RW, RMS reprojection error slightly increased with higher KPL and decreased with higher TPL, from 0.19 RMS at 10000 KPL and 0.25 RMS at 2000 TPL to 0.19 RMS at 220000 KPL and 0.19 RMS at 60000 TPL (Figure 2.6). Although the deviation at a lower KPL and TPL was not as high as with RW imagery, the same occurred when using data collected with FW. RMS reprojection error decreased with higher KPL and TPL, from 0.16 RMS at 10000 KPL and 0.20 RMS at 2000 TPL to 0.16 RMS at 670000 KPL and 0.16 RMS at 60000 TPL. The RMS reprojection error reached a minimum point from which no matter how high KPL or TPL was, the matching algorithm could not reduce the error by finding more key and tie points. This point was at 160000 KPL and 46000 TPL for RW and 540000 KPL and 46000 TPL for FW. The lowest RMS reprojection error for RW was obtained at KPL 170000 and 58000 TPL and at 310000 KPL and 34000 TPL for FW (Table 2.2).

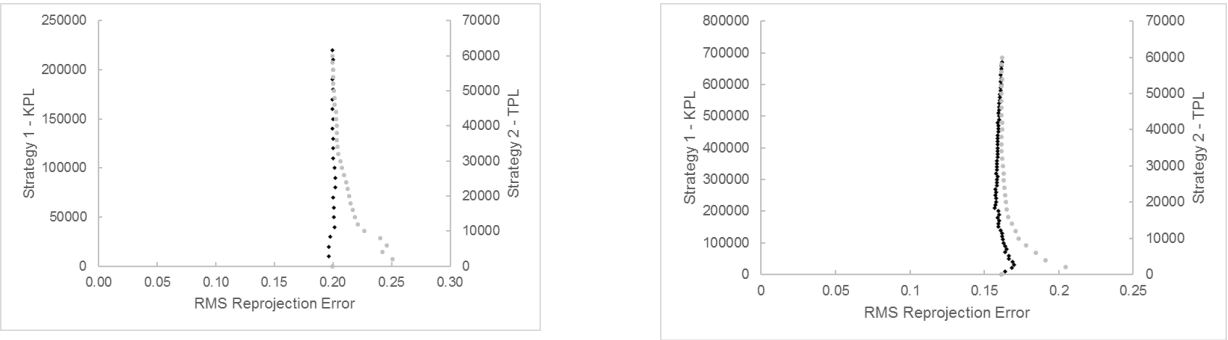

Figure 2.6 RMS reprojection error results from the alignment tests of imagery obtained with RW (left) and FW (right) UAV. Black points represent to S1-KPL and grey points to S2-TPL

Effective overlap showed the average number of projections for each of the used and unused tie points in the sparse cloud. Considering that KPL is the maximum number of points that the algorithm extracts from each photo, and that TPL sets the limit at which tie-points with the lower number of projection will be removed, the effective overlap in FW and RW imagery was augmented when KPL increased and decreased with a higher TPL. As with the RMS reprojection error, effective overlap neither decreased nor increased from an equilibrium point. This was found at 100000 KPL and 38000 TPL for RW data (effective overlap 3.39), and at 590000 KPL and 30000 TPL for FW data (effective overlap 2.68) (Figure 2.7).

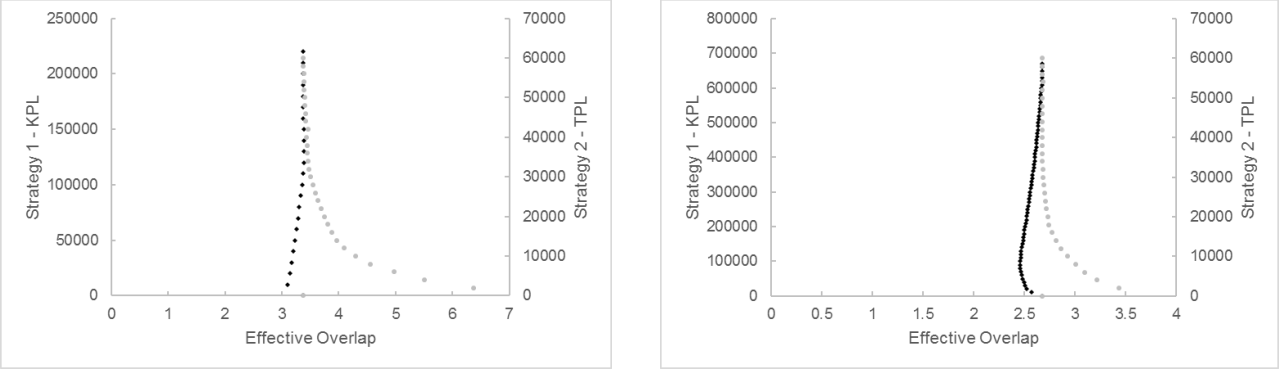

Figure 2.7 Effective overlap results from the alignment tests of imagery obtained with RW (left) and FW (right) UAV. Black points represent to S1-KPL and grey points to S2-TPL

RW imagery with the lowest RMS reprojection error was aligned with a KPL of 170000 and TPL of 58000. Small deviations were also obtained in the final alignment of imagery taken with the RW platform. Out of 110 photos, 105 were aligned and a lower RMS reprojection error was obtained (0.19). The average number of projections for each used and unused tie point in the sparse cloud (effective overlap) remained at approximately three for every alignment (Table 2.2). Gradual selection and manual removal of outliers contributed to the decline of RMS reprojection error in the sparse point cloud (0.10 RW and 0.08 FW). After outlier removal, the final sparse clouds had 328377 and 97842 points for RW and FW alignments, respectively. The imagery obtained from the FW was best aligned with combination values of 310000 and 34000 for KPL and TPL, respectively. With the selected KPL, a total of 78 out of 83 images were aligned. Compared to the number of points obtained from the best clouds computed with S1 and S2, the deviation of the statistic measurements of the final sparse point cloud was small (Table 2.2). The KPL and TPL combination contributed in the same way to a lower RMS reprojection error. Mean key point size and effective overlap were also examined and similarly, no big deviations were found. The processing time for the final photo alignment increased to approximately 1.6 minutes.

Table 2.2 Description values for bests alignments obtained in Strategy 1, Strategy 2 and final photo alignment. RMS reprojection error is given in units of tie point scale

	Best alignments in S1		Best alignments in S2		Final photo alignment	
	RW	FW	RW	FW	RW	FW
Key Point Limit	170000	310000	0	0	170000	310000
Tie Point Limit	0	0	58000	34000	58000	34000
Aligned Cameras	105 of 110	78 of 83	105 of 110	78 of 83	105 of 110	78 of 83
Points	568381	158592	568360	245158	568209	157968
RMS reprojection error	0.19	0.15	0.19	0.16	0.19	0.15
Effective overlap	3.38	2.56	3.38	2.67	3.38	2.56
Processing Time [min]	53.3	49.85	52.9	107.65	53.15	51.45

In addition to point cloud statistical measurements, photo alignments also revealed differences in the adjusted imaging sensor characteristics. Although the same imaging system was implemented in both UAVs, the derived interior parameters were not the same when the adaptive camera model fitting was applied. Strong deviations were found in the principal point coordinates and radial distortions in the final photo alignment. For principal point coordinates Cx and Cy respectively, 11.21 and -27.59 was

adjusted for the camera mounted on the RW and 6.46 and -3.91 for FW. For k1, k2, k3, k4, the obtained radial distortion coefficients of the RW-camera were -0.007, 0.02, -0.06, 0, and -9.41e-05, -0.0004, 0, 0 for the FW-camera, respectively. Differences in the tangential distortions coefficients were not significant.

2.4.2. Vertical Accuracy of DEMs

Digital Surface Models were created by means of interpolation of dense point clouds, which for RW and FW consisted of a total of 18471606 and 12580569 points, respectively. A higher resolution of 2.10 cm/pxl was obtained with RW data and 2.86 cm/pxl for FW. With a mean absolute height of 519.19 meters, the height of the selected flat surface was accurately estimated with a RMSE of 0.04, mean error of 0.04 and a standard deviation of 0.007 meters. Sample skewness proved that residuals of both DEMs were normally distributed. Residuals of RW were lowly (-0.02) and of FW moderately skewed (-0.66). The distributions were not significantly skewed, since two times the standard error of the skewness ($SES = \sqrt{6/n}$) is 0.53 (RW) and 0.44 (FW). Residuals showed that in sparse aquatic reed beds, they are of a higher magnitude (greater than 54 and 88 cm for RW and FW, respectively). The statistical analysis showed that the RW-DEM was more accurate than the FW-DEM. A total of 85 independent RPs were used to assess the accuracy of RW-DEM and 120 for the FW-DEM. RPs were distributed along transects as seen in Figure 2.3. The generated RW-DEM had a mean error of 0.76 m and a RMSE of 1.05 m. The FW imagery produced the less accurate results, with a mean error of 1.01 m and a RMSE of 1.42 m. The analysis of heights obtained from the derivation of DEMs revealed that sparse aquatic reed beds and the seaward frontline can be delimited. Height of reeds and the variation of height per unit of surface would contribute to the determination of the areas corresponding to reeds with a dense or a sparse status (Figure 2.8).

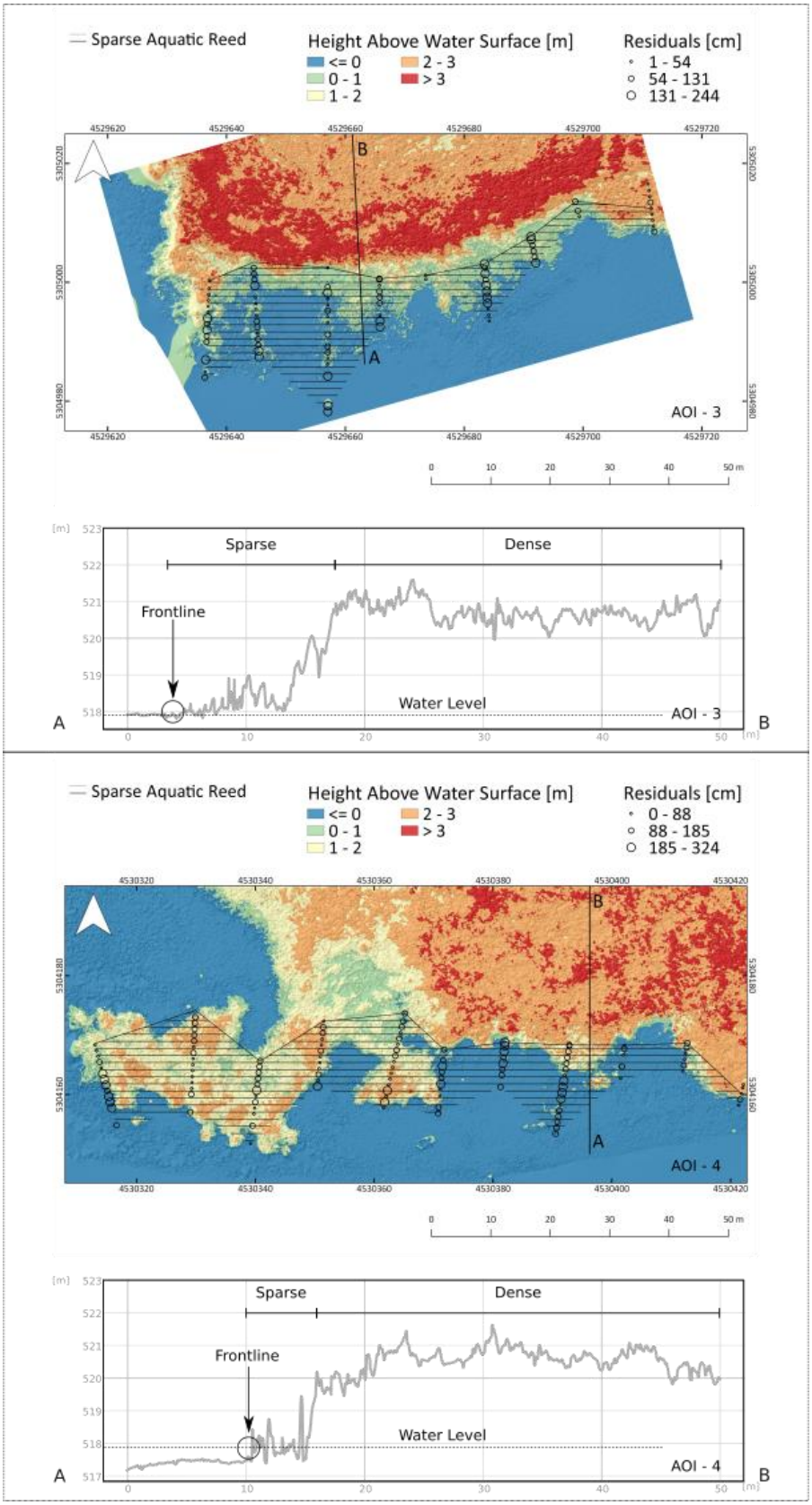

Figure 2.8 Spatial distribution of residuals in DEMs for AOI-3 (top) and AOI-4 (bottom). Example of two cross sections obtained from DEM derived from RW and FW imagery. The "Y" axis represents the absolute height in meters

2.5. *Discussion*

The results of this study suggest that close-range aerial photogrammetry is a powerful method for extent quantification of aquatic reed beds, especially in sparse populations. The proposed technical solution is in line with previous research focused on the study of wetlands or specific plant populations by means of remote sensing methods (Bourgeau-Chavez et al. 2015; Villa et al. 2013; Venturi et al. 2016; Marcaccio et al. 2015). By constructing and validating two DEMs derived from imagery recorded by two different UAVs but with the same imaging system, we assessed the accuracy of the UAV-SfM (Structure from Motion) workflow aimed at extracting heights of sparse aquatic reed beds. Fundamental for future monitoring projects, in this study we were able to determine adequate parameter settings for feature extraction with the lowest RMS reprojection error and with the highest number of images aligned, to model sparse aquatic reed beds with UAVs deployed in manual flight mode.

2.5.1. Alignments of RW and FW oblique imagery

Regarding of sparse aquatic reed beds, Structure from Motion procedures were able to align imagery independent of the flight strategy and camera angle. Compared to photogrammetric missions executed in autopilot mode and in NADIR (Jensen and Mathews 2016; Clapuyt et al. 2016; Wiseman and Van Sluijs 2015; Neugirg et al. 2016; Chen et al. 2015; Pérez-Ortiz et al. 2016), matching algorithms also allowed the feature extraction in oblique imagery collected manual mode. The availability of large features (e.g. houses, streets, docks) were seen as the key factor for detecting key points. The higher the altitude at which a UAV is deployed, the lower the spatial resolution, but the higher the availability of features for image alignment. This finding was supported by the RMS reprojection error calculated in Photoscan. Available information on the internal computing and matching algorithms applied by Agisoft Photoscan is very rare (Remondino et al. 2014; Santise et al. 2014). For matching and point extraction, it seems that a stereo SGM-like (Semi Global Matching) method is implemented as an image-matching algorithm (Remondino et al. 2014). Furthermore, it is mentioned that a SIFT-like (Scale Invariant Feature Transform) algorithm is applied, which solves for interior and exterior orientation parameters *'using a greedy algorithm followed by a more traditional bundle adjustment refinement'* (Santise et al. 2014). The photo alignment achieved with data from the RW aircraft had a higher RMS reprojection error (0.19) than the one obtained with FW data (0.15). In relation to the aligned images, RMS reprojection error, and effective overlap, the results obtained from the alignment test indicated that definition of KPL and TPL is crucial. In a world of images taken from a non-fixed and non-geometric object (aquatic reed beds) with variation in flight heights and camera angles, it is very important to limit the amount of valid and invalid matching points through the selection of KPL and TPL. Additionally, image alignment also revealed that photogrammetrically it is not strictly necessary to deploy UAVs in autopilot mode for collecting imagery. This result proves that imaging with UAVs can be deployed onsite regardless an automatic flight plan to support terrestrial monitoring without compromising the accuracy of the results.

2.5.2. Validation of heights estimated from DEM

The photogrammetric processing chain proved to be suitable in the digital surface modelling of sparse aquatic reed beds. Deviations in modelled vegetation heights are of a high magnitude compared to the ones calculated for flat surfaces, which can be explained mainly by three reasons. First, the physical

characteristics of the study object may have influenced the photogrammetric reconstruction. *Phragmites australis* moves easily even when small breezes occur or if the surf changes. This effect is greater in stocks where reeds are sparse. Error in the parallax caused by stem movements during data collection was observed as the source for the observed local disturbance of the bundle adjustment. Second, water surfaces have also been an obstacle in the photogrammetric reconstruction of aquatic reeds. Bright surfaces, random sunglint effects, and the constant surf cause wrong projections and therefore errors in the extraction of features. To avoid error during the photogrammetry process, (Long et al. 2016) it is proposed to mask these surfaces. However, this solution cannot be applied for sparse aquatic reed beds because there is the need to detect single stems growing sparsely in the lacustrine environment. This can be seen in the analysis of residuals and its spatial distribution (Figure 2.8). Third, the automatic removal of outliers could have eliminated points corresponding to aquatic reeds and consequently cause deviations in the heights represented in the DEM. Nevertheless, it is important to mention that matching algorithms and depth maps were sensitive enough to extract most of these features in sparse aquatic reed beds.

Flat, stable, and geometrical surfaces showed high agreement with the ones measured onsite (RMSE = 0.04 meters). In the same way, other studies have shown very low RMSE when validating flat surfaces (Uysal et al. 2015) and even with the same DGPS (Clapuyt et al. 2016, p. 6). When validating DEMs based on vegetation heights, a study where olive trees ranging in height from 1.16 to 4.38 meters (similar to aquatic reed heights) obtained high deviations as well (Zarco-Tejada et al. 2014). The estimation error of 0.35 meters (RMSE) was attributed to the method in which quantification was based on relative heights (Zarco-Tejada et al. 2014). Since height deviations in geometrical structures are of a lower magnitude than vegetation ones, assumptions about the limited accuracy of DGPS can be rejected. This suggests that it is not advisable to validate DEMs based on modelled vegetation heights.

2.5.3. Performance of UAV and camera systems

The quality to weight ratio of the mirrorless and interchangeable lens camera used in this study contributed to flight efficiency and photogrammetric modelling. Shot-to-shot cycle times in the Canon EOS M's in single-shot mode appeared to be slow for this study's purposes. For large/fine JPEGs, the cycle time was 1.94 seconds, 2.02 seconds for RAW mode, and 2.33 seconds for RAW + L/F JPEGs. This restriction affected data collection with FW more than with RW. Both UAVs were operated at the lowest possible flying speed to compensate for the slow cycle time. Increasing the flying altitude could have also contributed, but this would have compromised the spatial resolution. Since a spatial resolution of 2 cm/pixel was the minimum accepted value for mapping sparse aquatic reed beds, a higher altitude for compensating shutter sequence was not an option. Therefore, data acquisition with higher image overlaps would not be a problem for FW as long as the shot-to-shot cycle time is fast enough.

Within the bundle adjustment, the oblique images help the estimation of interior and exterior parameters (Cunliffe et al. 2016). It seemed that an accurate estimation of such parameters would depend on features to be extracted. The extraction of geometrical features (houses, docks, cars) gave a more precise estimate of interior parameters than irregular features (vegetation). Adjusted interior parameters obtained in this study after aligning RW and FW data confirmed this fact, but also spoke to the importance of image sharpness. Derivation of camera interior parameters by means of bundle triangulation is apparently possible with very high quality imagery and clear features for tie point

extraction. Among others, data with variable image blur, pixel resolution, low radiometric quality, shadows, and shiny or textured objects interfere in the accurate derivation of principal point coordinates, radial and tangential distortions. These factors are known to contribute to a noisy point cloud and difficulties in feature extraction (Remondino et al. 2014). Although the quality of RW imagery was good enough to approximate to the real camera interior parameters, calibration by capturing aquatic reed according to the obtained results is not recommended.

The presented study exhibited greater accuracy in height determination of RW and to FW for monitoring sparse aquatic reed beds. A RW in the form of a hexacopter delivered sharper imagery and consequently more accurate DEMs. It was more manoeuvrable and appropriate to areas where aquatic reeds are surrounded by tall vegetation (trees). Although not needed in this study, the greater payload allows for carrying of heavier imaging systems. The only detected disadvantage in the platform developed was the inability to land on water. On the other hand, FW allowed for coverage of much larger areas. This might be a decisive factor with regard to an operational application because delivering more stable results with regard to illumination conditions and at a better cost/area ratio are very important criteria for system selection. Close-range aerial photogrammetry offers new alternatives for small offices oriented in ecological mapping. Whether regular monitoring of small areas is requested and where entering the study area is not possible or can disturb the sensitive ecological zones, the presented methodology proved to be accurate and effective.

2.5.4. UAV and alternative data for height extraction of sparse aquatic reed beds

Structure from Motion algorithms have proved to be efficient in the extraction of features. Photogrammetry applied in UAV or satellite imagery, as well as Light Detection and Raging (LiDAR) are both valuable methods for 3D modelling. Point clouds produced out of these sources have different characteristics, since the recording method and output data differ. In vegetation stands, data along vertical structure can be obtained by LiDAR scanners (Corti Meneses et al. 2017; Zlinszky et al. 2014). Pulses of light emitted by LiDAR sensors pass through vegetation stands allowing the scanning of features. Differently, Structure from Motion (SfM) point clouds from either UAV or satellite imagery are derived by photogrammetric methods and only the recorded features on imagery are extracted (Mohan et al. 2017; Forsmoo et al. 2018; Chen et al. 2017). The detection and mapping of sparse aquatic reed beds strongly depends on the spatial resolution of data. The number of points per unit of surface gives the spatial resolution of point clouds. In the case of LiDAR scanners, the higher is the laser repetition rate, the more the features (points) for one scan are. In order to increase the number of points, a common practice with LiDAR systems is to execute several scans. Point density of SfM clouds is given by the pixel size of the optical imagery used for extracting features. Since more objects can be seen in very high spatial resolution images, higher number of matching points are detected and therefore more features can be extracted (points). Taking into account that reed stems and leaves have a mean diameter of 2 cm, single individuals distributed in shallow waters possibly cannot be extracted in imagery with spatial resolutions smaller than 0.5 m. This could also be case for airborne LiDAR, which a single stem cannot be scanned if the sensor is located around 400 m above ground and scanning with footprints of approximately 0.5 m (depending of laser beam divergence). As proven in this research, close-range aerial photogrammetry, which provides high density point clouds (e.g. 2260 points/m² in this study) from imagery with pixel resolutions higher than 3 cm is a suitable methodology for mapping sparse

aquatic reed beds. Besides its 3D-modelling effectivity, this is also a low-cost tool (Westoby et al. 2012), making it accessible for small companies working in vegetation mapping or environmental monitoring.

2.6. Conclusions

The presented methodology allowed for accurate and efficient feature extraction of aquatic reed beds; an advantage compared to previously applied methods. Based on data taken with the same imaging system, efficiency of Rotary Wing (RW) and Fixed Wing (FW) platforms in capturing high quality data for extraction heights of sparse aquatic reed beds was evident. Image alignment tests were essential in the extracting of sparse aquatic reed beds. Recording imagery in manual flight mode was not an obstacle in the feature extraction for bundle adjustment algorithms. The determined values for image alignment with the lowest RMS reprojection error were KPL 170000 and TPL 58000, and KPL 310000 and TPL 34000 for RW and FW, respectively. Accuracy assessments revealed the agreement of calculated DEM (RMSE = 0.04 m). Both UAVs proved principal applicability for monitoring purposes. FW flew over larger areas and its adaptation for starting and landing on water surfaces was a comparative advantage. DEM derived from RW imagery was more accurate when validating reed heights (RMSE = 1.05 m) due to sharper and higher spatial resolution imagery. Not considering the type of platform, sparse aquatic red beds were detected and accurate extraction was possible using photogrammetric methods. Results proved that sparse and dense aquatic reed beds, as well as frontline can be identified by analysing heights variations. However, density classification and surface quantification was beyond the scope of this study. The employed system camera proved to be a good compromise between image quality and weight. These results advance the knowledge of the application of UAVs for height extraction and therefore delivering more information for a more adequate and accurate aquatic reed monitoring

3. Quantification of Extent, Density and Status of Aquatic Reed Beds Using Point Clouds derived from UAV-RGB Imagery

A similar version of this chapter was published: Meneses, Nicolás Corti; Brunner, Flo; Baier, Simon; Geist, Juergen; Schneider, Thomas (2018): Quantification of Extent, Density and Status of Aquatic Reed Beds Using Point Clouds derived from UAV-RGB Imagery. In *Remote Sensing* 10 (12), p. 1869. DOI: 10.3390/rs10121869.

3.1. Abstract

Quantification of reed coverage and vegetation status is fundamental for monitoring and developing lake conservation strategies. The applicability of Unmanned Aerial Vehicles (UAV) three-dimensional data (point clouds) for status evaluation was investigated. This study focused on mapping extent, density, and vegetation status of aquatic reed beds. Point clouds were calculated with Structure from Motion (SfM) algorithms in aerial imagery recorded with Rotary Wing (RW) and Fixed Wing (FW) UAV. Extent was quantified by measuring the surface between frontline and shoreline. Density classification was based on point geometry (height and height variance) in point clouds. Spectral information per point was used for calculating a vegetation index, used as indicator for vegetation vitality. Status was achieved by combining data on density, vitality and frontline shape outputs. Field observations in areas of interest (AOI) and optical imagery were used for reference and validation purposes. A root mean square error (RMSE) of 1.58 m to 3.62 m for cross sections from field measurements and classification was achieved for extent map. The overall accuracy (OA) acquired for density classification was 88.6 % (Kappa = 0.8). The OA for status classification of 83.3 % (Kappa = 0.7) was reached by comparison with field measurements complemented by secondary RGB data visual assessments. The research shows that complex transitional zones (water-vegetation-land) can be assessed and support the suitability of the applied method providing new strategies for monitoring aquatic reed bed using low-cost UAV imagery.

3.2. Introduction

The Reed beds located in freshwater lakes around shores can be categorized in three ecological zones. Land, transitional and aquatic reeds have been mapped according to the lake's water level. Land reed grows in rarely flooded areas, has a lower stem density and height compared to the transitional reed, and is a stand mixed with other species (e.g. *Thypa, Scripus, Carex*). Transitional reed is flooded periodically and has the highest stem density and height. Between aquatic and transitional reed a significant break in height can often be noticed. Aquatic reed stands in water throughout the year and forms the reed expansion front, representing the boundary to the lakeside. It is the most sensitive area in a reed stock and under favourable conditions, it is able to develop further rhizomes and spread seaward. Aquatic reed is characterized by a lower stem density and a lower height. Aquatic reed, as well as transitional reed, are normally pure stands consisting of *Phragmites australis* (Grosser et al. 1997).

Aquatic reed beds play an important role in lake systems that can be linked to ecosystem services. They stabilize and protect the shores from erosion reducing waves energy with its dense root system and stems distribution (Rolletschek 1999). They support in the assimilation of nutrients, which is fundamental for the balance of nitrogen, phosphorus and silicon (Struyf et al. 2007; Mitsch et al. 2012).

Reed beds also function as habitat and nurture supply. The reed is decomposed by fungi and bacteria and constitutes nutrients for detritus and grazers, which are eaten by insects, toad bugs and omnivore water birds. The undisturbed aquatic reed and the reduced wave energy makes it a preferred site for the spawning of fish, reptiles and amphibians. Regarding of cultural ecosystem services, reed beds belong to the dominating elements of a pictorial landscape (Grosser et al. 1997). Growing at lakes shores, they are associated with near-natural landscape, which is considered as an important aspect for recreation (Holsten et al. 2013).

Decline of aquatic reed beds in central Europe during the last decades has already been documented (Dienst et al. 2004; Ostendorp 1989; Nechwatal et al. 2008). Suggested reasons for decline include direct destruction by land expansion, recreational traffic and summer mowing, mechanical destruction by waves, rubbish or driftwood. Further identified potential decline causes are the grazing by waterfowl and other animals (e.g. gray goose, swans, black coot, muskrat, nutria and grass carp) and domestic animals (e.g. cows and horses), and the degradation of the water and sediment quality caused by eutrophication (Ostendorp 1989). An increment in the frequency and severity of extreme events such as floods and drought is predicted (Erwin 2009; Vincent 2009). Changes in water regimes producing very low to extreme high water levels are also suspected to decline aquatic reed populations.

In order to monitor and develop adequate protection and conservation strategies, quantification of aquatic reed coverage and its status is fundamental. Aquatic reed extent is calculated by measuring the area between the shore and frontline. The shoreline is the boundary where water surface and land have the same height. The frontline is the limit at which the aquatic reed expansion front finishes seaward and its sinuosity can also be used as indicator for assessing status. Different approaches to describe a reed bed condition are available. Data collected in field such as stem density (number of stems per m^2), the percentage of panicle bearing shoots, or stem height are indicators of vitality (Ostendorp 1993a; Poulin et al. 2010). The collection of plant morphologic and phenotypical traits on field represents a traditional method for characterizing a reed stock. This type of collected data might deliver precise information but it is time and personnel consuming. Additionally, it causes a habitat disturbance and it is often not possible to access the high dense stocks (Schmieder and Woithon 2004a). Field observations have been supported by remote sensing methods, in which aquatic reed was conventionally mapped by manual visual interpretation and manual delineation of images recorded from satellite or airplanes (Dienst et al. 2004; Schmieder and Woithon 2004a; Samiappan et al. 2016). This is also truth for historical monitoring at lake Chiemsee in which aquatic reed beds were quantified through the analysis of aerial imagery provided by the state office for surveying "Landesamt für Digitalisierung, Breitband und Vermessung". Accurate allocation of the frontline and density quantification was however restricted by spatial resolution and variation in spectral information due to different collecting times (Hoffmann and Zimmermann 2000).

Emerging remote sensing technologies such as hyperspectral sensors, light detection and ranging (LiDAR), and Unmanned Aerial Vehicles (UAV) offer new possibilities in the monitoring of aquatic reed beds. Most common in vegetation analysis are optical systems registering the spectral reflectance of surfaces (Onojeghuo and Blackburn 2011; Poulin et al. 2010; Schmieder and Woithon 2004a; Villa et al. 2013). However, the reflectance is only recorded from the upper surface of objects missing valuable information from lower structures (e.g. under storey) in a vegetation stand. LiDAR data delivers information in three dimensions (point clouds), which supports a better characterization of vegetation

structure and also without habitat disturbance (Corti Meneses et al. 2017; Zlinszky et al. 2012; Onojeghuo and Blackburn 2011). Although the intensity of laser can be used for classification purposes, LiDAR lacks of spectral information characteristic of optical data. An alternative to produce 3D data with spectral information is by close-range aerial photogrammetry. Technological advances improve the performance of UAVs, being capable of flying longer, auto piloted, and carrying heavier loads. A wide range of instruments have already been tested on UAVs such as visible band, near-infrared, or multispectral cameras, as well as thermal cameras and laser scanners (Colomina and Molina 2014). For instance, UAVs equipped with VNIR and thermal sensors record data at decimetre or centimetre spatial resolutions for more accurate monitoring and stress characterization, which represents "a capacity unavailable from satellite based systems" (McCabe et al. 2016).

Optical imagery collected with UAV can be photogrammetrically processed for the generation of 3D information. The development of automated computer vision technique structure from motion (SfM) facilitates the remote sensing of structural and spectral characteristics of vegetation with UAVs (Dandois et al. 2017). It enables a high-resolution three-dimensional observation of the vegetation canopy structure by matching overlapped images and generating three-dimensional models (Westoby et al. 2012). Three-dimensional coordinates of an object can be extracted if it is imaged from two different perspectives and without the need of camera positional information (Tonkin et al. 2014). With series of overlapping images, objects can be matched, the geometric accuracy is improved and the probability of occlusions (shadowed or invisible areas in an image) is reduced. For the goal addressed in this study, the generating of image-based point clouds requires images with a high-spatial resolution and a multi-image overlap (White et al. 2013). Spectral information available in optical imagery collected with UAVs allows calculation of vegetation indexes. For instance, in agricultural applications, spectral data has been used to assess vegetation health and nutrient supply, where the high resolution enabled the separation of single plants from the ground (Ren et al. 2017). Implementing multispectral sensors to calculate the normalized different vegetation index (NDVI) have also been used to describe the status of crops and applied thermal spectral sensors to assess the water supply via the crop water stress index (CWSI) (Katsigiannis et al. 2016). The temporal flexibility of UAVs has been also tested in forestry to create time series of multispectral imagery with five narrow bands (red, green, blue, red edge, NIR) to detect appearing stress in crowns of *Pinus radiate* (Dash et al. 2017). Spectral signatures of reed can be also used as an indicator for vegetation status. Vital leafs of reed show a high reflectance in the green and infrared colour and a high absorption in the red wavelength (Gitelson et al. 2003). Reduced vitality is accompanied by degradation and shrinking cells resulting in higher red and lower NIR reflectance.

Analysis of point clouds in combination with the available spectral information are expected to allow a better characterization of vegetation stocks. Crop damage has already been estimated by analysing the relations between vegetation canopy height and NDVI values (Stanton et al. 2017). Discrimination of vegetation types can also be achieved with close-range aerial photogrammetry (Weiss and Baret 2017). In terms of mapping products, the present study faced the challenge of developing an approach, which is consistent with the official monitoring method in terms of extent, density and status determination. High-resolution imagery and three-dimensional information derived from close-range aerial imagery may be suitable in assessment of vegetation. UAVs in combination with SfM could also contribute in the coverage quantification, categorization of vegetation density and status assessment for aquatic reed beds. This study assessed the classification of aquatic reed bed using close-range aerial photogrammetry. The UAV platform and imaging system were chosen from the consumer sector and affordable for small

companies specialized in UAV mapping for environmental applications. The core objectives addressed were to determine the accuracy of 1) the determination of aquatic reed bed frontline and extent, 2) the classification of aquatic reed density, and 3) the status classification of aquatic reed.

3.3. Material and Methods

3.3.1. Study Area

The study area is located approximately 80 km South-Eastern of Munich city in Bavaria (Germany). Lake Chiemsee is one of the last intact inland waters in central Europe (Hoffmann and Zimmermann 2000). Although a significant decline of reed bed has occurred also at the Chiemsee, essential aquatic reed populations are still present. The populations of *Phragmites australis* are not older than approximately 100 years. Visual interpretations of aerial images have revealed that the development of aquatic reed had reached its maximum expansion in 1937 (Grosser et al. 1997). Along the following 20 years reed population remained stable and before the end of 1957, a starting decrease was documented. Until 1973, 14 % of the reed bed declined in terms of biomass and special extent and reduced further 31 % in the following years. In 1982 the reed population slowly stabilized (decreasing 7 %) (Grosser et al. 1997). Further monitoring projects revealed a population increase of 4,5 % in between 1991 and 1998 (Hoffmann and Zimmermann 2000).

3.3.2. Description of UAV Point Clouds

Point clouds were photogrammetrically calculated based on aerial imagery collected by UAVs in two different areas of interest (AOI). Surveying missions were deployed on September 21st in 2015 with Rotary-Wing (RW) and Fixed-Wing (FW) UAVs for AOI-1 and AOI-2 (Figure 3.1), respectively. Selected AOIs differentiate regarding the structure and represent different characteristics of aquatic reed bed types. AOI-1 and AOI-2 are located at the north-west shore at the border of the community Breitbrunn. From the water to the landside AOI-1 is characterized by a gradually increase in stem height. Expansion front is frayed causing small vegetation inlets. In AOI-2 reeds grow in groups with increasing height.

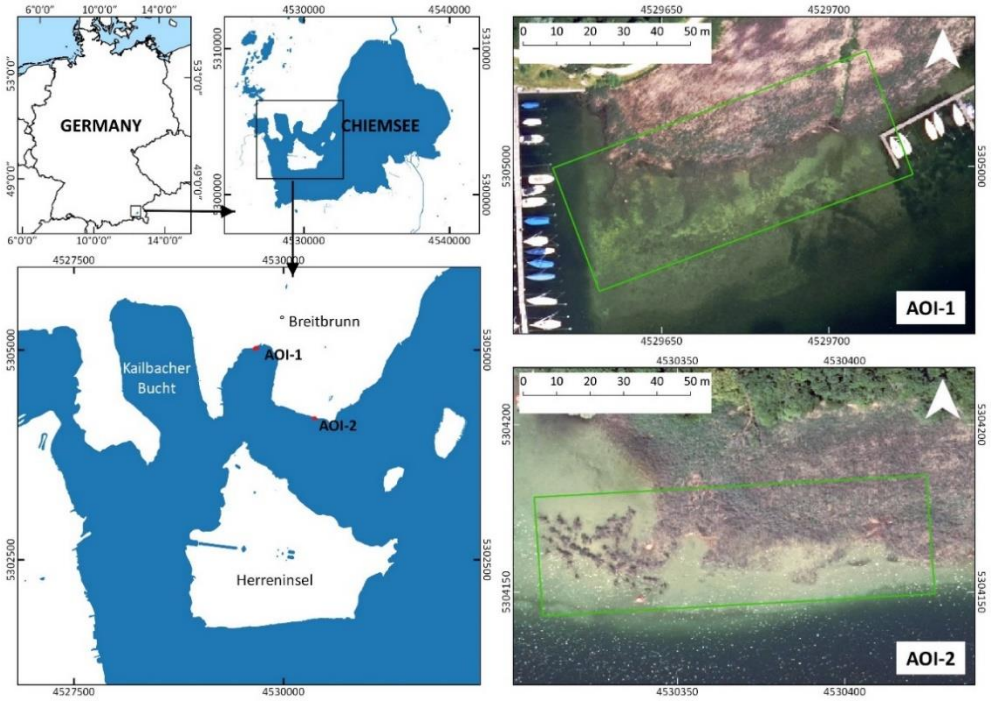

Figure 3.1 Lake Chiemsee at country level and location of Areas of Interest (AOI). Background is an orthorectified aerial image of the LDBV. Coordinate System is DHDN Gauss Krüger Zone 4 (EPSG 31468)

Point clouds were generated through the implementation of structure from motion (SfM) algorithms. The mean flying altitude for RW and FW survey was 46 m and 146 m, respectively. As an effect of the different flying altitude, the point clouds differed in the point density. RW imagery (AOI-1) allowed clouds with point density of 2260 points/m², and 1230 points/m² for the FW imagery (AOI-2). Point clouds were georeferenced with ten Ground Control Points (GCP) in case of AOI-1 and eight GCPs for AOI-2. The coordinate reference system used was DHDN Gauss-Krüger Zone 4. Each single point in clouds has geographic coordinates (x, y, z) and a value for each colour channel (Red, Green, Blue). Detailed explanation of point cloud calculation can be found in (Meneses et al. 2018).

3.3.3. Reference and Validation Data

Field measurements, orthomosaics from RW and FW UAVs, and aerial imagery were used for reference and validating classifications. Field data were generated thorugh field measurements from September 15th in 2015 based on the protocols (Meneses et al. 2018; Corti Meneses et al. 2017). They consisted on shoreline perpendicular cross-sections, square sample plots, and shoreline and frontline boundaries. The data available for every cross-section was the stem height and for square sample plots the number of stems per square meter, number of green and dry stems with and without panicles, and diameter of stems. Square measurements were taken along each cross section in sparse and in dense reed beds (Figure 3.2). Since measurements took place from water to land side, the frontline corresponds to the first occurring reed stem. The water level on the day of the field measurements was at 517.96 m.a.s.l. (Bayerisches Landesamt für Umwelt 2017a). As well as GCPs, transect points were recorded by a differential GPS (Trimble Geo XT).

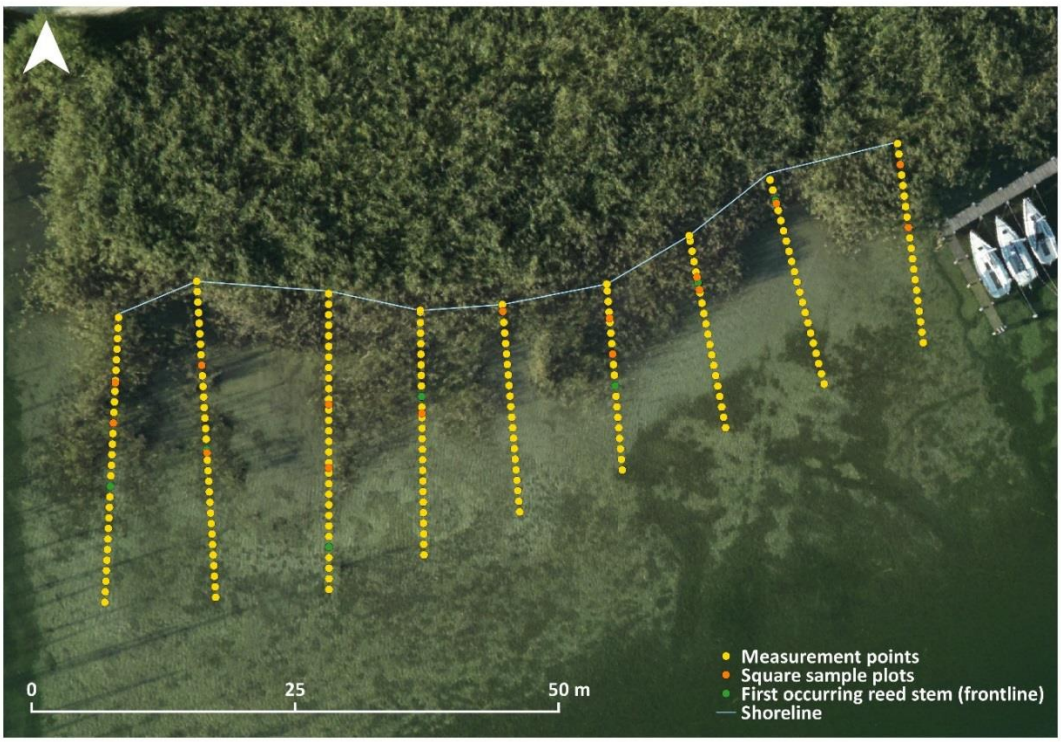

Figure 3.2 Validation data for AOI-1. Observations were measured every meter along cross-sections. Along transects square sample plots were placed. Background is an optical image collected during the LiDAR survey by the company AHM

Orthomosaics were created from RW and FW UAVs datasets after running SfM algorithms. Using the same sensor (Canon EOS-M) with 22 mm optics the spatial resolution is controlled by flying height. AOI-1 achieved a spatial resolution of 2.1 cm/pix and 2.86 cm/pix for AOI-2. In the same way, orthoimagery was referenced in DHDN Gauss-Krüger Zone 4. Additionally, a set of aerial imagery (10 cm spatial resolution) was recorded on the same day of UAV surveys (21st of September 2015) but by a different sensor (Hasselblad H3DII-39 camera, 39 MP) mounted in an aircraft (Airborne Hydro Mapping - AHM) and used as additional verification source.

3.3.4. Classification of Reed Extent and Density in UAV point clouds

The software OPALS 2.2.0 (Orientation and Processing of Airborne Laser Scanning data) developed by the Vienna University of Technology, was used for the analysis of the point clouds. OPALS is a software based on modules (processing tools), which use information about points stored as attributes (Pfeifer et al. 2014). The developed classification script was applied for both AOIs. The classification of aquatic reed beds for extent quantification was implemented considering the differences in point heights (z value of a point). The first step was the classification of points in the classes "Water" and "No Water". The height of water surface provided by the water management office was used as reference to discriminate points corresponding to water/lake-bottom and aquatic reed. Once points corresponding to land and water were identified, categorization of "Aquatic Reed" points was achieved.

Consistent with the instructions of the last official reed survey at the Chiemsee, the density classes for this study were also assigned to "Dense" and "Sparse" aquatic reed beds (Hoffmann and Zimmermann

2000). The visual examination of cross-sections along AOIs revealed that density classification can be obtained based on the geometric distribution of points in height (Z axis). Within the class "Aquatic Reed", absolute height and variation of points in height are suitable attributes for threshold definition and then classification (Figure 3.3). These attributes were calculated with the module *PointStats*. It calculates statistics by selecting a group of points within a specific volume (*searchMode*) and measuring them from a specific reference point (*refModel*). Since the analysis was based on distribution of points in the Z axis, a cylinder was used for point selection. Its radius (*searchRadius*) was defined to 0.5 m with the purpose of being consistent and match the measurements on field (stems/m²). A plane passing through the origin (*zeroPlane*) was employed as reference for point measurements. The statistics used for classification were the mean height (*Zmean*) and the variance of point height (*ZVariance*).

The statistic *Zmean* is calculated considering all the points within the cylinder with reference to the *zeroPlane*. The advantage of using the mean height instead of the absolute height is that differences are avoided resulting in heights that are more homogeneous across the cloud. The statistic *ZVariance* gives a value of height variations for a group of points with reference to the *zeroPlane*. The smaller the variation, the more points have the same height. Contrarily to dense stocks, additional features are imaged in areas of sparse aquatic reed beds. Points of leaves, stems, or ground can be found in the cloud, which increases the height variation value (Figure 3.3). Furthermore, the variance shows abrupt changes in the reed bed, such as ripped areas of the reed front. *ZVariance* was calculated with the same settings as the *Zmean*. The closer is the value to 0, the lower the variance and consequently the higher the stand density.

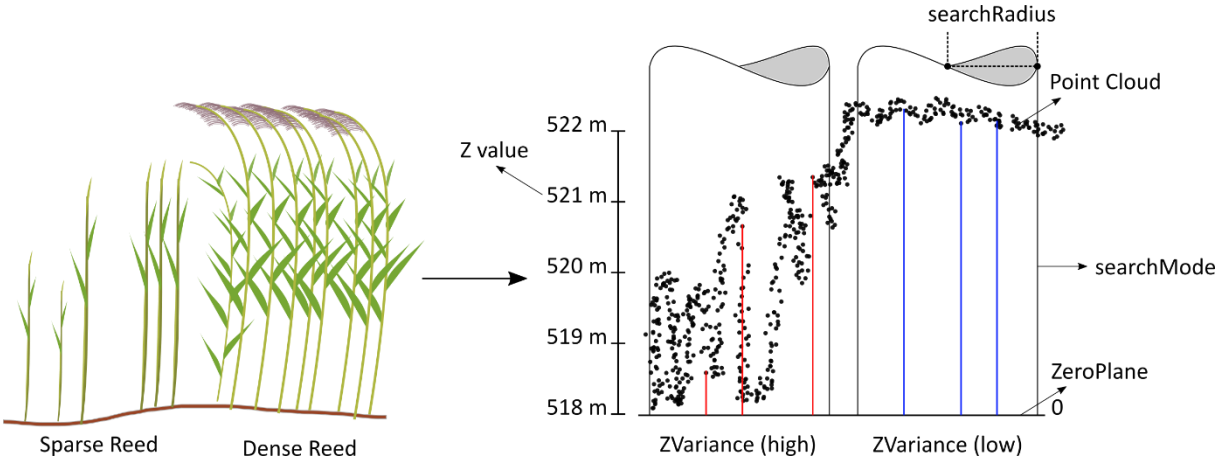

Figure 3.3 Statistics calculated for point clouds derived from optical imagery after applying structure from motion algorithms. Red and blue lines represent the distances measured from reference plane (ZeroPlane) to the selected points within a cylinder

3.3.5. Estimation of vegetation status

The status of aquatic reed was calculated on basis of a colour index and frontline sinuosity. Band intensity based indices are less sensitive to brightness fluctuations and are therefore more useful than applying only a single colour channel (Meyer and Neto 2008). Woebbecke's excess green (*ExG*) (Woebbecke et al. 1995) minus the excess red (*ExR*) (George E. Meyer 1999) was found to be most effective in separating these classes as well as reed from the ground of the lake, because the index

illustrates clear differences in its values. Other studies (Meyer and Neto 2008; Lameski et al. 2017) have also tested the *ExG-ExR* as a useful vegetation index. *ExG-ExR* index is calculated as:

$$\mathrm{ExG} = 2 * \mathrm{g} - \mathrm{r} - \mathrm{b}, \mathrm{ExR} = 1.4 * \mathrm{r} - \mathrm{g}$$

Where r, g, and b were the chromatic coordinates

$$r = \frac{R^*}{R^*+G^*+B^*} \ , \ g = \frac{G^*}{R^*+G^*+B^*} \ , \ b = \frac{B^*}{R^*+G^*+B^*}$$

And, R*, G* and B* were the normalized RGB values (0–1) defined

$$R^* = \frac{R}{R_m}, \ G^* = \frac{G}{G_m}, \ B^* = \frac{B}{B_m}$$

R, G and B are the actual values for each colour channel of one point. The R_m, G_m and B_m are the maximum tonal values of each colour (Meyer and Neto 2008). The maximum values per channel in the UAV point cloud were 65280, which approximately corresponds to a 16bit colour depth. That information was obtained by using the module *OpalsInfo*. The mean value was calculated for the *ExG-ExR* with the using same *searchMode*, *searchRadius*, and *refModel* used for the mean height or the height variance (Figure 3.4).

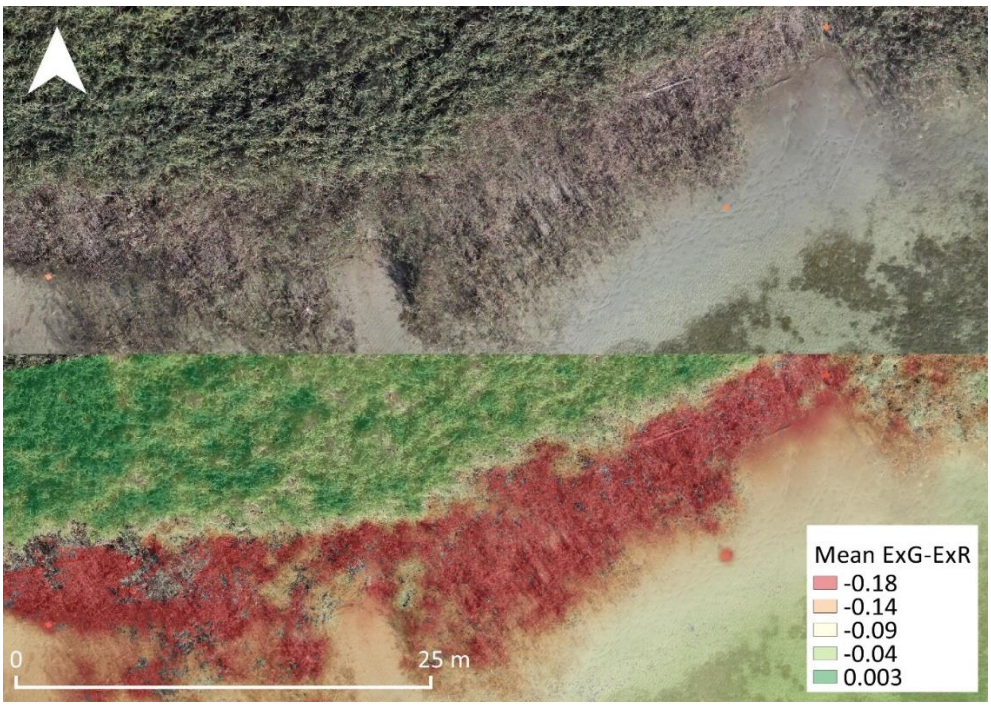

Figure 3.4 Colour index Mean ExG-ExR calculated for AOI-1. Orthomosaic in the background was created using the same imagery implement for point cloud calculation

The frontline sinuosity is another element to analyse whether aquatic reed beds are facing stressing factors. The frontline sinuosity is the ratio of the length along the frontline (curvilinear length) and the straight distance between two points (Euclidean distance). Frayed, ripped, or not zoned aquatic reed beds can be allocated by measuring the frontline sinuosity. Frontline sinuosity is calculated as:

$$Frontline\ Sinuosity = \frac{Frontline\ length\ [m]}{Frontline\ Euclidean\ distance\ [m]}$$

if the sinuosity index of a reach is 1.3 or greater, the reach is considered as meandering, a straight reach has a sinuosity index of 1 and reaches which is having sinuosity indices between 1.05 and 1.3 are defined as sinuous (Sapkale et al. 2016). Sinuosity index was calculated every 10 meters sections (Total of 18) and the mean value was used for determined if the frontline in the AOIs is low or high sinuous.

Based on the spectral reflectance of reed bed components obtained with *ExG-ExR* index, areas with a majority of reeds with green leaves and stems (Vital) were discriminated from dried/dying reeds (less vital). Finally, density and vitality classifications were then combined with frontline sinuosity ratio to derive the status. The classes "Stressed" and "Unstressed" were employed for the status classification. The lower the density and vitality, the more stressed a stand is. Contrarily, unstressed stocks consist of a dense and green vegetation coverage.

3.3.6. Validation of classification results

3.3.6.1. Reed Bed Extent Quantification and Frontline Assessment

Extent of aquatic reed beds were obtained by measuring the area between shoreline and frontline. Since with photogrammetric methods and optical imagery the allocation of shoreline is not possible, the shoreline measured on site was used to calculate the coverage. Regarding the frontline, its accuracy was assessed using the DGPS points defined as frontline. For both AOIs, 20 transect measurements were checked about conformity. Length differences between cross sections measured on field and on modelled data was assessed using the Root Mean Square Error (RMSE).

3.3.6.2. Accuracy Assessment of Density and Vegetation Status Classification

Accuracy of aquatic reed bed density and vegetation status was assessed by means of an error matrix. It is an effective method since every single class is evaluated individually. Producer's Accuracy (PA), User's Accuracy (UA), and Kappa coefficient are the indicators obtained to evaluate the match between field and estimated measurements. PA reveals how well samples for this class are assigned. UA indicates the probability that a classified sample represents the assigned class in real (Lillesand et al. 2015). Kappa coefficient is an indicator to which percentage correct values of an error matrix are "true" agreement (value 1) versus "chance" agreement (value 0) (Congalton and Green 2009). A third class which represents water, was added to fill empty areas. Thereby, the differentiation of reed and water was also evaluated.

Data collected from 33 squared sample plots and 682 randomly stratified (classes) sample points were used to assess density map. The true agreement of each sample point was then verified. Regarding the status map, the same strategy was chosen but instead of square sample plots, 384 observations at 1 m distance along transects were used. Measurements reported without reed above the water surface were assigned as "Water", whilst the remaining observations to either "Stressed" or "Unstressed" reed. This grouping was implemented in order to be consistent with the classified categories. The allocation of unstressed reed was completed by verifying the status, using the reference image provided by Airborne Hydro Mapping (AHM) Company according to the interpretation key (Table 3.1).

Table 3.1 Description of categories for aquatic reed bed status according to (Grosser et al. 1997) (Hoffmann and Zimmermann 2000)

Category	General Description
Stressed Reed	Sparse and parallel stripes along the reed bed edge (due to either floods, wind storms, or driftwood accumulation), a lane/aisle perpendicular to the shore (for docks, boat traffic, bathing, fish traps), the dissolution of reed beds though decreasing stem density, frayed, ripped, not zoned reed edge and in single clumps (through erosion or flood), and seaward stubble fields of past reed beds.
Unstressed Reed	Characterized by a closed and evenly growing stock. Their seaward stock limit is evenly curved and uninterrupted. There is a gradual decline in crop density and the middle stem height instead. The reed is stock-forming over large areas and without gaps in the interior.

3.4. Results

3.4.1. Point Cloud Classification

Aquatic reed bed extent, density, and status were obtained with the implementation of the developed decision tree (Figure 3.5). Knowledge from field observations, visual inspections of point clouds, and additional independent aerial imagery were fundamental in the categorization process. Calculation of statistical parameters provided variables for more accurate and unbiased classifications. Considering statistical parameters for every point cloud, several classes were categorized. Aquatic reed was identified by allocating the land-water line with the water surface level for the day of flight. Density of aquatic reed beds was achieved by considering the mean height (*ZMean*) and height variance (*ZVariance*). The threshold for the mean height parameter was set to 519.5 m, which is 1.45 m with reference to the water surface level (518.05 m). The classification threshold for variance was defined to 0.1 for points with heights smaller than 1.45 m and variance greater than 0.1 were assigned as “Sparse”, whilst points with opposite values as “Dense”. *ExG-ExR* index was calculated to determine areas with dominance of vital stems. The threshold for the classification based on the index was determined to -0.105 and assigned classes were “Vital” and “Less Vital”. The threshold assigned for frontline sinuosity was assigned to 0.5. A reed bed with values smaller than 0.5 were classified as “high sinuosity”. The combination of density results and colour index contributed in the achievement of classification or reed status. Status was assigned to the classes “Stressed” and “Unstressed” aquatic reed.

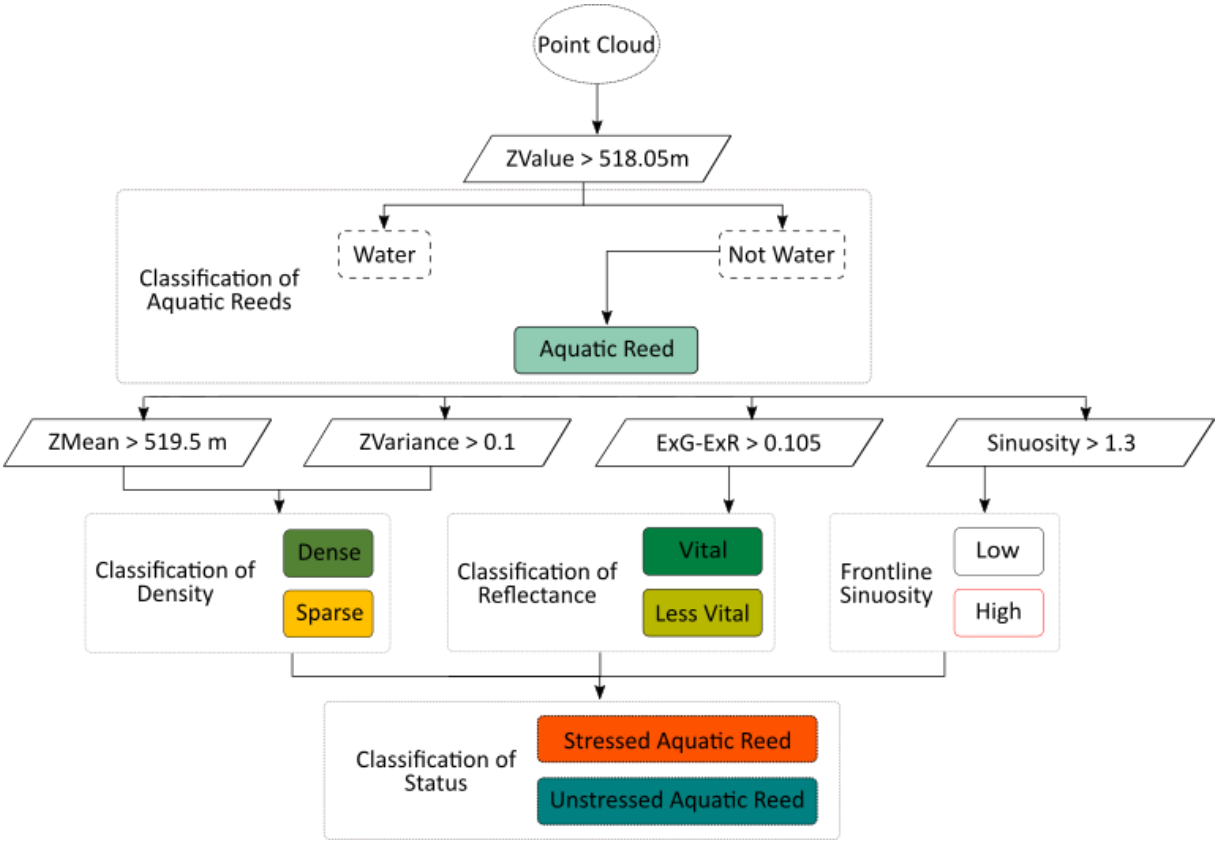

Figure 3.5 Decision tree implemented for classification of aquatic reed status. Ellipse represent to input data. Classification thresholds are written inside parallelograms. Dashed boxes are intermediate classes.

3.4.2. Extent Quantification and Frontline Assessment

The extents for AOI-1 and AOI-2 were 656 m² and 986 m², respectively. In both cases the classified areas were smaller than the measured area (760 m² and 1179 m² for AOI-1 and AOI-2 respectively). The RMSEs of cross sections confirmed that the classified extent of AOI-2 had a higher agreement. The RMSE of AOI-1 was 3.62 m and 1.58 m for AOI-2. Frontline sinuosity index for AOI-1 was μ 2.9 ± α 1.8 and μ 3.02 ± α 1.8 for AOI-2. Since sinuosity index for both AOIs is greater than 1.3, frontlines were categorized as high sinuous. The evaluation of the classified reed frontlines resulted in a true agreement only 63.6 % of the all the measurements for AOI-2. Seven out of eleven points of the measured extent showed an alignment. For AOI-1, seven out of nine points were correctly identified, which resulted in 77.8 % agreement. The overall agreement of the reed fronts for both AOIs amounts was 70 %.

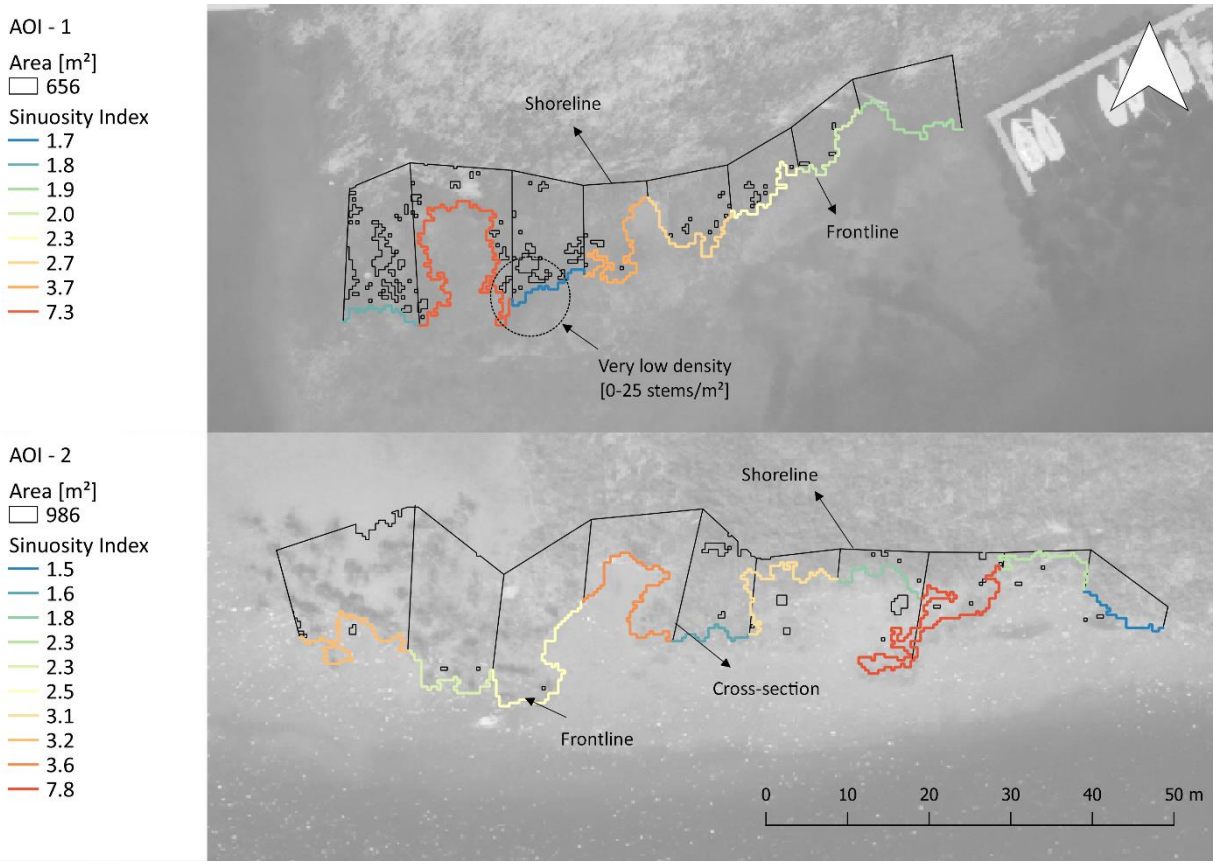

Figure 3.6 Extent quantification for AOI-1 and AOI-2. Blacked outline polygons represent areas derived from UAV point clouds. Coloured lines represent the calculated sinuosity index in 10 meter sections. Background is an orthorectified image of the LDBV

3.4.3. Accuracy Assessments of Density and Status of Aquatic Reeds

The accuracy assessment based on the 33 square measurements resulted in an overall accuracy (OA) of 81.82 %. Since there were no square measurements in water areas, the Kappa statistic was computed as 0. The user's and producer's accuracy of the class "Sparse" was equal (88.46 %). Out of 26 samples, 23 were classified correctly as "Sparse" and three samples were in areas classified as "Water". Four sample points lying in "Dense" reed bed were correctly assigned (User's accuracy = 100 %), and the remaining three to "Sparse", giving a total of seven samples. This explains why the Producer's accuracy is only 57.14 %. The visual accuracy assessment reveals an OA of 88.56 % and a Kappa statistic of 0.8. Out of 682 sample points, 604 points were classified correctly against RGB imagery. The gained experience in field when measuring and describing status classes (**Table 3.1**) were fundamental for this assessment. Water has the highest User's accuracy with 89.58 %. Producer's accuracy for the class dense reed obtained a value of 68.33 % resulted from 19 points, which were assigned as dense reed, but are rather sparse reed. The lowest but not bad user's accuracy of dense reed (82 %) was assessed because 9 out of 50 points were classified as sparse reed.

The status classification achieved an OA of 82.9 % and Kappa statistics of 0.691. The User's accuracies laid in close value ranged from 81 % (water) to 90 % (unstressed reed). Only two points out of 20 dense reed sample points were wrongly assigned to "Stressed" reed. Regarding of the Producer's accuracy, the water category has the highest value with 92.51 %, resulting in only 14 miss-assigned samples. The

"Unstressed" category has the lowest value (69.23 %), because 8 samples were wrong assigned since they are "Stressed" reed.

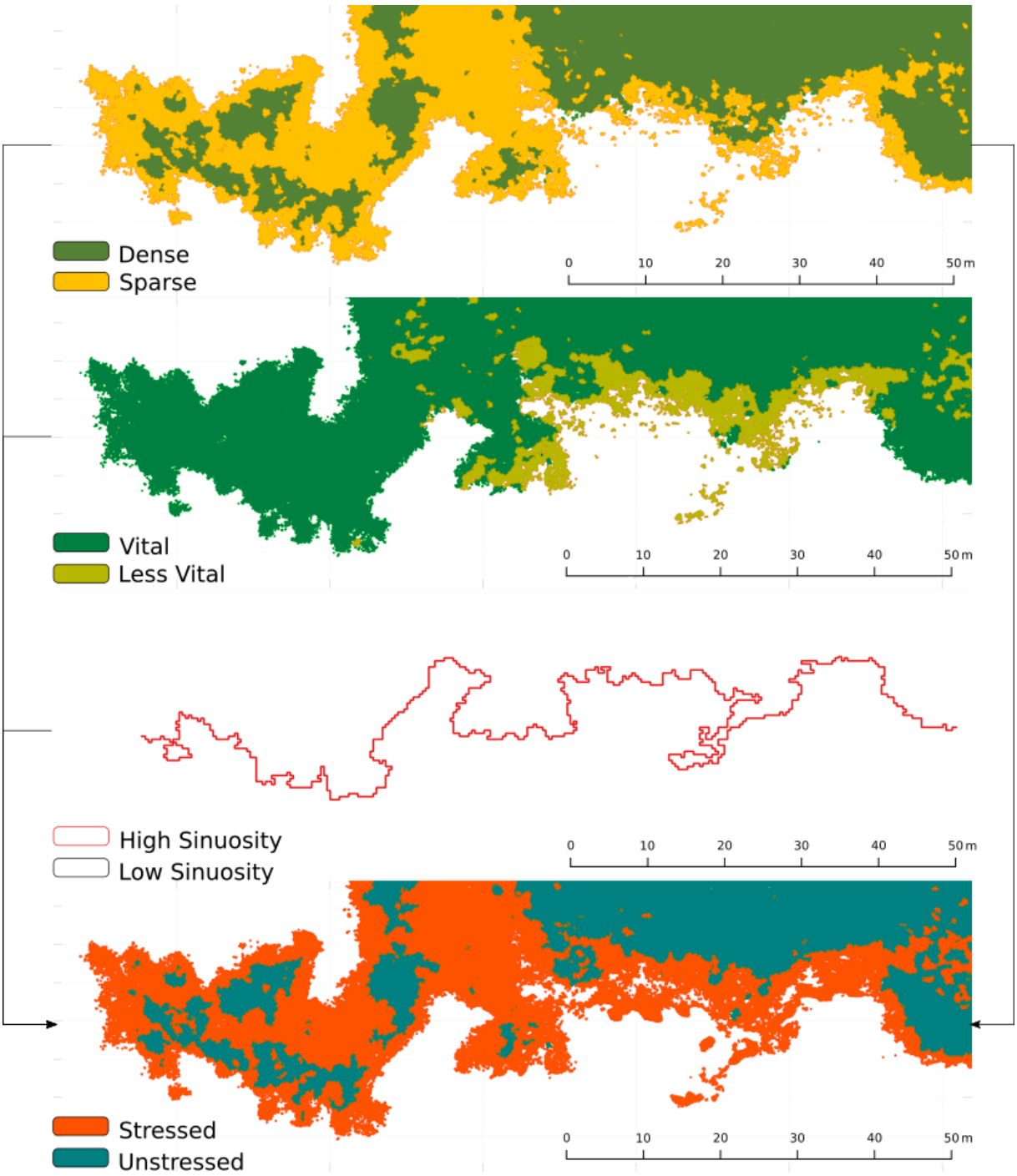

Figure 3.7 Status classification for AOI-2 achieved with the combination of density map, vitality and shape of the frontline (sinuosity) maps obtained with height and variance values, and colour index ExG-ExR, respectively

3.5. Discussion

The results of this study suggest that statistical measurements in point clouds are powerful method for aquatic reed bed assessment and represent an accurate alternative to commonly applied methodologies. Evaluation of point clouds estimated with Structure from Motion (SfM) algorithms in close-range aerial imagery is suitable for frontline allocation, extent quantification, density classification, and status determination of aquatic reed beds. The proposed decision tree for point cloud classification is easily reproducible, consistent and objective, since it is not influenced by criteria of the operator and based on thresholds. The suggested point cloud processing chain enabled new possibilities for aquatic reed bed monitoring in short frequencies. Particularly in dynamic ecosystems, like wetlands, repeated and continuous recordings are substantial for ecologists (Marcaccio et al. 2015). Allocation of frontline was achieved with the modelled height of reed. Spatial distribution of points was fundamental in the analysis of stock density. Spectral signature stored in every point was crucial to determine the status of aquatic reed beds.

3.5.1. Frontline allocation and extent quantification

Allocation of frontline was accurately achieved with the modelled heights of aquatic reed beds. Point cloud geometry (height) contributed to bypass sunglint effects, shadowed areas and spatial resolution, which are common issues when imagery is interpreted only spectrally (Hoffmann and Zimmermann 2000). In terms of accuracy and habitat disturbance, the presented method proved to be more suitable than monitoring in the field. Data collected along transects every 10 meters delivered points where reed emerged from water, but no exact allocation of the frontline boundaries. A frontline mapped onsite could be improved by shortening the distances between each transect or with GPS tracking, but this would increase the effort and make the monitoring less operational. In addition, this would represent a higher disturbance to the habitat due to mechanical damage. Although frontline was accurate allocated, the analysed data type did not allow the mapping of the shoreline. Since SfM algorithms are only capable of extracting the features recorded in optical imagery, structures bellow canopy surface cannot be considered. This represents a disadvantage in comparison to other technologies, such as LiDAR data in which light pulses are able to penetrate the vegetation canopy (Zlinszky et al. 2012; Alexander et al. 2015; White et al. 2013). For this study purposes, the shoreline allocated during field observations was used for extent quantification. The shoreline provided by the official water authorities could also be used in case no field observations are available. Additionally, point clouds derived from optical close-range imagery are also of a higher density. Point density in clouds obtained with LiDAR in the same study area where 200 points/m² (Corti Meneses et al. 2017), whilst UAV data produced clouds with 2260 points/m². Higher point density from SfM, relates to the small ground sampling distance and high image overlap (White et al. 2013). A higher point cloud density enables a better detection of reeds growing especially in highly sparse populations. Therefore, more stems can be modelled, which leads to an accurate allocation of the frontline.

3.5.2. Density and status assessment of aquatic reed beds

Density and status classifications showed a high level of consistency compared to the observations onsite. The applied software facilitated the calculation of statistical parameters implementing neighbour points in a defined space and proved to be applicable for the classification of UAV point clouds. Photogrammetric methods provided two valuable attributes to describe reed bed density. Besides height (Ostendorp 1989; Zlinszky et al. 2012; Grosser et al. 1997; Poulin et al. 2010; Luo et al. 2017), the

variance proved to be an additional parameter for reed bed characterization. The spatial distribution of points in combination with the mean height facilitated the characterization of aquatic reed bed density. Furthermore, the point clouds allowed the classification of aquatic reed bed status involving the structural and spectral information (RGB values). The fusion of three dimensional structures and spectral information is declared as "state of the art" for characterizing ecosystem vegetation and improves the understanding of vegetation status compared to the application of only the structure or the spectral reflectance (Dandois et al. 2017). The overall accuracy of 83.33 % (Kappa = 0.691) confirmed the efficiency of the RGB-based ExG-ExR to for status classification of aquatic reed. This result is similar to a LiDAR study, which categorized wetland vegetation using LiDAR data into four types and achieved accuracies from 62.5 % to 84.6 % (Zlinszky et al. 2012). Vegetation indices, based on RGB channels have been successfully used to describe the vegetation status (Kefauver et al. 2015; Du and Noguchi 2017; Casadesús et al. 2007) and also as a component to define above ground biomass (Li et al. 2016). Thereby, they can be approached for imagery that is recorded by cost-effective consumer cameras. Nevertheless, the development of smaller multispectral cameras had increased their approach in context with UAVs and vegetation status (Michez et al. 2016; Candiago et al. 2015; Dash et al. 2017; Ren et al. 2017; Colomina and Molina 2014; Katsigiannis et al. 2016) where NDVI is preferred in the most cases. In general, plant health deterioration leads to reflectance decrease in the NIR and a reflectance increase in the visible colour range due to the chlorophyll content in leaves. Therefore, UAVs with a multispectral camera with similar spatial resolution could improve the classification result. Compared to a consumer camera, such a sensor would currently result in higher cost and heavier weight. More weight would decrease the flight time and thus area recorded by the sensor becomes smaller. Furthermore, the equipment for this study was chosen as low cost and consumer graded, to represent a monitoring method that is widely applicable, e.g. for small common environmental planning offices.

3.6. Conclusion

Suitability of three-dimensional data (3D) derived from close-range aerial imagery for monitoring aquatic reed beds was assessed. Point clouds calculated with Structure from Motion (SfM) algorithms in imagery collected with two low cost and consumer graded UAVs were used for classification purposes. The implementation of the statistically calculated parameters "mean height" and "height variance" were suitable to reproduce aquatic reed bed density and frontline sinuosity. In combination with spectral information per point in the cloud, status of aquatics reed beds was mapped. This qualitative component was used to support the density classification for assessing the status of aquatic reed bed. In context of aquatic reed bed monitoring, this study demonstrated a new strategy based on data from low-cost UAVs for assessing and detecting changes. The developed strategy represents a constant classification method, which is easily reproducible for other stands of common reed possibly even for other plants and purposes. The implementation of short time series for change detection analysis, can improve the understanding of the complex aquatic reed decline causes, which is essential to design conservation strategies. The presented methodology fits environmental requirements in governmental policies. This low cost method can be implemented making it flexible and appropriate for supporting terrestrial mapping activities executed specially by small offices dealing with environmental issues.

4. Evaluation of Green-Lidar Data for Mapping Extent, Density and Height of Aquatic Reed Beds at Lake Chiemsee

A similar version of this chapter was published: Corti Meneses, Nicolás; Baier, Simon; Geist, Juergen; Schneider, Thomas (2017): Evaluation of Green-LiDAR Data for Mapping Extent, Density and Height of Aquatic Reed Beds at Lake Chiemsee, Bavaria—Germany. In *Remote Sensing* 9 (12), p. 1308. DOI: 10.3390/rs9121308.

4.1. Abstract

Aquatic reed is an important indicator for the ecological assessment of freshwater lakes. Monitoring is essential to document its expansion or deterioration and decline. The applicability of Green-LiDAR data for the status assessment of aquatic reed beds of Bavarian freshwater lakes was investigated. The study focused on mapping diagnostic structural parameters of aquatic reed beds by exploring 3D data provided by the Green-LiDAR system. Field observations were conducted over 14 different areas of interest along 152 cross-sections. The data indicated the morphologic and phenologic traits of aquatic reed, which were used for validation purposes. For the automatic classification of aquatic reed bed spatial extent, density and height, a rule-based algorithm was developed. LiDAR data allowed for the delimitating of the aquatic reed frontline, as well as shoreline, and therefore an accurate quantification of extents (Hausdorff distance = 5.74 m and RMSE of cross-sections length 0.69 m). The overall accuracy measured for aquatic reed bed density compared to the simultaneously recorded aerial imagery was 96% with a Kappa coefficient of 0.91 and 72% (Kappa = 0.5) compared to field measurements. Digital Surface Models (DSM), calculated from point clouds, similarly showed a high level of agreement in derived heights of flat surfaces (RMSE = 0.1 m) and showed an adequate agreement of aquatic reed heights with evenly distributed errors (RMSE = 0.8 m). Compared to field measurements, aerial laser scanning delivered valuable information with no disturbance of the habitat. Analysing data with our classification procedure improved the efficiency, reproducibility, and accuracy of the quantification and monitoring of aquatic reed beds.

4.2. Introduction

Reed beds provide important structural elements of lake ecosystems. Along a horizontal gradient that runs from the lake towards the bank, reed stocks are classified into three different ecological zones that occur either in water, transition, or in land zones (Ostendorp 1993b). The water reed at the expansion front of a reed stock is considered the most sensitive zone of a reed bed (Grosser et al. 1997). According to their definition, land reed beds are located in areas above water level, comprising an onshore/shoreward stock of multiple species, and usually growing in meadows (Grosser et al. 1997). Aquatic reed beds grow in locations that were flooded throughout the year. Lakewards stocks are pure stands of *Phragmites australis*, and are characterized by their low stem density (stems/m^2) and longer sparse fertility (Grosser et al. 1997). Stocks of this macrophyte act as a buffer between land and water. They provide a key habitat for several endangered species (Ostendorp 1993b), they physically protect banks from erosion, and they provide a food resource for various arthropods, birds, and mammals (Ostendorp et al. 2003). Aquatic reed beds are threatened, mainly due to mechanical, hydrological, anthropogenic, biological, and climatic causes (Ostendorp et al. 2003; Crisman et al. 2014; Nechwatal et al. 2008; Schmieder et al. 2004; Schmieder et al. 2002; Ostendorp et al. 2001; Ostendorp 1989). Global

warming influences, such as an increase in water temperature, extreme drought, and heavy rain events could additionally affect the growth and status of aquatic reed populations of freshwater lakes (Gigante et al. 2011; Tóth 2016).

Changes in the abundance and density of reed beds can be quantified through the implementation of field measurements and remote sensing methodologies. Although on-site evaluations deliver highly accurate results, they are associated with high personnel, time, and financial expenses, as well as ecological disturbance of protected habitats (Schmieder and Woithon 2004a). Visual interpretation of multispectral aerial imagery has been the standard method to bypass this problem (Schmieder et al. 2002; Krumscheid et al. 1989; Kristiansen and Petersen 2000; Dienst et al. 2004). In the same way, analysis of satellite imagery has also been implemented (Davranche et al. 2010; Villa et al. 2013; Brix et al. 2014; Bourgeau-Chavez et al. 2015). These methodologies have contributed to the global monitoring of reed beds in wetlands and large lakes, where tens of hectares are covered by this type of vegetation. In the monitoring of small lakes with a limited presence of aquatic reed beds, spatial resolutions provided by satellite constellations are still too coarse for identifying stocks that are sparsely distributed or only comprise single reed individuals. This difficulty poses a serious limitation to monitoring spatial occurrence.

The accurate identification of aquatic reed beds by analysis of optical imagery is affected by sun illumination, plant phenology, and spatial resolution. The position of the leaves' and the stems' incidence angle towards the sun causes differences in the spectral response and therefore, causes variances in the extent of quantification of sparse aquatic reed beds (Schmieder et al. 2002). The imagery of official surveys is recorded normally for updating cadaster data and topographic maps, and not usually in the growth season (i.e., August to mid-September) when aquatic reed beds have their peak growth and maximum vitality. Accurate assessment is additionally hindered by shades, light reflection on the water surface, or vegetation reflectance. Although spatial resolution is sufficient for other purposes, sparse aquatic reeds cannot be identified in imagery with spatial resolutions lower than 20 cm per pixel (Melzer et al. 2001; Hoffmann and Zimmermann 2000).

Technological advancements in remote sensing science offer new possibilities in the characterisation of reed beds based on 3D data analysis. Very high spatial resolution multispectral imagery recorded with unmanned aerial vehicles and close range aerial photogrammetry have already supported the accurate mapping of land and aquatic reed beds (Venturi et al. 2016). In the same way, the biomass of wetland *Phragmites australis* (Luo et al. 2017), of wetland vegetation mapping (Zlinszky et al. 2012; Onojeghuo and Blackburn 2011; Gilmore et al. 2008), and characterisation of the land reed bed habitat quality (Onojeghuo et al. 2010) have all been achieved by applying Light Detection and Ranging (LiDAR) technologies alone or in combination with other data types (e.g., hyperspectral data). Nevertheless, the level of agreement at which height of, extent of, and density of aquatic reed beds can be mapped with LiDAR data remains unknown.

The new LiDAR system configured to function in the green wavelength of the electromagnetic spectrum offers new possibilities in the research of aquatic reed beds. Green light, the opposite of infrared, propagates in water by reflecting off the bottom surface, or in medium content materials (Mandlburger et al. 2013). In addition, green light not only propagates in water but can also reflect off land surfaces. These characteristics make the Green-LiDAR scanner suitable in mapping bathymetry (Costa et al. 2009),

bottom structures (Wedding et al. 2008; Tulldahl and Wikström 2012), or even for topo-bathymetric applications (Mandlburger et al. 2015; Yamamoto et al. 2012). Extents are important in the monitoring of aquatic reed beds, in which the mapping of the shoreline and the frontline are crucial. The technological benefits of a Green-LiDAR scanner could contribute to the accurate mapping of red bed boundaries. The frontline is scanned from reed stems and leaves above the water surface and thanks to green light propagation, the shoreline can be obtained independent of the water surface level during surveying.

Aquatic reed is an important indicator for the ecological assessment of freshwater lakes listed by the European Water Framework Directive (EU-WFD). As in other European countries, German federal state environmental agencies have to regularly report on the ecological status of freshwater lakes which involves a substantial monitoring effort. The core objective of the present study was to evaluate the applicability of Green-LiDAR technology in aquatic reed monitoring. We addressed the following research questions by focusing on the accuracy of diagnostic determination:

- How accurate is the estimation of aquatic reed extent in LiDAR point clouds?
- How accurate is the estimation of aquatic reed density in LiDAR point clouds?
- How accurately can aquatic reed bed DSMs be calculated from LiDAR point clouds?

4.3. Material and Methods

4.3.1. Study Area

The Chiemsee is the largest lake in Bavaria (80 km²) with a maximum depth of 73 m and a volume of 2048 hm³ (Bayerisches Landesamt für Umwelt 2017b). It is located approximately 80 km southeast of Munich at an approximate altitude of 518 meters above sea level (masl). During the last five decades, the spatial extent of the reed population has declined by about 50% at the Chiemsee (Grosser et al. 1997). Substantial reed beds at the Chiemsee are still existent and their decrease has been well documented which was why this lake was selected for our study. On the northwest side of the Chiemsee and at the Herreninsel, the most representative stocks of aquatic reed are still present (Hoffmann and Zimmermann 2000). Through an analysis of previous surveyed data, field observations, distribution stocks, and of water depth, the areas of interest (AOI) were selected for gathering validation data. The actual density of reed stems obtained from field observation was also considered. A total number of 14 AOIs with the occurrence of *Phragmites australis* at a mean area of 1694 m² (100 m in length at varying width) were selected for this study. AOIs were delimited at Aiterbacher Winkel (AOI-1), at the shores of Holzen (AOI-2,) at Keilbacher Eck (AOI-3), in Kailbacher Winkel (AOI-4 and -5), at Scheren (AOI-6), at the shores of town Mühln (AOI-7 and -8), and at Herreninsel (AOI-9, -10, -11, -12, -13, -14). In order to consider the variability of vegetation status, AOIs were selected in areas of different levels of protection: (a) protected all year long, (b) protected only during the avian breeding season, and (c) in areas without any form of environmental protection (Figure 4.1).

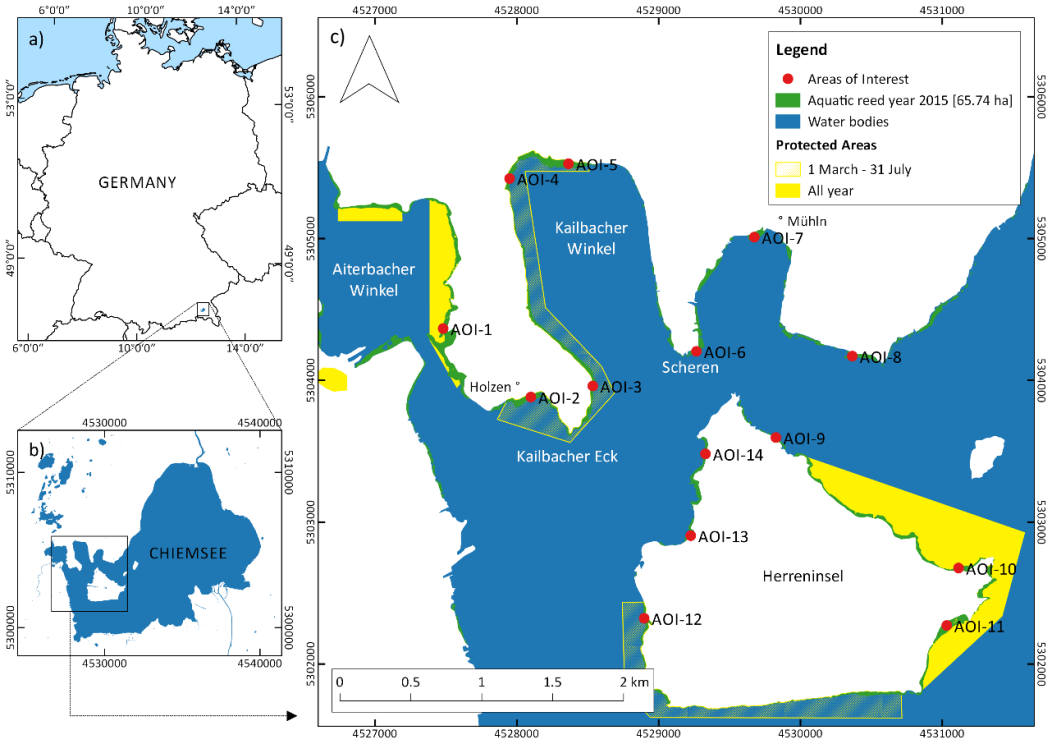

Figure 4.1 Location of the study area at country (a) and local level (b) and c) Distribution of Areas of Interest (AOIs) at the Chiemsee. Coordinate System is Deutsches Hauptdreiecksnetz (DHDN) Gauss Krüger Zone 4 (European Petroleum Survey Group (EPSG) 31468)

4.3.2. Airborne Laser Scanning Processing Chain

The analysis and classification of Airborne Laser Scanning (ALS) datasets was performed with the modular program system OPALS 2.2.0.0 (Pfeifer et al. 2014). The software provides modules for a complete processing chain of ALS data. Pre-processed LiDAR point clouds were imported into the OPALS data manager and the quality was assessed according to strip adjustment and outliers (noise). According to the information obtained from the quality control, no further calibration (e.g., strip adjustment, geometry calibration) was needed. Point cloud classification was then performed, and raster and vector file results were compared to field data and aerial imagery (Figure 4.2).

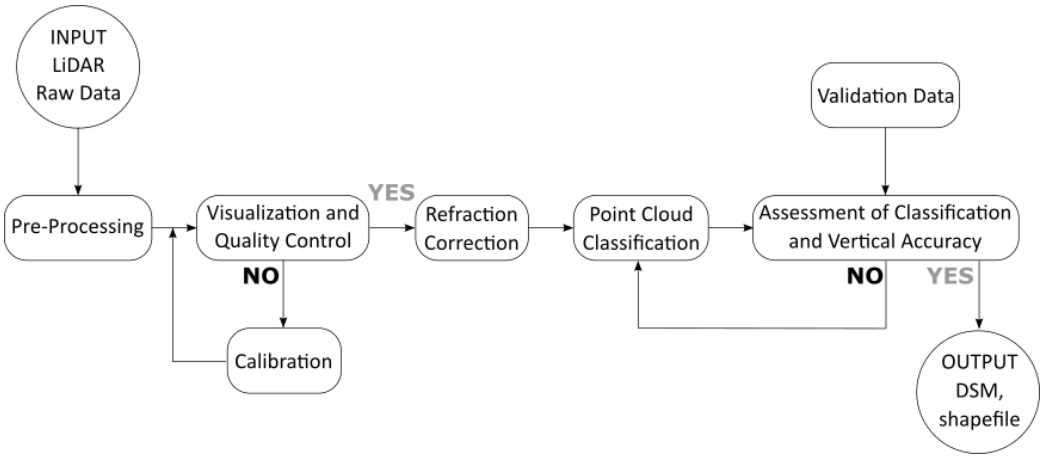

Figure 4.2 Airborne Laser Scanning (ALS) processing and decision chain applied for extracting heights of aquatic reed beds

The topo-bathymetric data collection took place on September 21, 2015, between 15h00 and 16h30 (UTC) during sunny weather conditions using the hydrographic laser scanner VQ-880G (Riegl LMS, Horn, Österreich). This device is a progressive palmer scanner with a laser beam in the green wavelength (532 nm) of the electromagnetic spectrum. The laser pulse repetition rate was set to 550 kHz and the laser beam divergence was set to 1 mrad. The mission was executed at an altitude of approximately 400 m above ground. The scan width was about 400 m and the footprint was 40 cm (diameter). A total of 58 strips was collected for the study area (29 back and forward scans). Point clouds were registered with the information obtained by a Position and Orientation System (POS) mounted on-board, and were improved by correction measurements sent by a Differential Global Positioning System (DGPS) base station on land. Orientation data was also recorded by the Inertial Measurement Unit (IMU) during flight. Aerial photographs with a 0.1 m spatial resolution were additionally recorded during the same flight for validation purposes.

Data pre-processing was executed by the data provider (AHM Airborne Hydro Mapping GmbH) using the software RiProcess. Strip adjustment was the first step in the pre-processing chain. The acquired accuracy was 10 cm (Standard Deviation). Secondly, based on the laser data, well distributed Ground Control Points (GCP) from roof corners and streets lane markers were defined across the study area. The 48 GCPs were measured by the research team with a tachymeter Leica TCRP 1201 R300 for fine registration. Absolute registration achieved an accuracy of 8 cm, and the point density of the raw data was approximately 200 points/m^2 (which included outliers). Finally, outliers were filtered and the point clouds from the specific AOIs were exported in Log ASCII Standard (LAS) 1.4 format.

Quality control was performed before processing the ALS data sets. Point clouds were firstly visually inspected. Attributes stored in the OPALS Data Manager (ODM) were examined in a 3D environment (opalsView) to identify potential errors in the already pre-processed product. Special attention was paid to the point geometry and the outlier filtering in water-land transition areas. An absence of points from water surfaces was identified in shallow water areas. Planar water surfaces cause specular reflections and therefore surface echo dropouts (Mandlburger et al. 2015). The overall low amount of noise in the point clouds delivered from the provider revealed that additional filtering was not needed. The package opalsQuality was then used for the quantification of point cloud quality. Cloud density and strip differences were analysed by means of density maps and statistical measurement.

Since light propagates differently in water than in air, the points under the water surface appeared to have shifted and therefore had to be corrected. The module implemented for the refraction correction was opalsSnellius (Mandlburger et al. 2013). This correction was computed with the refractive index, coordinates of origin, incidence angle, and specification of the water lever. First, to calculate the refractive index, the sine of the angle of incidence was divided by the sine of the angle of refraction (Smith et al. 2012). Refractive index varies depending on properties of transmission media (e.g., temperature, pH) and wavelength of incoming radiation. For variable temperature and salinity conditions, and for a green laser (532 nm wavelength), the refractive index is n = 1.33538 (Smith et al. 2012). Second, the coordinates of the laser origin and the incidence angle were obtained from the trajectory information recorded by IMU and POS. Third, the Air–Water Interface (AWI) was modelled in Quantum Geographic Information System (QGIS) by creating a raster in which all pixels values corresponded to the height of the water surface according to the daily measurements of the master data

gauge at Stock, Chiemsee (Bayerisches Landesamt für Umwelt 2017a). The water level used (517.93 m.a.s.l.) for the water surface definition was the measurement taken when the scanning flight took place. The laser penetration depth in the water body was about 10 m, which was approximately 8 m after correcting for light refraction.

4.3.2.1. Classification of Green-LiDAR Data

Statistical parameters for LiDAR point clouds were calculated for describing point attributes with the module opalsPointStats. OPALS calculates statistical features by first selecting points and then relating them to a reference model. The selection of points was based on an infinite vertical cylinder (searchMode = d2); the reference model was a "horizontalPlane". Since the laser footprint at ground level was around 0.4 m in diameter, the cylinder radius (searchRadius) was set to 0.2 m for the majority of calculations. In the model "horizontalPlane", the samples were reduced in relation to a plane passing through the feature point. Calculated statistics for identifying patterns in point clouds were ranked (rank) and point density (pdens). Rank statistic was calculated as the relative position (0 = local minimum and 100 = local maximum) of the feature point within its vertical neighbourhood. The feature pdens is the number of points in relation to the area/volume of the search cylinder. Since the usual measurement units for point density is points/m², a cylinder searchMode with a searchRadius of 0.5 m was selected as the most proximate value to a square meter (Figure 4.3). Filtering was crucial for the classification, since it allowed for points to be defined when a new attribute had to be calculated (processing filtering) in relation to the local neighbourhood (neighbourhood filtering). The classification was performed with the module opalsAddInfo. In order to define the threshold values, point clouds were inspected through cross-sections every metre with the module opalsSection. Special attention was placed on spatial distribution, density, and intensity of points. Cross-sections revealed that height and vertical distribution of points are important factors to differentiate dense and sparse reed beds.

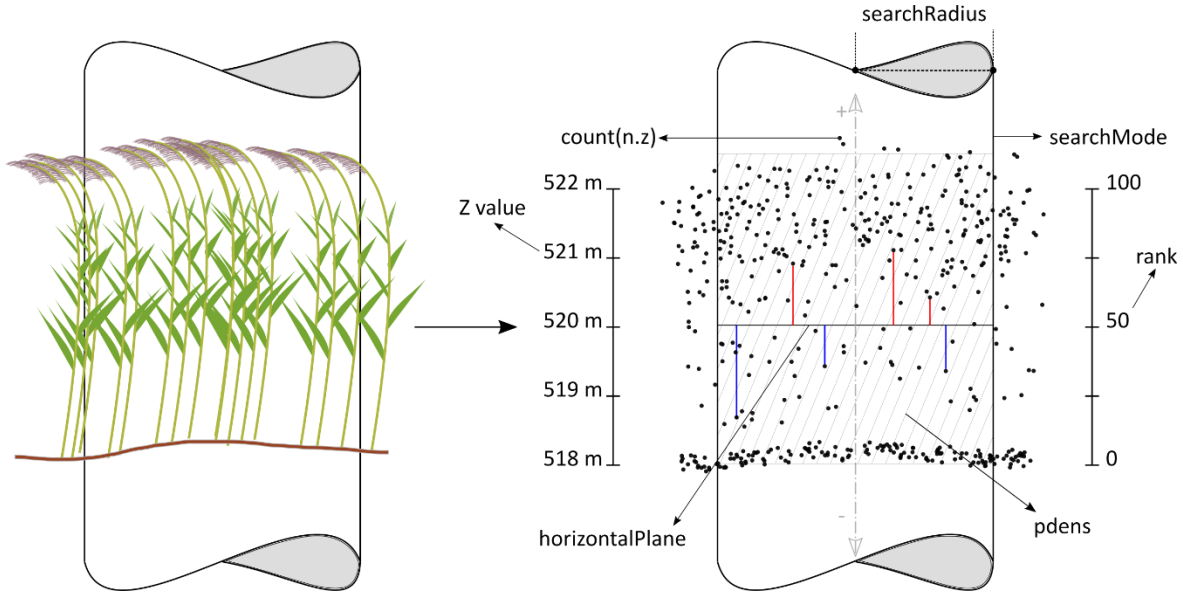

Figure 4.3 Graphical representation of methods and statistics used for classifying aquatic reeds in point clouds obtained from Green-Light Detection and Ranging (LiDAR)

4.3.2.2. Validation Data

Field data were collected by means of cross-sections and square sample plots. The measurements started by defining a one hundred-metre line parallel to the shore. A measuring tape was placed perpendicularly to this line every ten metres. Measurement started from the waterside and finished on the shoreline (i.e., the point at which water and land have the same height). At every metre along the cross-sections, water depth and reed stem height were measured to the nearest centimetre and decimetre, respectively. The frontline was then surveyed as the location in the cross-section where the first reed stem occurs. Plotting the coordinates of shorelines and frontlines in every cross-section in QGIS allowed the aquatic reed extents to be calculated. Based on expert knowledge, one or two square sample plots of 1 square metre each were placed where differences in stem density were identified. The parameter's density (stems/m^2), stem diameter, number of stems with and without shoots, and the number of green and dried (brown) stems were additionally recorded (Figure 4.4). Data collected from the square sample plots were used to verify the classification of point clouds. In addition, data from cross-sections (i.e., the height of reed stems) were used as independent data to validate the derived Digital Surface Models (DSM). Trimble Geo XT was the DGPS system implemented for measuring reference points. Post-processing was executed with the software Trimble GPS Pathfinder Office. The base station SOPAC Wettzell Daily with L2 and the Global Navigation Satellite System (GLONASS) capability was selected for differential correction. The coordinate reference system implemented was the Deutsches Hauptdreiecksnetz (DHDN) Gauss–Krüger Zone 4.

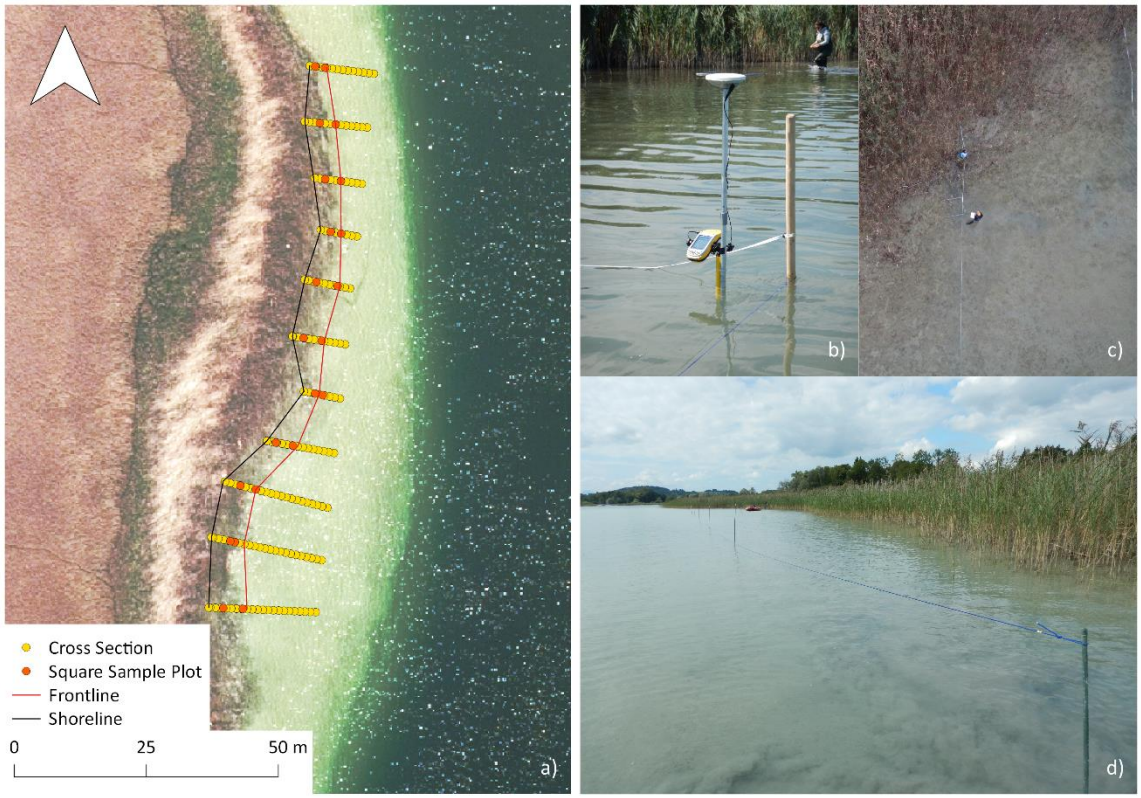

Figure 4.4 Collection of Reference Points (RPs) as an example of AOI-3 a). Background is an orthorectified aerial photograph in true colour of the Landesamt für Digitalisierung, Breitband und Vermessung (LDBV), 2015. Differential Global Positioning System (DGPS) b). Transect perpendicular to shoreline c). Transects every 10 meters intervals

4.3.2.3. Assessment of Aquatic Reed Extents and Classification Accuracy

Extents of aquatic reed beds were evaluated based on two criteria. First, the extents derived from LiDAR data for every AOI were compared with the ones obtained from field measurements, by means of correlation analysis. Since measured and derived surfaces can have the same extents but different shapes, the correlation analysis of the extents was complemented by an assessment of geometrical similarity. As a second criterion, the separation distance of two geometrical objects (polygons) in a metric space was measured (Hausdorff Distance Pairwise). The smaller the resulting value, the more similar the geometrical shapes are (QGIS Development Team 2017). In addition and to support this last metric, the Root Mean Squared Error (RMSE) of the lengths of cross-sections measured on the field in relation to the lengths obtained from LiDAR data was assessed.

The assessment of classification accuracy was achieved by a confusion or error matrix. The classification result was compared with independent validation data. Two approaches were implemented for the accuracy assessment of aquatic reed classification. First, the classification was compared with on-field collected data. A total of 249 square sample plots of 1 m² each were collected on-field and used for validation, out of which 127 and 152 were measured in dense and sparse aquatic reed beds, respectively. Second, RGB imagery with a resolution of 0.1 m/pxl, collected at the same time as the ALS survey took place, was used for visual interpretative validation. Samples were collected randomly and stratified (i.e., classes). Since the map has less than 12 classes and the study area is less than 1 million acres (4046.9 km²), a minimum of 50 points should be collected for every single class (Congalton and Green 2009). A total of 150 points were generated and proportionally distributed (Table 4.1) across the total extent of each class.

Table 4.1 Sample distribution according to extent of classes

Class	Area [m²]	Area [ha]	Number of Samples
Sparse Aquatic Reed	4843	0.4843	50
Dense Aquatic Reed	9037	0.9037	100

The error matrix shows a percentage of pixels from each class labelled correctly as well as the proportions of pixels erroneously labelled into a different class (Richards and Jia 2006). These percentages are expressed as the overall accuracy (OA), producer´s accuracy (PA) and user´s accuracy (UA). Additionally, the chance of agreement was also calculated with the Kappa coefficient (Lillesand et al. 2015).

4.3.2.4. Accuracy Assessment of DSM

Two assessments were accomplished in order to validate the accuracy of estimated DSM. First, the height of a flat surface (i.e., quay, dock) in DSM was compared to the respective one acquired with an onsite survey. Second, the derived aquatic reed heights were assessed on their elevation values in comparison with those measured at each AOI. Distribution type of the height residuals was calculated with the sample skewness and its significance. For a normal distribution, the Mean Error (ME), Standard Deviation (SD), and the Root Mean Square Error (RMSE) were obtained for evaluating the closeness agreement between the observed and the modelled height of reeds (Table 4.2). The rasterisation of the

point clouds was performed using a moving (tilted) plane interpolator (movingPlanes) in OPALS software. Detailed information about this interpolator can be found in (Pfeifer et al. 2014).

Table 4.2 Accuracy measures for Digital Surface Models (DSMs) presenting normal distribution of residuals

Mean Error	$\mu = \frac{1}{n}\sum_{i=1}^{n} \Delta h_i$	(Höhle and Höhle 2009)
Standard Deviation	$\sigma = \sqrt{\frac{1}{(n-1)}\sum_{i=1}^{n} (\Delta h_i - \mu)^2}$	(Höhle and Höhle 2009)
Root Mean Square Error	$RMSE = \sqrt{\frac{1}{n}\sum_{i=1}^{n} \Delta h_i^2}$	(Höhle and Höhle 2009; Luhmann et al. 2014)

n is the number of tested points in the sample (sample size) and Δh_i represents the difference between RP and Digital Service Models (DSMs) for a point i. The assessment of vertical accuracy was performed considering the Air–Water Interface (AWI) as the zero point. The relative stem height (RSH) was obtained by subtracting the absolute height (length from flower to sediment) minus the water depth. The same absolute height of the water surface used for modelling AWI was used for obtaining the RSH.

4.4. Results

4.4.1. Point Cloud Classification

The classification was performed at point level and by means of a decision tree. Development of the rule-based algorithm was based on combining previous knowledge from fieldwork and visual inspections of AOIs point clouds. By means of statistical parameters for every point cloud, several classes were categorised in every point cloud (Figure 4.5). Dense and Sparse Aquatic Reed beds were classified in consideration of the statistical parameters of height and density. With the obtained classes, quantification of extents, as well as the expansion of frontline and shoreline was possible. The classification procedures were executed after quality control. The absolute registration accuracy was 8 cm and strip differences averaged 0.022 m, SD 0.039 m, and RMSE 0.045 m. Registration accuracy and low strip differences were accepted as suitable for the study objectives and no further calibration was performed.

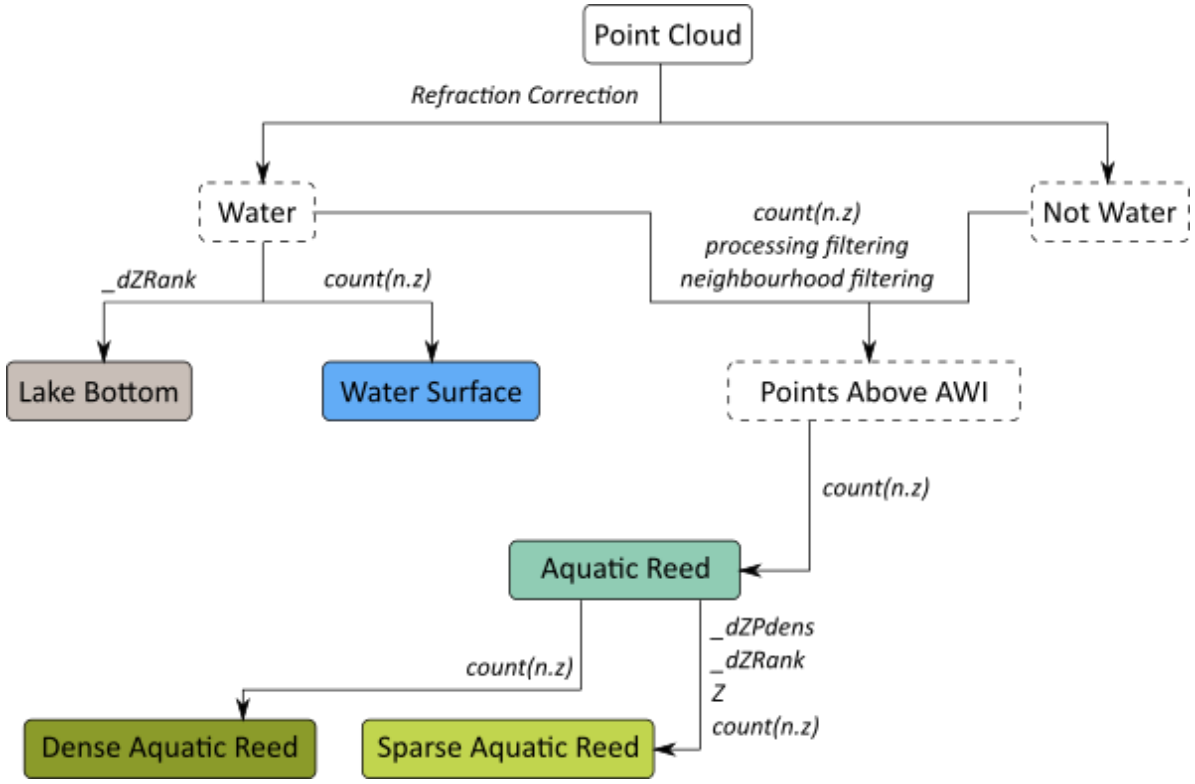

Figure 4.5 Classification scheme used in OPALS for density classification of aquatic reed beds. Dashed line boxes are intermediate classes and coloured boxes represent final classes. Point statistics and attributes used for classification thresholds are described

The structural characteristics obtained from cross-sections extracted in one-metre intervals through all point clouds were equally important. Spatial distribution of points and their height in relation to the AWI were key factors for density classification. The height of sparse aquatic reed beds for all AOIs varied between 1.80 and 2.40 m. A height of 2 m was found to be the most suitable value for an accurate automatic classification of all point clouds (Figure 4.6). The density of points was the second parameter considered for classification. Dense aquatic reed beds are characterised by tall reeds with a height greater than 2 m (520 masl), a large number of leaves in the upper canopy level, and bare thick stems in the lower canopy level. Regarding the LiDAR data, points were equally distributed in sparse stocks and accumulated in the upper canopy for dense stocks. This break in the spatial distribution was easily identifiable in the points between the AWI and the 1.5 m relative height (519.5 m). Once the density was calculated for all values under this height, the maximum frequent value in every AOI was always selected for classification thresholds. For clouds with 2–3 strips, this threshold value was 80 points/m^2. According to this definition, Sparse Aquatic Reed beds were classified and the remaining points without classification were assigned to Dense Aquatic Reed beds.

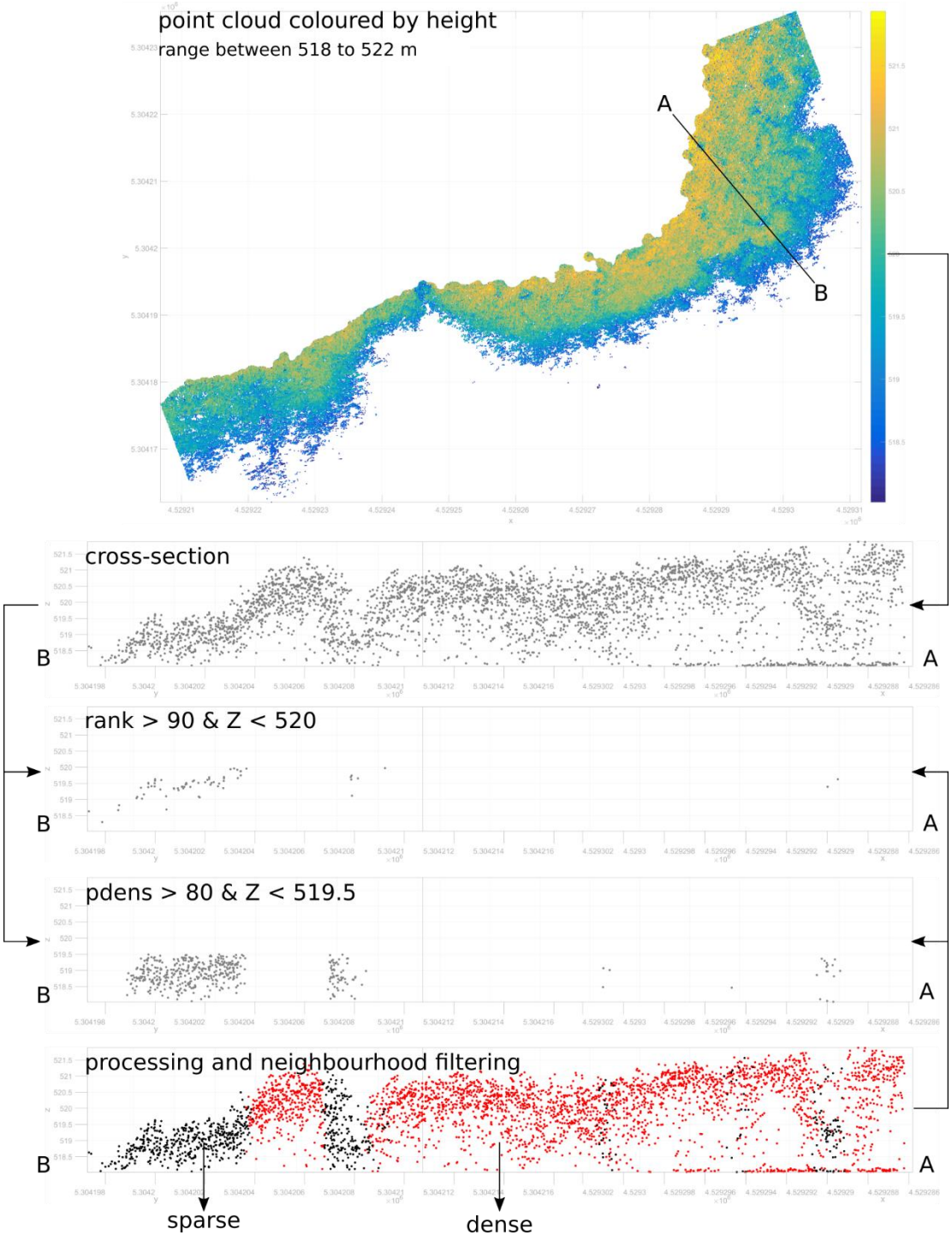

Figure 4.6 Classification of Sparse Aquatic Reed beds according to stem height below 2 m (rank), density of points under a height of 1.50 m (pdens), and in combination with processing and neighbourhood filtering. Grey colours represent to unclassified points, and black and red to areas of sparse and dense aquatic reeds, respectively

4.4.2. Assessment of Aquatic Reed Bed Extents

The result of the classification showed that a total of 1.388 ha (100%) were aquatic reed beds. More than half of the reed beds were identified as Sparse Aquatic Reed (65%—0.9037 ha) and the remaining 35% were identified as Dense Aquatic Reed (0.4843 ha). The correlation analysis between onsite and LiDAR

derived extents showed a highly positive correlation ($R^2 = 0.75$). However, similar extents do not mean similar border shapes and therefore correlation was complemented by a symmetrical assessment of polygon shapes and cross-section lengths (Figure 4.7). The methodology implemented for the aquatic reed front and shoreline delimitation showed a high similarity with the derived LiDAR results from the AOIs, especially in parallel frontlines and shorelines (e.g., AOI-1). Hausdorff distances ranged from 5.74 m (AOI-1) to 12.69 m (AOI-8). Similar results were obtained from the analysis of cross-sections lengths. The RMSE values ranged from 0.69 m (AOI-1) to 4.86 m (AOI-8).

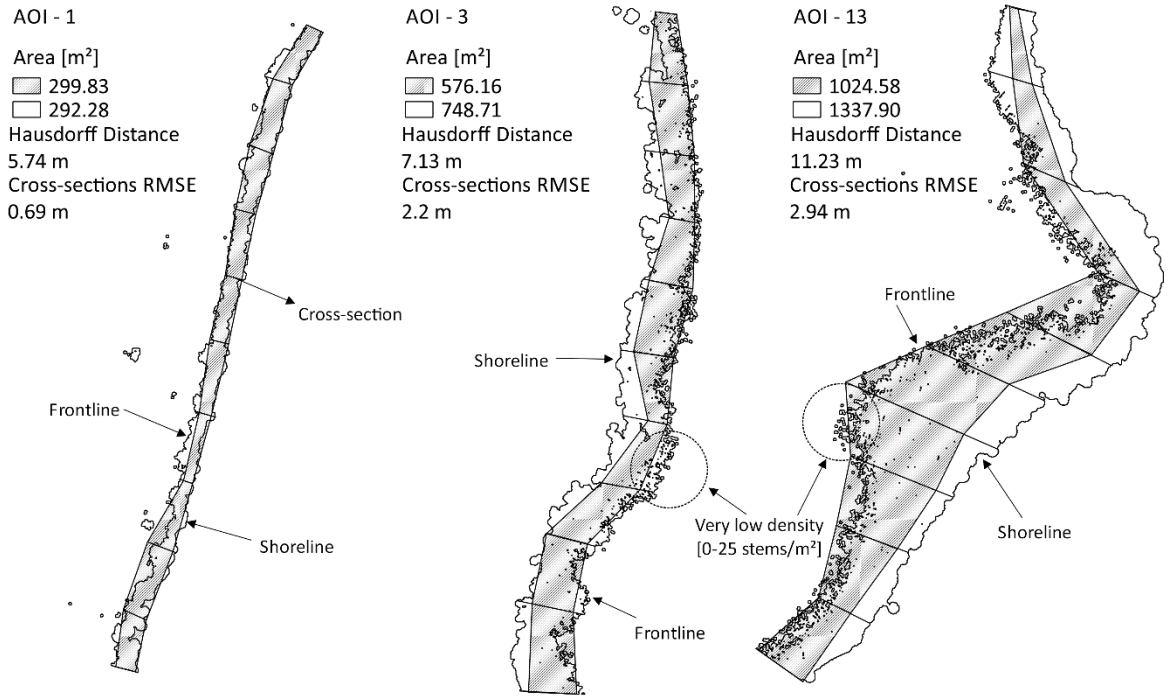

Figure 4.7 Examples of shape similarity measured onsite (grey fill) and derived from LiDAR data (black outline)

4.4.3. Assessment of Aquatic Reed Bed Densities

The first assessment of the vegetation density map revealed an overall accuracy (OA) of 72.7% for the validation compared to field data. The reference points (RP) used for this assessment obtained a 0.46 m horizontal and 0.54 m vertical precision after differential correction. The mean Horizontal and Vertical Dilution of Precision at which all the measurements (RPs) took place was 1.3 and 2.1, respectively. A mean of 17 measurements was recorded for every RP. The Producer's Accuracy (PA) showed that 85.6% of the sparse areas were correctly identified, but according to the User's Accuracy (UA) for the same class, this was true only 68.2% of the time (Table 4.3). Contrarily, 59.7% (PA) of dense areas were identified as such, with 80.4% (UA) of the classification truly corresponding to that category. The Kappa coefficient for this assessment suggests that the observed classification is 50% better than that which resulted by chance.

Table 4.3 Confusion matrix for classification assessed against field data (left) and aerial imagery (right)

Reference Data					Reference Data				
Classified Data	Dense	Sparse	Total	User's Accuracy (%)	**Classified Data**	Dense	Sparse	Total	User's Accuracy (%)
Dense	74	18	92	80.4	Dense	47	3	50	94
Sparse	50	1.07	157	68.2	Sparse	3	97	100	97
Total	124	125	249		Total	50	100	50	
Producer`s Accuracy (%)	59.7	85.6			Producer`s Accuracy (%)	94	97	150	
Overall Accuracy (%) = 72.7; Kappa = 0.5					Overall Accuracy (%) = 96; Kappa = 0.91				

Results differed for the second accuracy assessment of classified density. Very high-resolution aerial imagery (0.1 m/pxl) taken at the same time and during the same flight as the ALS was implemented for this task. An OA of 96% with the Kappa coefficient of 0.91 was obtained from the evaluation (Table 3). High classification accuracy was explained by the unbiased visual interpretative validation applied by the same operator (reed expert) and for all the AOIs represented on RGB data. Both classes (Dense and Sparse) showed a high level of UA and PA, for which the values were 94% and 97% for sparse and dense classes, respectively. An area on the ground will actually be what the classification reveals 94% and 97% of the time. In the same way, the proximity to one of the values from the Kappa coefficient indicates a "true" agreement with the classification (Figure 4.8).

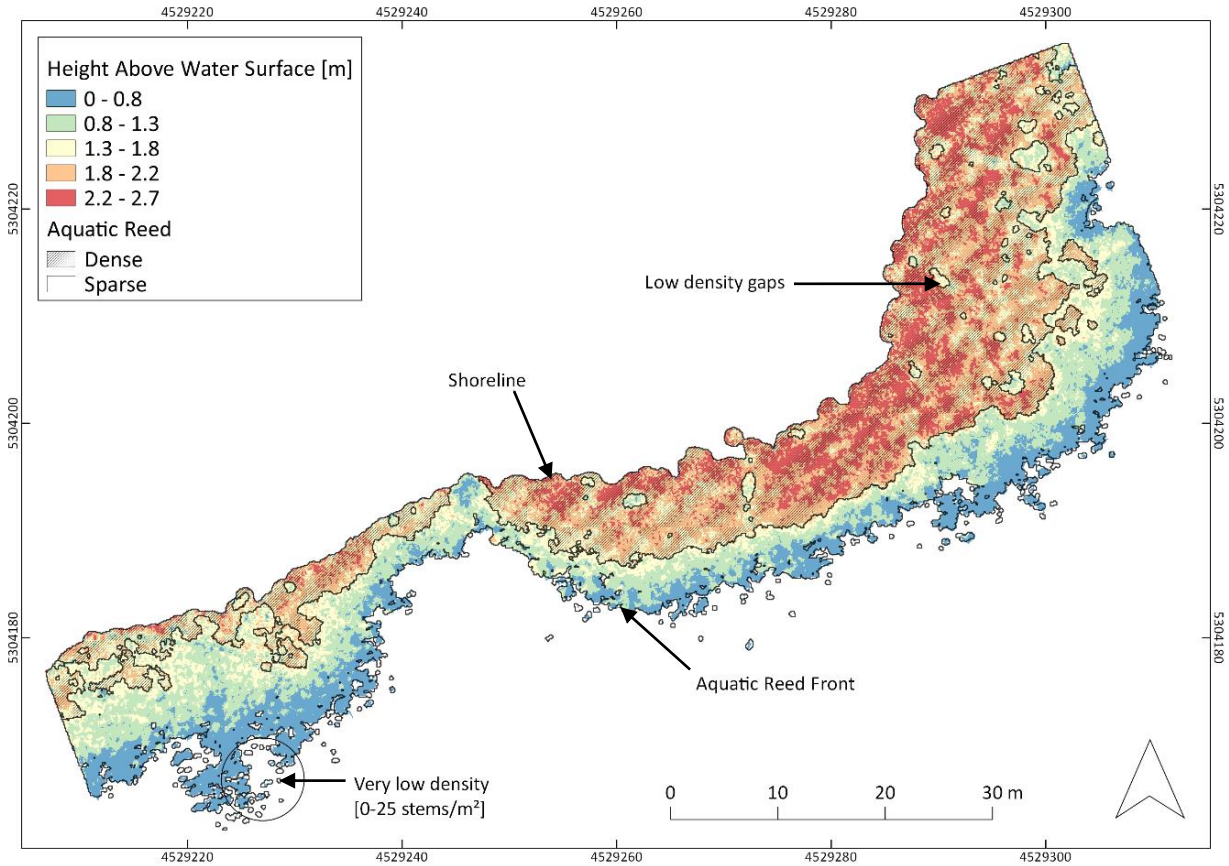

Figure 4.8 Classification of dense and sparse aquatic reed (AOI-6)

4.4.4. Accuracy Assessment for Calculated DSM of Aquatic Reed Beds

The moving tilted plane interpolator (movingPlanes) in combination with a defined number of neighbours (16) allowed for the creation of raster files with a minimum grid size of 10 centimetres. After evaluating observations against modelled height, an accuracy assessment for flat structures showed a total RMSE of 0.1 m, while for vegetation height, it showed a RMSE of 0.8 m. The distribution of the residuals in both assessments was not significantly skewed, since the skewness factors for all 14 AOIs were lower than two times the standard error of the skewness ($SES = \sqrt{6/n}$). In relation to the vegetation height assessment, a perfect normal distribution resulted in residuals from AOI-7 and -12. Meanwhile, the lowest and greatest asymmetries found were in AOI-5 (skewness = 0.52) and AOI-11 (skewness = −0.47). Overall, 1279 independent observations were used to assess the vertical accuracy of vegetation heights in DSM. The correlation analysis between the observed and predicted relative stem height (RSH) revealed a low positive correlation ($R^2 = 0.42$).

4.5. Discussion

This study suggests that ALS provides a highly accurate alternative to the currently applied field-based methodologies for aquatic reed bed monitoring. In contrast to classical monitoring, ALS involves no direct entry of the habitat and no disturbance of the species living there, and therefore, only samples of the study area are needed for field control. In addition, ALS can be carried out in a standardised way that will help increase accuracy at a reduced cost. In line with studies focused on reed bed or wetland habitat mapping (Luo et al. 2017; Onojeghuo and Blackburn 2011; Onojeghuo et al. 2010), ALS is an innovative technical solution compared to classical approaches based on analysis of satellite imagery or of airborne optical data sources (Schmieder et al. 2004; Stratoulias et al. 2015a; Fernandes et al. 2014). Compared to optical sensors in which recorded information on every image is only of top structures observable to an imaging sensor, ALS delivered valuable information in the horizontal as well as the vertical gradient. This technology allowed for characterisation of structural parameters in vegetation stands, and the usage of a Green-LiDAR provided relevant information about the water column and lake bottom in the areas of shallow waters, which was relevant to mapping the shoreline independent of the water surface level. In order to develop environmental protection measures, the material and methodologies implemented for monitoring aquatic reed beds should deliver reliable information on vegetation extents and status. LiDAR data, in combination with a decision tree algorithm, was developed to estimate the reproducibility of an ALS processing chain. The suitability of the applied system was assessed based on 1) an accurate estimation of aquatic reed extents; 2) density; 3) the accuracy of DSMs derived from LiDAR data.

4.5.1. *Mapping On-Field Concept and Extent Quantification*

The obtained quantification revealed that the ALS recorded data for an accurate delimitation of aquatic reed beds. Proposed field mapping of aquatic reed beds contributed to determining, not only structure parameters within the stand, but also to the delimitation of aquatic reed on the frontline, shoreline, and consequently led to the quantification of extent. Onsite measurements are invasive, and for shoreline, frontline, and extent, they are not nearly as accurate as ALS. High agreement of calculated extents from both datasets was seen in areas where the expansion of the frontline is parallel to the shoreline. With the methodology implemented, we observed that the greater the irregularity of the shoreline, the lower

the similarity of polygon shapes. A specific and different method for mapping the frontline and the shoreline could be implemented in such situations. For instance, real-time tracking of DGPS coordinates along aquatic reed fronts would deliver more accurate results, and at the same time, be more environmentally friendly than the executed onsite measures in 10-metre intervals. The same approach, however, cannot be recommended if the primary objective is mapping of the shoreline. It would cause ecological disturbance and damage to the reed population and would require more time and human resource efforts for mapping the entire lake. Additionally, it would compromise the gathering of other data types such as density and stem heights.

In the specific case of the Chiemsee, the official shoreline could have been used in combination with the exemplified frontline mapped with DGPS real-time tracking to calculate extents. It had been created based on aerial photographs from 1991 and it served as a separation between land and aquatic reed. The shoreline had been assumed to be the line of the mean water level (Hoffmann and Zimmermann 2000); however, the fact that water level under the canopy of aquatic reed beds cannot be recorded by optical imaging sensors, questions the reliability of the 1991 shoreline data. This is supported by the fact that the value for the mean water level was not reported and that the shoreline was delimited based on the spectral response of reeds. Even with modern photogrammetric technology, an accurate modelling of water levels below the canopy is unrealistic. Analysis of recorded vegetation spectra in Colour Infra-Red (CIR) imagery was therefore, a practical but not an accurate approach to the problem of shoreline delimitation. The LiDAR capability of detecting structures in the vertical gradient contributed to the extent quantification of aquatic reed stocks, based on the definition of the frontline and shoreline. Precise derivation of water levels under the reed beds canopy contributes to the characterisation of relevant ecological zones such as land, transition, and aquatic reed beds. Extent and heights derived from LiDAR data could also support volume calculations, such as the biomass above ground (Luo et al. 2017). Since LiDAR delivers not only data for accurate extent measurement but also data for the vegetation vertical structure, as well as not being an invasive method, it is comparatively and competitively more convenient than other measures in the field.

4.5.2. Classification of Aquatic Reed Bed Density

LiDAR data also allowed for an accurate classification of aquatic reed density. Without considering the nutrient supply of waters, density and height of aquatic reed beds are important indicators in determining whether a stand is spreading or declining (Grosser et al. 1997). A diminishing or sparse reed population can be seen in most cases by sparse and parallel strips at the reed bed edge (due to either floods, wind storms, or driftwood accumulation), a lane/aisle perpendicular to the shore (through docks, boot traffic, bathing, fish traps), diminishing reed beds with decreasing stem density, a frayed, ripped, or non-zoned reed edge, and growth in single clumps (through erosion or flood), and seaward stubble fields of previous reed beds (Grosser et al. 1997; Hoffmann and Zimmermann 2000). LiDAR data was suitable for deriving most of these parameters, and although not investigated in this study, cross-sections suggested that stubble fields of previous reed beds located underneath the water surface could also be mapped. The OA of 96% with a Kappa coefficient of 0.91 demonstrated the high level of agreement of maps derived from point clouds. Assessment of accuracy by using field measurement revealed the lack of consistency when data was gathered. While LiDAR data allows for a classification of the entire lake, field measurements vary according to phenology and growth rate. In addition, field data is typically collected by several workers and consequently, the selection of sparse stock can contain

a personal bias. This inconsistency was demonstrated in the accuracy assessment results (OA of 77.7% and a Kappa of 0.5), again suggesting the greater efficiency of LiDAR data. The few classification errors were a result of absent generalisation procedures. Vegetation phenology and anisotropy effects that were expected to influence the laser intensity values were not identified as a constraint for vegetation structure mapping. In the same way, surface echo dropouts caused by specular reflection also did not represent an obstacle, since the water level is the same for the entire lake, and the AWI was modelled with the official and freely available data from the water authority (Bayerisches Landesamt für Umwelt 2017a).

4.5.3. Reed Heights Measured on DSM

Deviations in the RMSE for aquatic reed and flat surfaces suggest that it is not advisable to validate a DSM based on vegetation heights. In the case of aquatic reed beds, structural characteristics of the study object may have influenced the laser scanning and derivation of point clouds. Reed beds, like any other grass-like plant, change position with wind action. In addition, aquatic reed beds are influenced by waves or surf changes. These effects caused apparent different stem heights when compared to the on-site field measurements. Since points corresponding to the upper canopy (reed crone) differ from strip to strip, some of these points may have been identified as outliers by filtering algorithms, and consequently, they could be removed from the point cloud in the pre-processing step. The interpolation method may have also influenced the generalisation of canopy heights.

4.5.4. LiDAR Processing Chain and ALS Data Collection

In addition to the type of data implemented, the classification methodology is also crucial in the analysis of LiDAR data. The implementation of a decision tree algorithm was consistently applied. Inspections of point clouds contributed to determining the parameters for classification thresholds. Thus, the presented methodology is objective and easily reproducible without the subjective influence of operators. For monitoring purposes, this also allows a more reliable comparison of results when datasets from different dates are compared. The uncertainty in the multi-temporal analysis is reduced since the resulting classification maps are obtained with the same thresholds and classification methodology.

Our results also confirmed the efficiency of ALS in terms of data collected per unit of time. ALS gathers information within a couple of hours, under the same water level, phenological and climatic conditions. With the proposed transect aquatic reed bed mapping protocol, a team comprising three researchers collecting biometric parameters in cross-sections every 10-m interval for 100 m needed approximately 3 h of work. The length of the Chiemsee (including the two islands) shoreline is 82.811 km. Thus, mapping the entire lakeshore would take approximately 10 months if a team were to work 8 h per day and 7 days per week. Due to the fast monthly growth rate of *Phragmites australis* and the fact that new stems are produced until late summer (Grosser et al. 1997), a considerable number of inconsistencies in data collection would be acquired, based on such field monitoring. Recording data within a short time period not only reduces the uncertainty of the measurements but also of the classification procedures. For instance, all AOIs were classified in the LiDAR data collections at once and the thresholds were suitable for all kind of *Phragmites australis* structures at the Chiemsee. However, during field work, every AOI was treated independently and classified according to the vegetation structures present on

each AOI. Thus, a classification developed for all objects cannot lead to the same result when every sample is independently categorised.

4.6. Conclusions

The presented methodology has demonstrated the suitability and the advantage of using LiDAR data for monitoring aquatic reed beds. The available information obtained from ALS allowed an accurate interpretation and mapping of vegetation structure. Points of the vegetation crown, upper and lower canopy, and ground all contributed to an improved characterisation of aquatic reed beds. The developed decision tree algorithm allowed for an automated classification of reed beds and of vegetation structure (extent, height, and density). With an overall accuracy of 96% and a Kappa coefficient of 0.91, aquatic reed beds could even be subclassified into sparse and dense stocks. Moreover, LiDAR-derived rasters and vector data allowed for the delimitation of the actual shoreline, aquatic reed front, and of sparse aquatic reed beds. ALS revealed several advantages compared to onsite-field monitoring methodology, including the absence of habitat and biological disturbance. The vertical accuracy of the derived DSMs similarly showed a high level of agreement in derived heights of flat surfaces (RMSE = 0.1 m) and an adequate agreement of aquatic reed heights with evenly distributed errors (RMSE = 0.8 m).

5. General Discussion

This study provides novel information on the detectability and quantification of aquatic reed beds using state of the art remote sensing methods. From all of the structural standard parameters recommended by official guidelines for measuring *in situ* and future monitoring, height, density, and extent were determined as essential and quantitative biometric parameters of aquatic reed beds that can accurately be measured in point clouds derived from UAVs and airborne Green-LiDAR data. In line with the study objectives, heights of aquatic reed beds were extracted using photogrammetry in close-range aerial imagery. These features can operationally and effectively be implemented for mapping density, extent, as well vegetation status when geometric is combined with spectral information. Furthermore, the thesis showed that Green-LIDAR is an additional technology, which contributes to the accurately monitoring of aquatic reeds especially when extent, density and height have to be measured. According to the new findings, this study for aquatic reeds adds to the previous studies that used remote sensing data for monitoring reed, and questions the quantification of aquatic reed beds for Lake Chiemsee based on official shoreline and standard colour infrared imagery provided by surveying authorities.

5.1. Extent quantification

The area measured between shoreline (land side) and frontline (lake side) is how the extent of aquatic reed beds is quantified. Data gathered with both systems (UAV and Green-LiDAR) in combination with an adequate processing method proved to be accurate in the allocation of the frontline. The break line between water surface and first reed stems (expansion front) was identifiable in point clouds obtained from either UAVs or Green-LiDAR. The abrupt change in height from almost flat surfaces (water surface) to vegetation (reed stems) determines the frontline. Sparsely distributed stems were detected and extracted thanks to the very high spatial resolution (< 3cm/pixel) of UAV optical imagery and a laser footprint of 40 cm. Low stem density in stands at the expansion front in combination with sun glint effects, sun illumination conditions and reed phenological stage did not represent a hindrance for the tested system in delimiting the frontline, as it was identified in official aerial photographs (Hoffmann and Zimmermann 2000; Melzer et al. 2001).

Regarding the shoreline, Green-LiDAR data demonstrated it could efficiently and accurately determine the boundary between land and aquatic reed beds. The scanning principle of Green-LiDAR helped to deliver information of vegetation features along the vertical structure (canopy to ground) in the vegetation stand. Precise derivation of water levels under the reed beds canopy contributed to the characterization of relevant ecological zones such as land, transition and aquatic reed beds (Figure 1.1). Additionally, LiDAR operating in the green wavelength of the electromagnetic spectrum provided relevant information about the water column and lake bottom in shallow waters, which was relevant to mapping the shoreline independently of the water surface level, on the day of recording. Results obtained in chapters 2 and 3 showed that it is not possible to allocate a shoreline with point clouds derived from UAVs. These results led to questioning the reliability of the official shoreline, which has been created by Bavarian governmental offices through visual interpretation of aerial imagery in 1991. This official shoreline could be used as reference for mapping reed density to have a standard that is necessary to compare reed areas of different years. However, in order to keep consistency in the research analysis, the shoreline allocated during field measurements was used for separating land reed and aquatic reed. The official shoreline at lake Chiemsee was implemented in 1973 for surface comparison of reed and it is still being used in 2015 (Epple 2016; Hoffmann and Zimmermann 2000). Since water

level under the canopy of aquatic reed beds cannot be recorded by optical imaging sensors, the value used for the mean water level was not reported, and the shoreline was delimited based on the spectral response of reeds, the absolute consistency of the 1991 shoreline is questionable.

Green-LiDAR data also proved to be suitable for allocating frontline and the calculation of vegetation extent. Very high spatial resolution of UAV imagery contributed as well to extracting dense point clouds, in which frontline was identifiable. However, UAV data had to be supported with secondary information sources (onsite measured shoreline) in order to quantify the extent. Spectral differences and georeferencing problems in imagery from transitional areas from water to land may cause difficulties in the allocation of frontline, which hinders the discrimination of expansion fronts in aerial photographs (Hoffmann and Zimmermann 2000). The positional error of the digital geometry data produced was a maximum of 0.25 m in aerial photographs with a high proportion of land. For images with large areas of reed bed the error was reported to 0.50 m (Schmieder et al. 2002). The error rates for the evaluation of areas above 0.06 ha averaged 2% and for areas <0.06 ha the error rate was up to 40%. However, the proportion of areas under 0.06 ha was low, resulting in an overall error of + 5%. (Rücker et al. 1999). Therefore, the presented results suggest, if aerial imagery is implemented for monitoring purposes, the analysis should be supported by additional datasets (DSM and shoreline) in order to quantify aquatic reed bed coverage.

5.2. Extraction of height and density parameters

Close-range aerial photogrammetry and Green-LiDAR proved to be suitable methods for delivering valuable information about stem height. Height extraction of sparse stocks (Chapter 2) and evaluation of height measurements (Chapter 4), suggest that it is not advisable to validate DSMs based on modelled vegetation elevations but on fixed structures (e.g. dock). Modelled flat, fixed and geometrical surfaces with UAV and Green-LiDAR data showed high agreement with the onsite measurements. The challenge of identifying sparse stocks in optical imagery was overcome through the feature extraction in very high spatial resolution close-range aerial data. Error in the parallax caused by stem movements during data collection was observed as the source for the observed local disturbance in the bundle adjustment. *Phragmites australis* moves easily in small breezes or surf changes and this movement effect increases in stocks where reeds are sparse. In Green-LiDAR data these effects caused apparent different stem heights when compared to the on-site field measurements. The analysis of point clouds suggests that points corresponding to the upper canopy (reed crone) may have been identified as outliers by filtering algorithms, which consequently could have been removed from the point cloud in the pre-processing step. Since elevation models in raster format were used for height assessments, an additional explanation for the identified variations may also be the applied interpolation methods.

Green-LiDAR and UAV data also allowed for an accurate classification of aquatic reed density. Without considering the nutrient supply of waters, the density and height of aquatic reed beds are important indicators in determining whether a stand is spreading or declining (Grosser et al. 1997). A diminishing or sparse reed population can be seen in most cases by sparse and parallel strips at the reed bed edge (due to either floods, wind storms, or driftwood accumulation), a lane/aisle perpendicular to the shore (through docks, boot traffic, bathing, fish traps), diminishing reed beds with decreasing stem density, a frayed, ripped, or non-zoned reed edge, and growth in single clumps (through erosion or flood), and seaward stubble fields of previous reed beds (Grosser et al. 1997; Hoffmann and Zimmermann 2000). As seen in chapter 4, Green-LiDAR point clouds were suitable for deriving most of these parameters.

Cross-sections suggested that stubble fields of previous reed beds located at lake bottom could potentially also be mapped, although not investigated in this study. Assessment of accuracy by using field measurements revealed the lack of consistency when data was gathered. While Green-LiDAR data allows for a classification of the entire lake, field measurements vary according to phenology and growth rate. In addition, field data is typically collected by several workers and the selection of sparse stock can contain a personal bias. In chapter 2, UAV point clouds showed a high level of agreement compared to the observations onsite. Although photogrammetric methods modelled only the recorded features, it provided two valuable attributes to describe reed bed density. Besides height (Ostendorp 1989; Grosser et al. 1997; Poulin et al. 2010; Zlinszky et al. 2012; Luo et al. 2017), the variance proved to be an additional parameter for reed bed characterization. The spatial distribution of points in combination with the mean height facilitated the characterization of aquatic reed bed density.

As mentioned above, emitted light pulses in LiDAR scanners travel through canopy and bounce on different vegetation elements and the reflections (returns) are recorded. This principle allows a characterization along the vertical structure of a stand. The 40 cm laser footprint delivered up to 5 returns per pulse after pre-processing, which decreases the amount of points per unit of surface. UAV data with spatial resolutions of 3 cm or less are more likely to detect single individuals of *Phragmites australis*. Point density in clouds obtained with UAV data produced clouds with 2260 points/m² (Chapter 2), while LiDAR in the same study area where 200 points/m² (Chapter 4). Higher point density obtained from SfM, relates to the small ground sampling distance and high image overlap (White et al. 2013). Low flying altitude decreases the recording area per survey, but a higher point cloud density enables a better extraction of especially sparse aquatic reed bed areas.

5.3. Mapping vitality

Point clouds derived from UAV imagery allowed the classification of aquatic reed bed status involving the structural and spectral information (Chapter 2). Vegetation mapping is commonly based on the interpretation of multi- or hyperspectral imagery (Onojeghuo and Blackburn 2011; Poulin et al. 2010; Schmieder and Woithon 2004a; Villa et al. 2015). Clouds with spectral information in each point contribute to the classification of a vegetation stock not only according its geometry but also the spectral reflectance of the different plant elements. The fusion of three dimensional structures and spectral information is declared as “state of the art” for characterizing ecosystem vegetation and improves the understanding of vegetation status compared to the application of only geometric or spectral information (Dandois et al. 2017). Vegetation indices, based on RGB channels have been successfully used to describe the vegetation status (Kefauver et al. 2015; Du and Noguchi 2017; Casadesús et al. 2007) and as a component to define aboveground biomass (Li et al. 2016). Thereby, they can be approached for imagery that is recorded by cost effective consumer cameras. Plant health deterioration leads to reflectance decrease in the NIR and a reflectance increase in the visible colour range due to the chlorophyll content in leaves. Therefore, UAVs with a multispectral camera could improve the classification result, however, compared to a consumer camera such a sensor would represent higher costs and heavier weights diminishing in this way the flight time and thus only small areas can be overflown.

5.4. Implications for monitoring

The unbiased measurement of aquatic reed diagnostic parameters presented in this dissertation overcomes the subjective expert knowledge based approach of the official mapping instructions. An important element to evaluate the usability of remote sensing technologies is based on the capability of the employed systems to deliver diagnostic relevant biometric data. Chapters 2 and 4 have shown that elemental features for a status assessment are height, density, and extent. These parameters are considered as stable variables, since they can be quantitative calculated and therefore comparable over time. The vitality of a stock was seen as an additional elemental feature for diagnostic assessments. However, the dependency on qualitative definitions and data variability when recorded by different remote sensing systems make it an unstable variable. Both systems delivered valuable data for measuring height and density. A competitive advantage of Green-LiDAR is the capability of scanning the stock from canopy to ground. Ground height information is fundamental for extracting surfaces and therefore, shoreline can be allocated, and areas with low amount of reeds in stock (gaps) and leaf-off stems can also be distinguished (Chapter 4). The photogrammetric clouds extracted from the RGB system mounted on UAV were also accurate in mapping diagnostic parameters (Chapter 3). Spectral information available in UAV data contributed to estimate of vitality through the calculation of vegetation indexes, which in combination with density and height the status was described and consequently monitoring performed

UAV and Green-LiDAR systems provide point clouds differing in resolution and total data recorded per unit of ground surface. UAV data has a higher number of points per unit of surface compared to LiDAR point clouds (Section 5.2). Recording and processing technologies explain the differences in point cloud density. Whilst photogrammetry is needed in feature extraction in UAV data, the time of flight of light pulses is fundamental in generating LiDAR point clouds. Photogrammetric extracted clouds with a dense number of points allows accurate calculation of Digital Elevation Models (DEM) (Section 2.4). In addition to DEMs, available information of the vertical structure in LiDAR data allows the measurement from base to top (Digital Height Models). In terms of area overflown per unit of time, aerial laser scanning overcomes UAVs. Airborne LiDAR provides data over large areas within a short period of time. The time required for UAV systems is on a different scale. Due to the low flying altitudes, a very low area coverage is achieved. Additional time must be taken into account for the logistics since the operations are executed from ground. When there is the need for monitoring specific areas of interest (AOI) of aquatic reed beds, UAVs are the convenient alternative in terms of cost. Considering the total area mapped of aquatic reed beds in this study with the most accurate system (1.388 ha), the cost per area (AOI) is € 8466 and € 18012 for UAV and LiDAR, respectively. Small companies working in the area of environmental planning benefit from the flexibility in deploying UAV missions, which the level of operability is difficult to overcome by other remote sensing systems. Extensive airborne LiDAR surveys have to be planned a long time in advance, extensive flight planning is required, aircraft availability have to be constantly checked, and a larger team of experts is needed.

The classification strategy implemented in this study proved that automatic classification of aquatic reed beds is possible. Derivation of diagnostic parameters of aquatic reed beds using either UAV or Green-LiDAR point clouds can be operationalized. UAV platforms satisfy the requirements of small companies focused in environmental management demand. In the same way Green-LiDAR has shown the actual technical possibilities for a detailed structural monitoring, independently of reed growing in aquatic or land environments. The proposed methods suggested are more cost effective, unbiased and offered improved information than previously performed on-site or remote sensing procedures. The

method could be transferable to other lakes, vegetation types, and the results can be used for change detection or monitoring. The above mentioned factors are fundamental to evaluate the suitability of remote sensing systems for aquatic reed monitoring. The selection of a specific platform will always depend on the objectives of the study. Both systems have fulfilled a specific mapping niche were they perform at their best. The preferred system will depend on the framework conditions of the monitoring campaign.

5.5. Outlook

Based on the analysis of point clouds generated by LiDAR or Structure-from-Motion algorithms applied in close-range aerial imagery, the quantification and mapping of height, density, extent and status of aquatic reed beds raised new unknowns in which future research should contemplate. The following scenarios can be proposed:

i. The study of further aquatic reed stands or similar vegetation types.

   In this study, the extraction of fundamental biometric parameters and classification strategies were established. The implementation of the presented approaches in different lakes at different latitudes, would contribute in complementing the knowledge of aquatic reeds and validating the methods as well the performance of airborne LiDAR and close-close range aerial photogrammetry under different flight conditions. Further validating the suitability of the presented approaches could be tested when its implementation is transferred to the monitoring or mapping of other grass-like plants in agriculture and forestry.

ii. The modelling of aquatic reeds.

   Beyond the photogrammetric extraction of height, future directions of aquatic reed research using close-range aerial imagery can be in the detailed modelling of reeds. The very high spatial and spectral resolution, which multispectral or hyperspectral sensors mounted on UAVs offer, could potentially contribute in extracting not only heights of aquatic reeds but also point coordinates from leaves, stems or panicles. Therefore, additional biometric parameters could be measured such as number of leaves per stem, number of panicles pro square meter, or even diameter of reed stems. Such quantitative variables would support the derivation of reed health models. In addition, the implementation of feature extraction in very high spatial resolution imagery (<5mm/pixel), would extract also different plant species growing in the same stand. This data could be used for analysis of vegetation stress or plan competition for resources.

iii. Analysis of Green-LiDAR amplitude and lake-bottom returns.

   The successful evaluation of Green-LiDAR data presented in this study was based on the geometric distribution of points in the cloud. An additional analysis in the variation of light amplitude in LiDAR sensors may support the evaluation of growth efficiency in reed stocks. For instance, the classification of points based on the amplitude could deliver information about

presence of leaves (dry or green), stems or panicles. These data in combination with the structure information presented in this study could be used for calculating productivity or biomass. Furthermore, stubble fields of previous reed beds located underneath the water surface could also be mapped with Green-LiDAR data. In this way, quantification and location of past stands of aquatic reeds in shallow waters can be mapped. This would allow more accurate measuring of decline (change detection), as well as defining areas where aquatic reeds could potentially be planted or regrowth if the adequate protection measures are carried out.

6. Conclusion

This dissertation set out to explore the possibilities of extracting quantitative and qualitative biometric variables for classifying the actual state of aquatic reeds. The findings of this research strengthen the idea that operational and effective monitoring can be achieved using state of the art remote sensing technologies. An important finding was that structural parameters (height, area, density) are particularly suitable for reed monitoring via UAV and LIDAR data. Qualitative criteria such as stress level could be determined through the classification of spectral information in point clouds. Based on the available studies, an automated and unbiased reed monitoring is possible. Through the implementation of remote sensing technologies and data, the proposed cost-efficient method delivers an improved information quality in comparison to previously performed on-site procedures, that cause habitat disturbance.

7. Publication list

7.1. Peer-reviewed publication included in this thesis

Meneses, Nicolás Corti (NCM); Baier, Simon; Reidelstürz, Patrick; Geist, Juergen; Schneider, Thomas (2018): Modelling heights of sparse aquatic reed (*Phragmites australis*) using Structure from Motion point clouds derived from Rotary- and Fixed-Wing Unmanned Aerial Vehicle (UAV) data. *Limnologica* 72, pp. 10–21. DOI: 10.1016/j.limno.2018.07.001.

Research topic was developed by TS and refined with NCM, JG, SB and PR. Data collection was coordinated by NCM and SB. PR was the UAV pilot and contributed to the manuscript with the technical information of UAVs and imaging sensors. NCM designed the processing chain, analyzed the data, validated the results, and wrote the first draft. Writing was continuously revised by JG and TS. All authors read and approved the final version of the manuscript.

Corti Meneses, Nicolás; Brunner, Florian; Baier, Simon; Geist, Juergen; Schneider, Thomas (2018): Quantification of Extent, Density, and Status of Aquatic Reed Beds Using Point Clouds Derived from UAV–RGB Imagery. *Remote Sensing* 10 (12), p. 1869. DOI: 10.3390/rs10121869.

The first project idea for this study was conceived by NCM and developed further during discussion with TS, JG and SB. NCM developed the methodology and FB processed and analysed the data under the constant direction of NCM The manuscript was drafted by NCM and FB with continuous input and revision by JG, TS, and SB. All authors read and approved the final version of the manuscript.

Corti Meneses, Nicolás; Baier, Simon; Geist, Juergen; Schneider, Thomas (2017): Evaluation of Green-LiDAR Data for Mapping Extent, Density and Height of Aquatic Reed Beds at Lake Chiemsee, Bavaria—Germany. *Remote Sensing* 9 (12), p. 1308. DOI: 10.3390/rs9121308.

The first project idea for this study was conceived by TS and developed further during discussion with NCM, JG and SB. NCM and SB coordinated the data collection. NCM developed the methodology for processing and analyzing the data. The manuscript was drafted by NCM with continuous input and revision by JG and TS. All authors read and approved the final version of the manuscript.

7.2. Selected oral contributions related to this thesis

Corti Meneses, Nicolás; Baier, Simon; Geist, Juergen; Schneider, Thomas (2018): UAV in der Gewässerfernerkundung. Erfahrungen im Schilfprojekt. Deutsches Zentrum für Luft- und Raumfahrt (DLR). February 22th 2018, Oberpfaffenhofen, Germany

Corti Meneses, Nicolás; Baier, Simon; Geist, Juergen; Schneider, Thomas (2016): Monitoring reed beds by using green LIDAR and UAV´s data. 3rd International Conference Water resources and wetlands. September 8-10th 2016, Tulcea, Romania

Corti Meneses, Nicolás; Baier, Simon; Geist, Juergen; Schneider, Thomas (2016): Workshop Manöverkritik, Datenqualität, Datenauswertung Chiemsee Befliegung. Technische Universität München, Limnologische Station. June 6th 2016, Iffeldorf, Germany

7.3. Selected poster presentation related to this thesis

Baier, Simon; Corti Meneses, Nicolás; Geist, Juergen; Schneider, Thomas (2017): Automatisierte Ableitung von Parametern zur Charakterisierung aquatischer Schilfbestände über 3D-Informationen aus Daten höchstauflösender Fernerkundungs-Systeme. Deutsche Gesellschaft für Limnologie (DGL) Tagung. September 25-29th 2017, Cottbus, Germany

Corti Meneses, Nicolás; Baier, Simon; Geist, Juergen; Schneider, Thomas (2016): Schilfmonitoring und Seeufer-Strukturkartierung bayerischer Seen unter Integration terrestrischer und fernerkundungsgestützer Methoden. Workshop "Gewässervermessung aus der Luft". February 10-11th 2016, Wien, Austria

Corti Meneses, Nicolás; Baier, Simon; Geist, Juergen; Schneider, Thomas (2015): Reed Monitoring and Shore Structure Mapping in the Bavarian lakes under Integration of Terrestrial and Remote Sensing Methods. Innsbruck Summer School of Alpine Research. July 5-11th 2015, Obergurgl, Austria

Acknowledgments

I especially thank Prof. Dr. Jürgen Geist for his constructive and scientific feedback. His patience, motivation, input and continuous support have helped me to complete this work and to develop myself as a research scientist. Also I especially like to thank my mentor and project supervisor Dr. Thomas Schneider, who has created a unique working atmosphere through his unparalleled manner and his incredible creativity. My special appreciation and gratitude to Dr. Uta Raeder who supported this research endeavor wherever she could. She works constantly and tireless on providing optimal conditions at the Limnological Research Station Iffeldorf and for motivating me to complete my research.

Of course I would like to thank my project colleague Simon Baier out of friendship and deepest fellowship. The cooperation with him, the countless conversations and discussions and above all the mutual motivation in difficult days was great gift. Also special thanks To my students Dana Lippert, David Epple, Florian Brunner for their contribution in the project and the scientific discussions and questions all of which allowed me to grow as a supervisor and scientist.

I would also like to thank my great friends from study times and native English speakers Jason Hartmann, Will Meister and Mobolaji Joseph for sharing this journey with me. Their unrestricted willingness to help was crucial to the final adjustments in my research papers as well as my dissertation

I want to sincerely thank my love Franzi. You have been a constant support during all challenging moments during my time in Germany. You are always there when I need you, listening to me and helping me. I am happy to be with you.

Finally my deepest thanks, appreciation, gratitude and humility are to my father and mother. All what I have achieved in my life is thanks to their unconditional love, patience, and example. Thanks parents.

This work was supported by the Bavarian State Ministry of the Environment and Consumer Protection through the project “Klimawandel beeinträchtigt Schilfbestände bayerischer Seen - Erfassung mittels moderner Monitoringmethoden”, which is part of the larger project “Bayerns Stillgewässer im Klimawandel - Einfluss und Anpassung” (TLK01U-66627). In particular, I would like to thank Prof. Dr. Tanja Gschlößl for her interest in the project.

References

Agisoft LLC (2017): Agisoft PhotoScan User Manual. Professional Edition. Version Version 1.3, checked on 11/3/2017.

Alexander, Cici; Deák, Balázs; Kania, Adam; Mücke, Werner; Heilmeier, Hermann (2015): Classification of vegetation in an open landscape using full-waveform airborne laser scanner data. In *International Journal of Applied Earth Observation and Geoinformation*, pp. 76–87. DOI: 10.1016/j.jag.2015.04.014.

Bayerisches Landesamt für Umwelt (2017a): Gewässerkundlicher Dienst Bayern. Available online at https://www.gkd.bayern.de/, checked on 6/1/2017.

Bayerisches Landesamt für Umwelt (2017b): Seen in Bayern - LfU Bayern. Available online at https://www.lfu.bayern.de/wasser/seen_in_bayern/index.htm, checked on 5/23/2017.

Bourgeau-Chavez, Laura; Endres, Sarah; Battaglia, Michael; Miller, Mary Ellen; Banda, Elizabeth; Laubach, Zachary et al. (2015): Development of a bi-national Great Lakes coastal wetland and land use map using three-season PALSAR and Landsat imagery. In *Remote Sensing* 7 (7), pp. 8655–8682. DOI: 10.3390/rs70708655.

Brix, Hans (1999): The European research project on reed die-back and progression (EUREED). In *Limnologica - Ecology and Management of Inland Waters* 29 (1), pp. 5–10. DOI: 10.1016/S0075-9511(99)80033-4.

Brix, Hans; Ye, Siyuan; Laws, Edward A.; Sun, Dechao; Li, Guosheng; Ding, Xigui et al. (2014): Large-scale management of common reed, Phragmitesaustralis, for paper production: A case study from the Liaohe Delta, China. In *Ecological Engineering*, pp. 760–769. DOI: 10.1016/j.ecoleng.2014.09.099.

Candiago, Sebastian; Remondino, Fabio; Giglio, Michaela de; Dubbini, Marco; Gattelli, Mario (2015): Evaluating Multispectral Images and Vegetation Indices for Precision Farming Applications from UAV Images. In *Remote Sensing* 7 (4), pp. 4026–4047. DOI: 10.3390/rs70404026.

Casadesús, J.; Kaya, Y.; Bort, J.; Nachit, M. M.; Araus, J. L.; Amor, S. et al. (2007): Using vegetation indices derived from conventional digital cameras as selection criteria for wheat breeding in water-limited environments. In *Ann Applied Biology* 150 (2), pp. 227–236. DOI: 10.1111/j.1744-7348.2007.00116.x.

Chen, Jianping; Li, Ke; Chang, Kuo-Jen; Sofia, Giulia; Tarolli, Paolo (2015): Open-pit mining geomorphic feature characterisation. In *International Journal of Applied Earth Observation and Geoinformation*, pp. 76–86. DOI: 10.1016/j.jag.2015.05.001.

Chen, Xiaowei; Cen, Minyi; Guo, Haitao; Zhang, Tonggang; Zhao, Chuan; Zhang, Baoming (2017): Chinese satellite photogrammetry without ground control points based on a public DEM using an efficient and robust DEM matching method. In *International Journal of Remote Sensing* 39 (3), pp. 704–726. DOI: 10.1080/01431161.2017.1390270.

Clapuyt, Francois; Vanacker, Veerle; Van Oost, Kristof (2016): Reproducibility of UAV-based earth topography reconstructions based on Structure-from-Motion algorithms. In *Geomorphology* 260, pp. 4–15. DOI: 10.1016/j.geomorph.2015.05.011.

Colomina, I.; Molina, P. (2014): Unmanned aerial systems for photogrammetry and remote sensing. A review. In *ISPRS Journal of Photogrammetry and Remote Sensing* 92, pp. 79–97. DOI: 10.1016/j.isprsjprs.2014.02.013.

Congalton, Russell G.; Green, Kass (2009): Assessing the accuracy of remotely sensed data. Principles and practices. 2. ed. Boca Raton [u.a.]: CRC Press/Taylor & Francis.

Corti Meneses, Nicolás; Baier, Simon; Geist, Juergen; Schneider, Thomas (2017): Evaluation of Green-LiDAR Data for Mapping Extent, Density and Height of Aquatic Reed Beds at Lake Chiemsee, Bavaria—Germany. In *Remote Sensing* 9 (12), p. 1308. DOI: 10.3390/rs9121308.

Costa, B. M.; Battista, T. A.; Pittman, S. J. (2009): Comparative evaluation of airborne LiDAR and ship-based multibeam SoNAR bathymetry and intensity for mapping coral reef ecosystems. In *Remote Sensing of Environment* 113 (5), pp. 1082–1100. DOI: 10.1016/j.rse.2009.01.015.

Crisman, Thomas L.; Alexandridis, Thomas K.; Zalidis, George C.; Takavakoglou, Vasileios (2014): Phragmites distribution relative to progressive water level decline in Lake Koronia, Greece. In *Ecohydrology* 7 (5), pp. 1403–1411. DOI: 10.1002/eco.1466.

Cunliffe, Andrew M.; Brazier, Richard E.; Anderson, Karen (2016): Ultra-fine grain landscape-scale quantification of dryland vegetation structure with drone-acquired structure-from-motion photogrammetry. In *Remote Sensing of Environment*, pp. 129–143. DOI: 10.1016/j.rse.2016.05.019.

Dandois, Jonathan; Baker, Matthew; Olano, Marc; Parker, Geoffrey; Ellis, Erle (2017): What is the Point? Evaluating the Structure, Color, and Semantic Traits of Computer Vision Point Clouds of Vegetation. In *Remote Sensing* 9 (4), p. 355. DOI: 10.3390/rs9040355.

Dash, Jonathan P.; Watt, Michael S.; Pearse, Grant D.; Heaphy, Marie; Dungey, Heidi S. (2017): Assessing very high resolution UAV imagery for monitoring forest health during a simulated disease outbreak. In *ISPRS Journal of Photogrammetry and Remote Sensing* 131, pp. 1–14. DOI: 10.1016/j.isprsjprs.2017.07.007.

Davranche, Aurélie; Lefebvre, Gaëtan; Poulin, Brigitte (2010): Wetland monitoring using classification trees and SPOT-5 seasonal time series. In *Remote Sensing of Environment* 114 (3), pp. 552–562. DOI: 10.1016/j.rse.2009.10.009.

Den Hartog, C.; Květ, J.; Sukopp, H. (1989): Reed. A common species in decline. In *Aquatic Botany* 35 (1), pp. 1–4. DOI: 10.1016/0304-3770(89)90062-4.

Dienst, Michael; Schmieder, Klaus; Ostendorp, Wolfgang (2004): Dynamik der Schilfröhrichte am Bodensee unter dem Einfluss von Wasserstandsvariationen. In *Limnologica - Ecology and Management of Inland Waters* 34 (1), pp. 29–36. DOI: 10.1016/S0075-9511(04)80019-7.

Dittrich, Bruno (2014): Lebensraum Schilf. In Alfred Schmitt (Ed.): Natur Neu Entdeckt. Naturfilmer Und Naturforscher Berichten. Basel: Birkhauser, pp. 116–128, checked on 1/23/2018.

Du, Mengmeng; Noguchi, Noboru (2017): Monitoring of Wheat Growth Status and Mapping of Wheat Yield's within-Field Spatial Variations Using Color Images Acquired from UAV-camera System. In *Remote Sensing* 9 (3), p. 289. DOI: 10.3390/rs9030289.

Epple, David (2016): Entwicklung des aquatischen Schilfs am Chiemsee anhand von Fernerkundungsdaten. Bachelor. Hochschule Weihenstephan, Triesdorf. Fakultät Umweltingenieurwesen.

Erwin, Kevin L. (2009): Wetlands and global climate change. The role of wetland restoration in a changing world. In *Wetlands Ecol Manage* 17 (1), pp. 71–84. DOI: 10.1007/s11273-008-9119-1.

Fernandes, Maria Rosário; Aguiar, Francisca C.; Silva, João M.N.; Ferreira, Maria Teresa; Pereira, José M.C. (2013): Spectral discrimination of giant reed (Arundo donax L.). A seasonal study in riparian areas. In *ISPRS Journal of Photogrammetry and Remote Sensing* 80, pp. 80–90. DOI: 10.1016/j.isprsjprs.2013.03.007.

Fernandes, Maria Rosário; Aguiar, Francisca C.; Silva, João M.N.; Ferreira, Maria Teresa; Pereira, José M.C. (2014): Optimal attributes for the object based detection of giant reed in riparian habitats. A comparative study between Airborne High Spatial Resolution and WorldView-2 imagery.

In *International Journal of Applied Earth Observation and Geoinformation* 32, pp. 79–91. DOI: 10.1016/j.jag.2014.03.026.

Fogli, S.; Marchesini, R.; Gerdol, R. (2002): Reed (Phragmites australis) decline in a brackish wetland in Italy. In *Marine environmental research* 53 (5), pp. 465–479.

Forsmoo, Joel; Anderson, Karen; Macleod, Christopher J. A.; Wilkinson, Mark E.; Brazier, Richard; Smit, Izak (2018): Drone-based structure-from-motion photogrammetry captures grassland sward height variability. In *J Appl Ecol* 94, p. 237. DOI: 10.1111/1365-2664.13148.

George E. Meyer, Timothy W. HindmanKoppolu Laksmi (1999): Machine vision detection parameters for plant species identification (3543). In *Proc.SPIE*. Available online at http://dx.doi.org/10.1117/12.336896.

Gigante, Daniela; Venanzoni, Roberto; Zuccarello, Vincenzo (2011): Reed die-back in southern Europe? A case study from Central Italy. In *Comptes rendus biologies* 334 (4), pp. 327–336. DOI: 10.1016/j.crvi.2011.02.004.

Gilmore, Martha S.; Wilson, Emily H.; Barrett, Nels; Civco, Daniel L.; Prisloe, Sandy; Hurd, James D.; Chadwick, Cary (2008): Integrating multi-temporal spectral and structural information to map wetland vegetation in a lower Connecticut River tidal marsh. In *Remote Sensing of Environment* 112 (11), pp. 4048–4060. DOI: 10.1016/j.rse.2008.05.020.

Gitelson, Anatoly A.; Gritz, Yuri; Merzlyak, Mark N. (2003): Relationships between leaf chlorophyll content and spectral reflectance and algorithms for non-destructive chlorophyll assessment in higher plant leaves. In *Journal of plant physiology* 160 (3), pp. 271–282. DOI: 10.1078/0176-1617-00887.

Grosser, Stephan; Pohl, Wolfgang; Melzer, Arnulf (1997): Untersuchung des Schilfrückgangs an bayerischen Seen. Forschungsprojekt des Bayerischen Staatsministeriums für Landesentwicklung und Umweltfragen. München (Schriftenreihe / Bayerisches Landesamt für Umweltschutz).

Harvey, M.C.; Rowland, J.V.; Luketina, K.M. (2016): Drone with thermal infrared camera provides high resolution georeferenced imagery of the Waikite geothermal area, New Zealand. In *Journal of Volcanology and Geothermal Research*, pp. 61–69. DOI: 10.1016/j.jvolgeores.2016.06.014.

Hoffmann, Florian; Zimmermann, Stefan (2000): Chiemsee Schilfkataster. 1973, 1979, 1991 und 1998. Wasserwirtschaftsamt Traunstein. Limnologische Station der Technische Universität München.

Höhle, Joachim; Höhle, Michael (2009): Accuracy assessment of digital elevation models by means of robust statistical methods. In *ISPRS Journal of Photogrammetry and Remote Sensing* 64 (4), pp. 398–406. DOI: 10.1016/j.isprsjprs.2009.02.003.

Holsten, Bettina; Schoenberg, Wiebke; Jensen, Kai (Eds.) (2013): Schutz und Entwicklung aquatischer Schilfröhrichte. Ein Leitfaden für die Praxis. 1. Nachdruck Dezember 2013. Flintbek: LLUR (Schriftenreihe LLUR SH Gewässer D, 23), checked on 1/18/2018.

Hotes, Stefan; Adema, Erwin B.; Grootjans, Ab P.; Inoue, Takashi; Poschlod, Peter (2005): Reed die-back related to increased sulfide concentration in a coastal mire in eastern Hokkaido, Japan. In *Wetlands Ecology and Management* 13 (1), pp. 83–91. DOI: 10.1007/s11273-003-3091-6.

Jaud, Marion; Passot, Sophie; Le Bivic, Réjanne; Delacourt, Christophe; Grandjean, Philippe; Le Dantec, Nicolas (2016): Assessing the accuracy of high resolution digital surface models computed by PhotoScan® and MicMac® in sub-optimal survey conditions. In *Remote Sensing* 8 (6). DOI: 10.3390/rs8060465.

Jensen, Jennifer L; Mathews, Adam J. (2016): Assessment of image-based point cloud products to generate a bare earth surface and estimate canopy heights in a woodland ecosystem. In *Remote Sensing* 8 (1). DOI: 10.3390/rs8010050.

Katsigiannis, Panagiotis; Misopolinos, Lazaros; Liakopoulos, Vasilis; Alesxandridis, Thomas K.; Zalidis, George (Eds.) (2016): An Autonomous Multi-Sensor UAV System for Reduced-Input Precision Agriculture Applications. Mediterranean Conference of Control and Automation; Mediterranean Control Association; Institute of Electrical and Electronics Engineers; Control Systems Society; Robotics and Automation Society; Mediterranean Conference on Control and Automation; MED. Piscataway, NJ: IEEE, checked on 1/18/2018.

Kefauver, Shawn C.; El-Haddad, George; Vergara-Diaz, Omar; Araus, José Luis (2015): RGB picture vegetation indexes for High-Throughput Phenotyping Platforms (HTPPs). In Christopher M. U. Neale, Antonino Maltese (Eds.). SPIE Remote Sensing. Toulouse, France, Monday 21 September 2015: SPIE (SPIE Proceedings), 96370J, checked on 1/16/2018.

Kristiansen, J. N.; Petersen, B. M. (2000): Remote sensing as a technique to asses reedbed suitability for nesting Greylag geese Anser anser. In *Ardea* 88 (2), pp. 253–257.

Kršák, B.; Blišťan, P.; Pauliková, A.; Puškárová, P.; Kovanič, Ľ.; Palková, J.; Zelizňaková, V. (2016): Use of low-cost UAV photogrammetry to analyze the accuracy of a digital elevation model in a case study. In *Measurement*, pp. 276–287. DOI: 10.1016/j.measurement.2016.05.028.

Krumscheid, P.; Stark, H.; Peintinger, M. (1989): Decline of reed at Lake Constance (Obersee) since 1967 based on interpretations of aerial photographs. In *Aquatic Botany* 35 (1), pp. 57–62. DOI: 10.1016/0304-3770(89)90066-1.

Lameski, Petre; Zdravevski, Eftim; Trajkovik, Vladimir; Kulakov, Andrea (2017): Weed Detection Dataset with RGB Images Taken Under Variable Light Conditions. In Dimitar Trajanov, Verica Bakeva (Eds.): ICT Innovations 2017. Cham: Springer International Publishing, pp. 112–119.

Large, Andrew R. G.; Heritage, George Leonard (Eds.) (2009): Laser scanning for the environmental sciences. Wiley InterScience (Online service). Chichester, U.K, Hoboken, N.J: Wiley-Blackwell.

Li, Wang; Niu, Zheng; Chen, Hanyue; Li, Dong; Wu, Mingquan; Zhao, Wei (2016): Remote estimation of canopy height and aboveground biomass of maize using high-resolution stereo images from a low-cost unmanned aerial vehicle system. In *Ecological Indicators*, pp. 637–648. DOI: 10.1016/j.ecolind.2016.03.036.

Lillesand, Thomas M.; Kiefer, Ralph W.; Chipman, Jonathan W. (2015): Remote sensing and image interpretation. 7th ed. Hoboken, N.J.: John Wiley.

Long, Nathalie; Millescamps, Bastien; Guillot, Benoît; Pouget, Frédéric; Bertin, Xavier (2016): Monitoring the topography of a dynamic tidal inlet using UAV imagery. In *Remote Sensing* 8 (5). DOI: 10.3390/rs8050387.

Luhmann, Thomas; Kyle, Stephen; Böhm, Jan; Robson, Stuart (Eds.) (2014): Close-range photogrammetry and 3D imaging. 2. ed. Berlin: De Gruyter (De Gruyter textbook).

Luo, Shezhou; Wang, Cheng; Xi, Xiaohuan; Pan, Feifei; Qian, Mingjie; Peng, Dailiang et al. (2017): Retrieving aboveground biomass of wetland Phragmites australis (common reed) using a combination of airborne discrete-return LiDAR and hyperspectral data. In *International Journal of Applied Earth Observation and Geoinformation*, pp. 107–117. DOI: 10.1016/j.jag.2017.01.016.

Mandlburger, G.; Pfennigbauer, M.; Pfeifer, N. (2013): Analyzing near water surface penetration in laser bathymetry – A case study at the River Pielach. In *ISPRS Ann. Photogramm. Remote Sens. Spatial Inf. Sci.* II-5/W2, pp. 175–180. DOI: 10.5194/isprsannals-II-5-W2-175-2013.

Mandlburger, Gottfried; Hauer, Christoph; Wieser, Martin; Pfeifer, Norbert (2015): Topo-Bathymetric LiDAR for Monitoring River Morphodynamics and Instream Habitats. A Case Study at the Pielach River. In *Remote Sensing* 7 (5), pp. 6160–6195. DOI: 10.3390/rs70506160.

Marcaccio, J. V.; Markle, C. E.; Chow-Fraser, P. (2015): Unmanned aerial vehicles produce high-resolution, seasonally-relevant imagery for classifying wetland vegetation. In *Int. Arch. Photogramm. Remote Sens. Spatial Inf. Sci.* XL-1/W4, pp. 249–256. DOI: 10.5194/isprsarchives-XL-1-W4-249-2015.

McCabe, Matthew F.; Houborg, Rasmus; Lucieer, Arko (2016): High-resolution sensing for precision agriculture. From Earth-observing satellites to unmanned aerial vehicles. In Christopher M. U. Neale, Antonino Maltese (Eds.). SPIE Remote Sensing. Edinburgh, United Kingdom, Monday 26 September 2016: SPIE (SPIE Proceedings), p. 999811, checked on 1/16/2018.

Melzer, Arnulf; Zimmermann, Stefan; Wissen, Ulrike (2001): Maßnahmenplanung zur Entwicklung der aquatischen Röhrichte am Starnberger See. Wasserwirtschaftsamt München. München.

Meneses, Nicolás Corti; Baier, Simon; Reidelstürz, Patrick; Geist, Juergen; Schneider, Thomas (2018): Modelling heights of sparse aquatic reed (Phragmites australis) using Structure from Motion point clouds derived from Rotary- and Fixed-Wing Unmanned Aerial Vehicle (UAV) data. In *Limnologica* 72, pp. 10–21. DOI: 10.1016/j.limno.2018.07.001.

Meyer, George E.; Neto, João Camargo (2008): Verification of color vegetation indices for automated crop imaging applications. In *Computers and Electronics in Agriculture* 63 (2), pp. 282–293. DOI: 10.1016/j.compag.2008.03.009.

Michez, Adrien; Piégay, Hervé; Lisein, Jonathan; Claessens, Hugues; Lejeune, Philippe (2016): Classification of riparian forest species and health condition using multi-temporal and hyperspatial imagery from unmanned aerial system. In *Environmental Monitoring and Assessment* 188 (3), pp. 1–19. DOI: 10.1007/s10661-015-4996-2.

Mitsch, William J.; Zhang, Li; Stefanik, Kay C.; Nahlik, Amanda M.; Anderson, Christopher J.; Bernal, Blanca et al. (2012): Creating Wetlands. Primary Succession, Water Quality Changes, and Self-Design over 15 Years. In *BioScience* 62 (3), pp. 237–250. DOI: 10.1525/bio.2012.62.3.5.

Mohan, Midhun; Silva, Carlos; Klauberg, Carine; Jat, Prahlad; Catts, Glenn; Cardil, Adrián et al. (2017): Individual Tree Detection from Unmanned Aerial Vehicle (UAV) Derived Canopy Height Model in an Open Canopy Mixed Conifer Forest. In *Forests* 8 (9), p. 340. DOI: 10.3390/f8090340.

Nechwatal, Jan; Wielgoss, Anna; Mendgen, Kurt (2008): Flooding events and rising water temperatures increase the significance of the reed pathogen Pythium phragmitis as a contributing factor in the decline of Phragmites australis. In *Hydrobiologia* 613 (1), pp. 109–115. DOI: 10.1007/s10750-008-9476-z.

Neugirg, F.; Stark, M.; Kaiser, A.; Vlacilova, M.; Della Seta, M.; Vergari, F. et al. (2016): Erosion processes in calanchi in the Upper Orcia Valley, Southern Tuscany, Italy based on multitemporal high-resolution terrestrial LiDAR and UAV surveys. In *Geomorphology*, pp. 8–22. DOI: 10.1016/j.geomorph.2016.06.027.

Onojeghuo, A. O.; Blackburn, G. A.; Latif, Z. A. (Eds.) (2010): Characterising Reedbed habitat quality using Leaf-off LiDAR Data. 21 - 23 May 2010, Mahkota Hotel, Melaka, Malaysia ; proceedings. Universiti Teknologi MARA; Institute of Electrical and Electronics Engineers; International Colloquium on Signal Processing and Its Applications; CSPA. Piscataway, NJ: IEEE, checked on 5/23/2017.

Onojeghuo, Alex Okiemute; Blackburn, George Alan (2011): Optimising the use of hyperspectral and LiDAR data for mapping reedbed habitats. In *Remote Sensing of Environment* 115 (8), pp. 2025–2034. DOI: 10.1016/j.rse.2011.04.004.

Ostendorp, Wolfgang (1989): 'Die-back' of reeds in Europe - a critical review of literature. In *Aquatic Botany* 35 (1), pp. 5–26. DOI: 10.1016/0304-3770(89)90063-6.

Ostendorp, Wolfgang (1991): Damage by episodic flooding to Phragmites reeds in a prealpine lake: proposal of a model. In *Oecologia* 86 (1), pp. 119–124. DOI: 10.1007/BF00317398.

Ostendorp, Wolfgang (1993a): Reed bed characteristics and significance of reeds in landscape ecology. Konstanz.

Ostendorp, Wolfgang (1993b): Schilf als Lebensraum.

Ostendorp, Wolfgang; Dienst, Michael; Schmieder, Klaus (2003): Disturbance and rehabilitation of lakeside Phragmites reeds following an extreme flood in Lake Constance (Germany). In *Hydrobiologia* 506-509, pp. 687–695. DOI: 10.1023/B:HYDR.0000008622.60094.6d.

Ostendorp, Wolfgang; Tiedge, Eva; Hille, Sven (2001): Effect of eutrophication on culm architecture of lakeshore Phragmites reeds. In *Aquatic Botany* 69 (2), pp. 177–193. DOI: 10.1016/S0304-3770(01)00137-1.

Pérez-Ortiz, María; Peña, José Manuel; Gutiérrez, Pedro Antonio; Torres-Sánchez, Jorge; Hervás-Martínez, César; López-Granados, Francisca (2016): Selecting patterns and features for between- and within- crop-row weed mapping using UAV-imagery. In *Expert Systems with Applications*, pp. 85–94. DOI: 10.1016/j.eswa.2015.10.043.

Pfeifer, N.; Mandlburger, G.; Otepka, J.; Karel, W. (2014): OPALS – A framework for Airborne Laser Scanning data analysis. In *Computers, Environment and Urban Systems* 45, pp. 125–136. DOI: 10.1016/j.compenvurbsys.2013.11.002.

Poulin, Brigitte; Davranche, Aurélie; Lefebvre, Gaëtan (2010): Ecological assessment of Phragmites australis wetlands using multi-season SPOT-5 scenes. In *Remote Sensing of Environment* 114 (7), pp. 1602–1609. DOI: 10.1016/j.rse.2010.02.014.

Puliti, Stefano; Olerka, Hans; Gobakken, Terje; Næsset, Erik (2015): Inventory of Small Forest Areas Using an Unmanned Aerial System. In *Remote Sensing* 7 (8), pp. 9632–9654. DOI: 10.3390/rs70809632.

QGIS Development Team (2017): QGIS Geographic Information System. Version 2.18. Available online at http://qgis.osgeo.org.

Rea, Naomi (1996): Water levels and Phragmites: Decline from lack of regeneration or dieback from shoot death. In *Folia Geobotanica* 31 (1), pp. 85–90.

Remondino, Fabio; Spera, Maria Grazia; Nocerino, Erica; Menna, Fabio; Nex, Francesco (2014): State of the art in high density image matching. In *Photogrammetric Record* 29 (146), pp. 144–166. DOI: 10.1111/phor.12063.

Ren, David D. W.; Tripathi, Siddhant; Li, Larry K. B. (2017): Low-cost multispectral imaging for remote sensing of lettuce health. In *J. Appl. Remote Sens* 11 (1), p. 16006. DOI: 10.1117/1.JRS.11.016006.

Reshetyuk, Yuriy; Mårtensson, Stig Göran (2016): Generation of Highly Accurate Digital Elevation Models with Unmanned Aerial Vehicles. In *Photogrammetric Record* 31 (154), pp. 143–165. DOI: 10.1111/phor.12143.

Richards, J. A.; Jia, Xiuping (2006): Remote sensing digital image analysis. An introduction. 4th ed. Berlin, New York: Springer.

Rolletschek, Hardy (1999): The impact of reed-protecting structures on littoral zones. In *Limnologica - Ecology and Management of Inland Waters* 29 (1), pp. 86–92. DOI: 10.1016/S0075-9511(99)80043-7.

Rücker, Achim; Grosser, Stephan; Melzer, Arnulf (1999): Geschichte und Ursachen des Röhrichtrückgangs am Ammersee (Deutschland). In *Limnologica - Ecology and Management of Inland Waters* 29 (1), pp. 11–20. DOI: 10.1016/S0075-9511(99)80034-6.

Samiappan, Sathishkumar; Turnage, Gray; Hathcock, Lee; Casagrande, Luan; Stinson, Preston; Moorhead, Robert (2016): Using unmanned aerial vehicles for high-resolution remote sensing to map invasive Phragmites australis in coastal wetlands. In *International Journal of Remote Sensing* 15 (5), pp. 1–19. DOI: 10.1080/01431161.2016.1239288.

Santise, M.; Fornari, M.; Forlani, G.; Roncella, R. (2014): Evaluation of dem generation accuracy from UAS imagery. In *International Archives of the Photogrammetry, Remote Sensing and Spatial Information Sciences - ISPRS Archives* 40 (5), pp. 529–536. DOI: 10.5194/isprsarchives-XL-5-529-2014.

Santoso, Fendy; Garratt, Matthew A.; Pickering, Mark R.; Asikuzzaman, Md (2016): 3D Mapping for Visualization of Rigid Structures: A Review and Comparative Study. In *IEEE Sensors Journal* 16 (6), pp. 1484–1507. DOI: 10.1109/JSEN.2015.2498940.

Sapkale, Jagdish B.; Kadam, Yuvraj U.; Jadhav, Indrajeet A.; Kamble, Seema S. (2016): River in Planform and Variation in Sinuosity Index : A Study of Dhamni River, Kolhapur (Maharashtra), India. In *International Journal of Scientific & Engineering Research* 7 (2), checked on 9/6/2018.

Schmieder, Klaus (2004): European lake shores in danger — concepts for a sustainable development. In *Limnologica - Ecology and Management of Inland Waters* 34 (1), pp. 3–14. DOI: 10.1016/S0075-9511(04)80016-1.

Schmieder, Klaus; Dienst, Michael; Ostendorp, Wolfgang (2002): Auswirkungen des Extremhochwassers 1999 auf die Flächendynamik und Bestandsstruktur der Uferröhrichte des Bodensees. In *Limnologica - Ecology and Management of Inland Waters* 32 (2), pp. 131–146. DOI: 10.1016/S0075-9511(02)80004-4.

Schmieder, Klaus; Dienst, Michael; Ostendorp, Wolfgang; Jöhnk, Klaus (2004): Effects of water level variations on the dynamics of the reed belts of Lake Constance. In *Ecohydrology and Hydrobiology* 4 (4), pp. 469–480.

Schmieder, Klaus; Woithon, Annette (2004a): Einsatz von Fernerkundung im Rahmen aktueller Forschungsprojekte zur Gewässerökologie an der Universität Hohenheim. In *Bayerische Akademie für Naturschutz und Landschaftspflege* 2 (03), pp. 39–45, checked on 1/16/2018.

Schmieder, Klaus; Woithon, Annette (2004b): Einsatzt von Fernerkundung im Rahmen aktueller Forschungsprojekte zur Gewässerökologie an der Universität Hohenheim. In Elisabeth Obermaier (Ed.): Erfassung und Beurteilung von Seen und deren Einzugsgebieten mit Methoden der Fernerkundung. Tagungsband der ANL-Fachveranstaltung vom 11. bis 12. September in Laufen, 2/03. Laufen: Bayerische Akademie für Naturschutz und Landschaftspflege (ANL) (Laufener Seminarbeiträge, 2003,2), pp. 39–45.

Smith, Mark; Vericat, Damià; Gibbins, Chris (2012): Through-water terrestrial laser scanning of gravel beds at the patch scale. In *Earth Surf. Process. Landforms* 37 (4), pp. 411–421. DOI: 10.1002/esp.2254.

Stanton, Carly; Starek, Michael J.; Elliott, Norman; Brewer, Michael; Maeda, Murilo M.; Chu, Tianxing (2017): Unmanned aircraft system-derived crop height and normalized difference vegetation index metrics for sorghum yield and aphid stress assessment. In *J. Appl. Remote Sens* 11 (2), p. 26035. DOI: 10.1117/1.JRS.11.026035.

Stark, H.; Dienst, M. (1989): Dynamics of lakeside reed belts at Lake Constance (Untersee) from 1984 to 1987. In *Aquatic Botany* 35 (1), pp. 63–70. DOI: 10.1016/0304-3770(89)90067-3.

Stratoulias, Dimitris; Balzter, Heiko; Sykioti, Olga; Zlinszky, Andras; Toth, Viktor R. (2015a): Evaluating Sentinel-2 for Lakeshore Habitat Mapping Based on Airborne Hyperspectral Data. In *Sensors (Basel, Switzerland)* 15 (9), pp. 22956–22969. DOI: 10.3390/s150922956.

Stratoulias, Dimitris; Balzter, Heiko; Zlinszky, András; Tóth, Viktor R. (2015b): Assessment of ecophysiology of lake shore reed vegetation based on chlorophyll fluorescence, field spectroscopy and hyperspectral airborne imagery. In *Remote Sensing of Environment* 157, pp. 72–84. DOI: 10.1016/j.rse.2014.05.021.

Struyf, Eric; van Damme, Stefan; Gribsholt, Britta; Bal, K.; Beauchard, O.; Middelburg, Jack J.; Meire, Patrick (2007): Phragmites australis and silica cycling in tidal wetlands. In *Aquatic Botany* 87 (2), pp. 134–140. DOI: 10.1016/j.aquabot.2007.05.002.

Sukopp, Herbert; Markstein, Barbara (1989): Changes of the reed beds along the Berlin Havel, 1962-1987. In *Aquatic Botany* 35 (1), pp. 27–39. DOI: 10.1016/0304-3770(89)90064-8.

Tonkin, T. N.; Midgley, N. G.; Graham, D. J.; Labadz, J. C. (2014): The potential of small unmanned aircraft systems and structure-from-motion for topographic surveys. A test of emerging integrated approaches at Cwm Idwal, North Wales. In *Geomorphology* 226, pp. 35–43. DOI: 10.1016/j.geomorph.2014.07.021.

Tonkin, T.N.; Midgley, N.G.; Cook, S.J.; Graham, D.J. (2016): Ice-cored moraine degradation mapped and quantified using an unmanned aerial vehicle: A case study from a polythermal glacier in Svalbard. In *Geomorphology*, pp. 1–10. DOI: 10.1016/j.geomorph.2015.12.019.

Tóth, Viktor R. (2016): Reed stands during different water level periods. Physico-chemical properties of the sediment and growth of Phragmites australis of Lake Balaton. In *Hydrobiologia* 778 (1), pp. 193–207. DOI: 10.1007/s10750-016-2684-z.

Tulldahl, H. Michael; Wikström, Sofia A. (2012): Classification of aquatic macrovegetation and substrates with airborne lidar. In *Remote Sensing of Environment* 121, pp. 347–357. DOI: 10.1016/j.rse.2012.02.004.

Uysal, M.; Toprak, A.S.; Polat, N. (2015): DEM generation with UAV Photogrammetry and accuracy analysis in Sahitler hill. In *Measurement*, pp. 539–543. DOI: 10.1016/j.measurement.2015.06.010.

van der Putten, Wim H. (1997): Die-back of Phragmites australis in European wetlands: an overview of the European Research Programme on Reed Die-back and Progression (1993–1994). In *Aquatic Botany* 59 (3), pp. 263–275. DOI: 10.1016/S0304-3770(97)00060-0.

Venturi, Sara; Di Francesco, Silvia; Materazzi, Filippo; Manciola, Piergiorgio (2016): Unmanned aerial vehicles and Geographical Information System integrated analysis of vegetation in Trasimeno Lake, Italy. In *Lakes and Reservoirs: Research and Management* 21 (1), pp. 5–19. DOI: 10.1111/lre.12117.

Vermaat, Jan E.; Bos, Bas; van der Burg, Peter (2016): Why do reed beds decline and fail to re-establish? A case study of Dutch peat lakes. In *Freshw Biol* 61 (9), pp. 1580–1589. DOI: 10.1111/fwb.12801.

Villa, Paolo; Bresciani, Mariano; Bolpagni, Rossano; Pinardi, Monica; Giardino, Claudia (2015): A rule-based approach for mapping macrophyte communities using multi-temporal aquatic vegetation indices. In *Remote Sensing of Environment* 171, pp. 218–233. DOI: 10.1016/j.rse.2015.10.020.

Villa, Paolo; Laini, Alex; Bresciani, Mariano; Bolpagni, Rossano (2013): A remote sensing approach to monitor the conservation status of lacustrine Phragmites australis beds. In *Wetlands Ecol Manage* 21 (6), pp. 399–416. DOI: 10.1007/s11273-013-9311-9.

Vincent, W. F. (2009): Effects of Climate Change on Lakes, pp. 55–60. DOI: 10.1016/B978-012370626-3.00233-7.

Wedding, Lisa M.; Friedlander, Alan M.; McGranaghan, Matthew; Yost, Russell S.; Monaco, Mark E. (2008): Using bathymetric lidar to define nearshore benthic habitat complexity. Implications for management of reef fish assemblages in Hawaii. In *Remote Sensing of Environment* 112 (11), pp. 4159–4165. DOI: 10.1016/j.rse.2008.01.025.

Weiss, Marie; Baret, Frédéric (2017): Using 3D Point Clouds Derived from UAV RGB Imagery to Describe Vineyard 3D Macro-Structure. In *Remote Sensing* 9 (2), p. 111. DOI: 10.3390/rs9020111.

Westoby, M. J.; Brasington, J.; Glasser, N. F.; Hambrey, M. J.; Reynolds, J. M. (2012): 'Structure-from-Motion' photogrammetry. A low-cost, effective tool for geoscience applications. In *Geomorphology* 179, pp. 300–314. DOI: 10.1016/j.geomorph.2012.08.021.

White, Joanne; Wulder, Michael; Vastaranta, Mikko; Coops, Nicholas; Pitt, Doug; Woods, Murray (2013): The Utility of Image-Based Point Clouds for Forest Inventory. A Comparison with Airborne Laser Scanning. In *Forests* 4 (3), pp. 518–536. DOI: 10.3390/f4030518.

Wiseman, Dion J.; Van Sluijs, Jurjen Der (2015): Alternative methods for developing and assessing the accuracy of UAV-derived DEMs. In *International Journal of Applied Geospatial Research* 6 (3), pp. 58–77. DOI: 10.4018/ijagr.2015070104.

Woebbecke, D. M.; Meyer, G. E.; Bargen, K. Von; Mortensen, D. A. (1995): Color Indices for Weed Identification Under Various Soil, Residue, and Lighting Conditions. In *Transactions of the ASAE* 38 (1), pp. 259–269. DOI: 10.13031/2013.27838.

Yamamoto, Kristina H.; Powell, Rebecca L.; Anderson, Sharolyn; Sutton, Paul C. (2012): Using LiDAR to quantify topographic and bathymetric details for sea turtle nesting beaches in Florida. In *Remote Sensing of Environment* 125, pp. 125–133. DOI: 10.1016/j.rse.2012.07.016.

Zarco-Tejada, P.J.; Diaz-Varela, R.; Angileri, V.; Loudjani, P. (2014): Tree height quantification using very high resolution imagery acquired from an unmanned aerial vehicle (UAV) and automatic 3D photo-reconstruction methods. In *European Journal of Agronomy*, pp. 89–99. DOI: 10.1016/j.eja.2014.01.004.

Zlinszky, András; Mücke, Werner; Lehner, Hubert; Briese, Christian; Pfeifer, Norbert (2012): Categorizing wetland vegetation by airborne laser scanning on Lake Balaton and Kis-Balaton, Hungary. In *Remote Sensing* 4 (6), pp. 1617–1650. DOI: 10.3390/rs4061617.

Zlinszky, András; Schroiff, Anke; Kania, Adam; Deák, Balázs; Mücke, Werner; Vári, Ágnes et al. (2014): Categorizing Grassland Vegetation with Full-Waveform Airborne Laser Scanning. A Feasibility Study for Detecting Natura 2000 Habitat Types. In *Remote Sensing* 6 (9), pp. 8056–8087. DOI: 10.3390/rs6098056.